

# JGR Solid Earth

## RESEARCH ARTICLE

10.1029/2019JB017604

### Key Points:

- Submarine volcanism in Amerasia Basin of the western Arctic Ocean produced flows dated by  $^{40}\text{Ar}/^{39}\text{Ar}$  geochronology at circa 118–112 Ma (low-Ti tholeiite I of the Northwind Ridge) and circa 105–100 Ma (low-Ti tholeiite II) and circa 90–70 Ma (high-Ti tholeiite)—both from Healy Spur
- The low-Ti tholeiites I at Northwind Ridge that erupted at circa 118–112 Ma resulted from melting of a subcontinental lithospheric mantle (SCLM) source within the spinel stability field and were precursor to melting and eruption of magmas from isotopically more depleted sources, including the asthenosphere
- Melting events that produced the circa 105–100 Ma low-Ti tholeiites II and circa 90–70 Ma high-Ti tholeiites may be related to ascent of a plume head and the concomitant melting that yielded bimodal distribution of basaltic compositions, typical of plume-related continental flood basalts (CFB) provinces elsewhere on Earth

### Supporting Information:

- Supporting Information S1

### Correspondence to:

S. B. Mukasa,  
mukasa@umn.edu

### Citation:

Mukasa, S. B., Andronikov, A., Brumley, K., Mayer, L. A., & Armstrong, A. (2020). Basalts from the Chukchi borderland:  $^{40}\text{Ar}/^{39}\text{Ar}$  ages and geochemistry of submarine intraplate lavas dredged from the western Arctic Ocean. *Journal of Geophysical Research: Solid Earth*, 125, e2019JB017604. <https://doi.org/10.1029/2019JB017604>




Received 27 FEB 2019

Accepted 8 MAY 2020

Accepted article online 11 MAY 2020

©2020. American Geophysical Union.  
All Rights Reserved.

## Basalts From the Chukchi Borderland: $^{40}\text{Ar}/^{39}\text{Ar}$ Ages and Geochemistry of Submarine Intraplate Lavas Dredged From the Western Arctic Ocean

Samuel B. Mukasa<sup>1</sup> , Alexandre Andronikov<sup>2</sup>, Kelley Brumley<sup>3</sup> , Larry A. Mayer<sup>4</sup> , and Andrew Armstrong<sup>4</sup>

<sup>1</sup>Department of Earth and Environmental Sciences, University of Minnesota, Minneapolis, MN, USA, <sup>2</sup>Czech Geological Survey, Prague, Czech Republic, <sup>3</sup>Fugro, Inc., Houston, TX, USA, <sup>4</sup>Center for Coastal and Ocean Mapping/Joint Hydrographic Center, Jere A. Chase Ocean Engineering Laboratory, Durham, NH, USA

**Abstract** Submarine volcanism in the western Arctic Ocean, known as Amerasia Basin, is attributed to a mantle plume based on geophysics and meager geochemical evidence. Basaltic samples dredged from Chukchi Borderland within the basin have produced minimum  $^{40}\text{Ar}/^{39}\text{Ar}$  ages for eruption at circa 118–112, circa 105–100, and circa 90–70 Ma, which we use to constrain tectonic models for basin opening. Major oxide and trace element concentrations and Sr, Nd, and Hf isotopic ratios of the lavas show that the circa 118–112 Ma samples from Northwind Ridge are tholeiites (low-Ti tholeiite I) with low degrees of rare-earth element (REE) fractionation, high overall heavy rare-earth element (HREE), and Mg# (*Mg-number*), which suggests magma derivation from a garnet-free source followed by minor crystal fractionation. Strontium, Nd, and Hf isotope systematics for these lavas and ratios of highly incompatible trace elements point toward a lithospheric source. Eruptions at circa 105–100 and circa 90–70 Ma, both at Healy Spur, produced two types of lavas: low-Ti tholeiite II—which are generally older than high-Ti tholeiite—both common in continental flood basalt (CFB) provinces and both with trace element abundance patterns typifying a garnet-free source and significant crystal fractionation for the high-Ti tholeiite. The isotope characteristics for both groups are common features of asthenospheric sources. Composition-time relationships for the lavas suggest inception of melting in the subcontinental lithospheric mantle (SCLM)—probably due to introduction of a heat source by a plume—followed later (at ca. 105–100 and ca. 90–70 Ma) by asthenospheric melting possibly triggered by plume rise.

**Plain Language Summary** Using U.S. Coast Guard research icebreaker *Healy*, we dredged basaltic lava flows from the bathymetrically high Chukchi Borderland on the floor of the western Arctic Ocean—an area known as Amerasia Basin—to determine eruption history using radioactivity thereby providing time constraints on the plate tectonic evolution of the region. We also measured the major oxide and trace element compositions as well as the lead, strontium, neodymium, and hafnium isotopic ratios of the lavas to decipher the geochemical character of the source materials deep inside the Earth. This work is part of the push for data collection in the last decade for Extended Continental Shelf (ECS) purposes under the U.N. Convention for Law of the Sea (UNCLOS), Article 76. Submarine eruptions along Chukchi Borderland occurred at circa 118–112, circa 105–100, and circa 90–70 Ma, producing three geochemically distinct rock types akin to lavas in continental flood basalt (CFB) in other magmatic provinces on Earth. These lava compositions are in stark contrast to the compositions of submarine lavas in the eastern Arctic where oceanic crust of significant width developed and separated previously joined continental landmasses and their continental shelves.

## 1. Introduction

The floor of the Arctic Ocean, a vast area surrounding the North Pole, is divided into two main basins: Amerasia Basin (approximately 1,500 by 1,900 km)—bordering eastern Siberia, Alaska, and the Canadian Arctic Archipelago—and Eurasia Basin, which borders western Siberia and Greenland and is floored by the Gakkel Ridge at its median axis (Figure 1). Amerasia Basin is composed of several tectonic elements, including a deep basin (>3,800 m) known as Canada Basin (Figures 1 and 2) and a few smaller basins, bordered by the high standing Chukchi Borderland and the bathymetrically high Alpha Ridge and Mendeleev

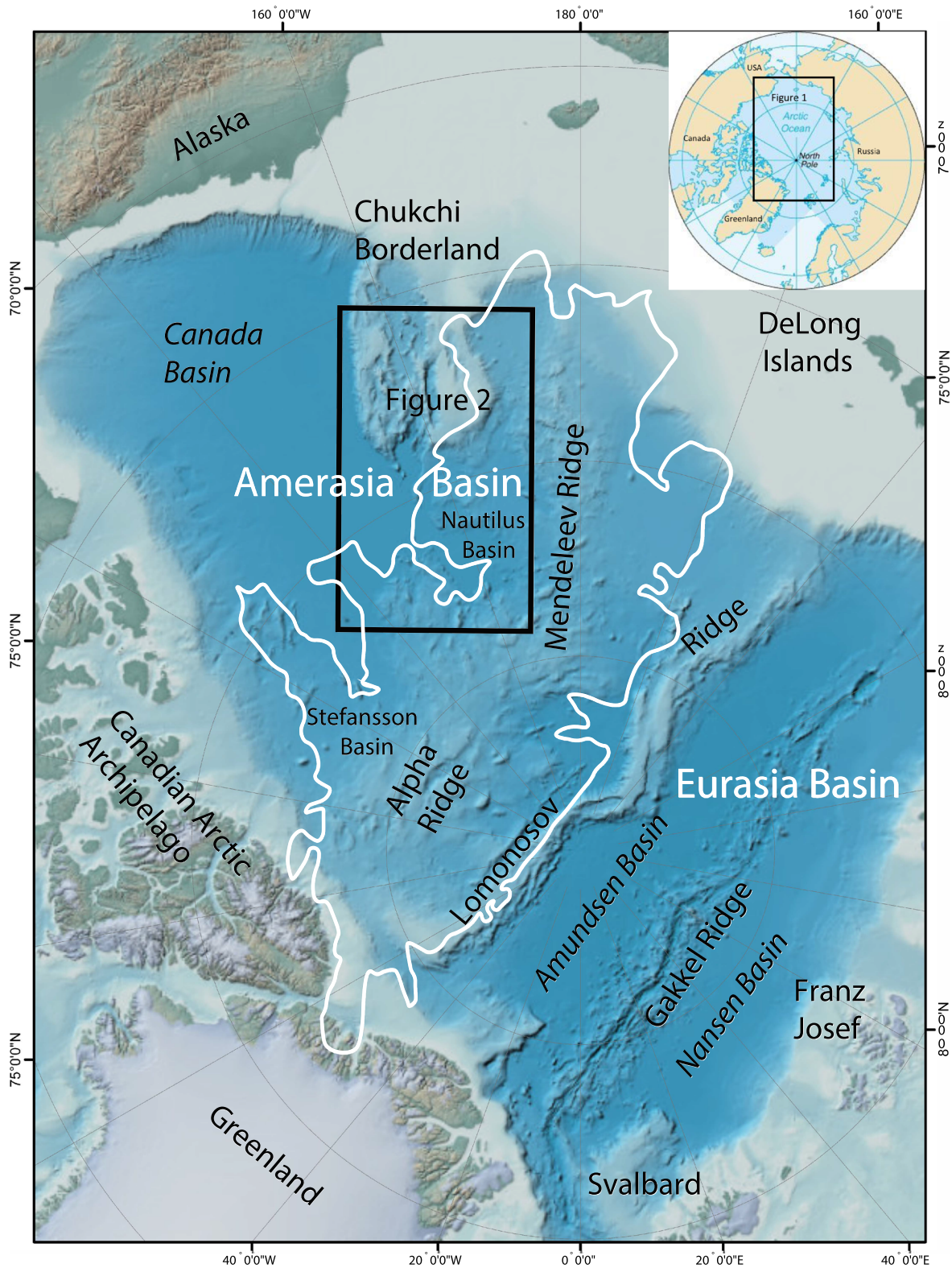


**Figure 1.** Map of the Arctic polar region showing the major bathymetric features, including Chukchi borderland, the area sampled in this study. The area covered by this map is indicated on the inset map in the top right-hand corner. The area for Figure 2 is indicated by the black rectangle in the middle of the map. The white shape in the middle of the map outlines the extent of the high Arctic large Igneous Province (HALIP), based on the high Arctic magnetic high (HAMH) of Gaina et al. (2011) as summarized in Oakey and Saltus (2016). Note that the HALIP does not delineate Mesozoic and Cenozoic magmatic activity in the area as this extends into the Canadian Arctic archipelago, DeLong Islands, Franz Josef, and Svalbard.

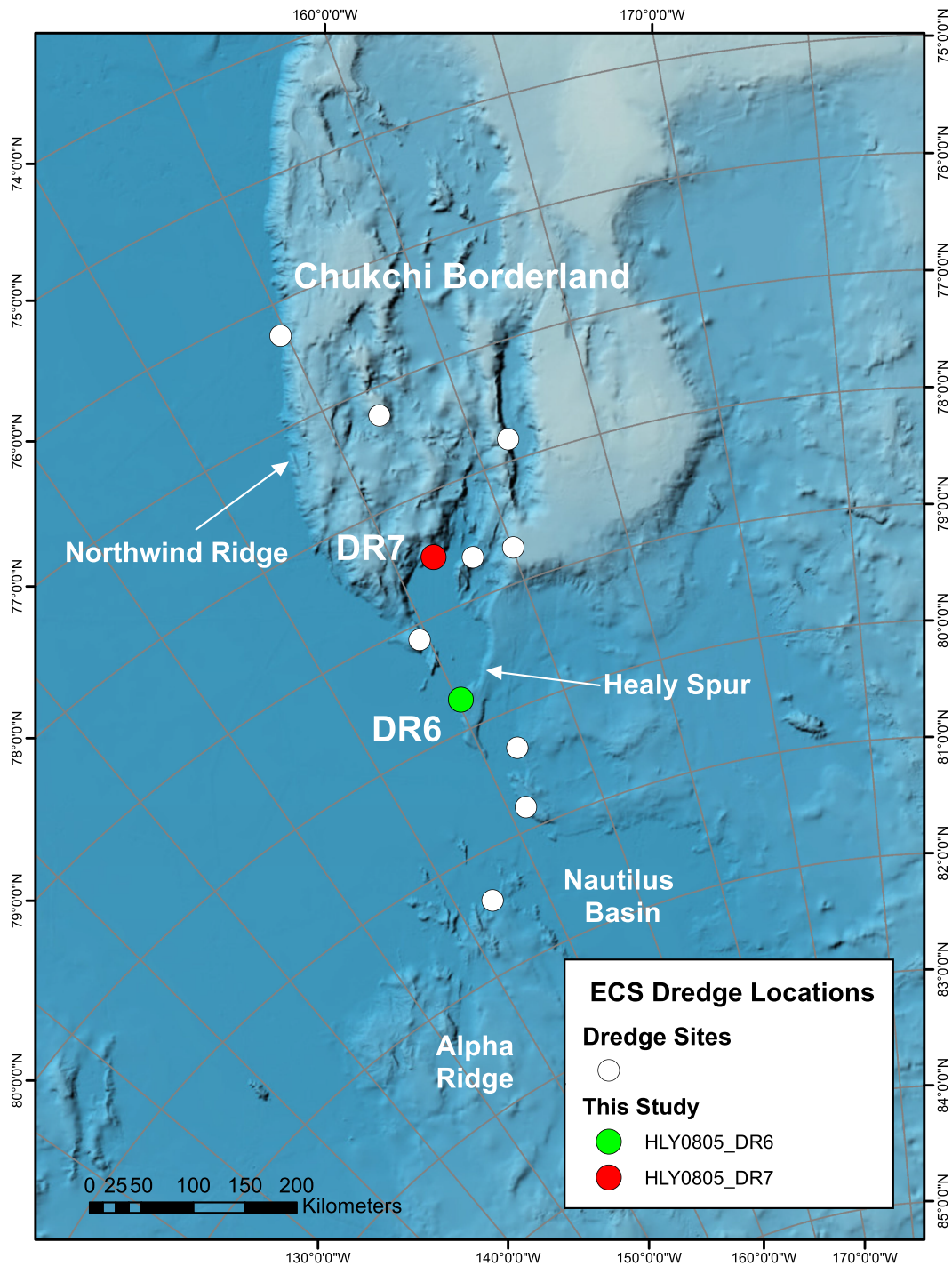


**Figure 2.** Bathymetric map of the Chukchi Borderland, Healy Spur, and Alpha Ridge region showing all of the dredge locations for the extended continental shelf (ECS) study. The samples discussed in this paper came from dredge sites DR6 and DR7.

Ridge (Figure 1). While the presence of oceanic crust in the Canada Basin and the continental nature of the Chukchi Borderland is now reasonably well established (e.g., Chian et al., 2016; Grantz et al., 1998; Hutchinson et al., 2017), there is little consensus about the nature of Alpha Ridge and Mendeleev Ridge and the kinematic history of Amerasia Basin as a whole. These features have been ascribed different origins, including continental rifting, seafloor spreading, and plume activity, as summarized in the section below.

A push for data collection in the last decade for Extended Continental Shelf (ECS) purposes under the U.N. Convention for Law of the Sea (UNCLOS), Article 76 has resulted in new information about Amerasia Basin, particularly its bathymetry, tectonic evolution, and geochemistry of the basaltic lavas along its margins (e.g., Brumley et al., 2015; Chian et al., 2016; Døssing et al., 2013; Evangelatos et al., 2017; Flinders et al., 2014; Miller et al., 2018; Mosher et al., 2012). Sea ice retreat during the summer months as the result of recent climate change has made navigation easier and opened up opportunities for multibeam bathymetric mapping and dredging in the western Arctic Ocean. In August–September 2008, as part of the U.S. Extended Continental Shelf Program (Mayer & Armstrong, 2008), seven dredges were collected aboard the icebreaker U.S. Coast Guard Cutter *Healy*, including HLY0805-DR7 from a slope edge of the Chukchi Borderland at the northern end of the Northwind Ridge, another along a bathymetric high here called Healy Spur (HLY0805-DR6; Figure 2), and another on Alpha Ridge where it borders Nautilus Basin (HLY0805-DR1) (Andronikov et al., 2008; Brumley et al., 2008; Mayer et al., 2008). Four of the seven dredges were conducted on relatively gentle slopes ( $<30^\circ$ ) and therefore yielded mostly mud with various ice rafted debris (Brumley, 2009). Dredge HLY0805-DR1 from Alpha Ridge yielded monolithologic outcrop samples of silicic volcanoclastic sedimentary rocks interpreted to have been deposited in shallow water during a phreatomagmatic eruption (Brumley et al., 2013; Flinders et al., 2014).

The dredges discussed here (HLY0805-DR6 and DR7) were collected from steep escarpments with slopes up to  $50^\circ$  in water depths of over 3,500 m. These dredges recovered the largest and some of the first known submarine basalt samples from the Amerasia Basin seafloor. Van Wagoner et al. (1986), Mühe and Jokat et al. (1999), Jokat (2003), and Jokat et al. (2013) previously reported recovery of acoustic basement materials in the Alpha/Mendeleev Ridge area, but these included sedimentary rocks and only a few small basalt samples, none definitively from outcrop. The fresh broken surfaces of large blocks of rock (some  $>10$  kg) and the lithological similarity of the rocks recovered in our dredges, as well as identical Mn crust development on the unbroken surfaces of the samples at each site, suggest that the lava samples were broken away from autochthonous submarine outcrops. Here, we report the first results of  $^{40}\text{Ar}/^{39}\text{Ar}$  dating, as well as chemical and radiogenic isotope (Pb, Nd, Sr, and Hf) compositions of the dredged volcanic samples from Healy Spur and Northwind Ridge, both parts of the Chukchi Borderland (Figure 1). The data are used to test tectonic models for development of Amerasia Basin and to infer the mantle melting processes that produced the variety of lava compositions observed through time in a part of the Arctic Ocean that has never been studied systematically from the petrological and geochemical perspectives.

## 2. Tectonic Setting

Most authors agree that the Late Jurassic to Early Cretaceous is the time when a continental block in the Arctic Region started to break apart and Amerasia Basin began to form (e.g., Grantz et al., 1979; Grantz & May, 1983; Lawver et al., 2002). However, the prebreakup geometry and overall tectonic setting prior to opening are not well constrained. Studies by Lawver et al. (2002), Miller et al. (2002), and Kuzmichev (2009) inferred from the geology along the margins of Amerasia Basin that the North American and Eurasian plates had not yet separated in the early Mesozoic and that the Ural and Taimyr mountains were shedding sediments into basins along the broad shelf thought to have existed between the two continents.

All tectonic reconstruction models for development of Amerasia Basin agree that the Chukchi Borderland (Figure 1) is a continental fragment (Dietz & Shumway, 1961; Grantz et al., 1998; Hall, 1990; Jokat et al., 1992), and indeed, dredged basement rocks from the area have confirmed this view (Brumley, 2009; Brumley et al., 2015). It is generally accepted that Canada Basin may be underlain by oceanic crust due to a generally north/south linear gravity low interpreted to be a fossil spreading center (Coles & Taylor, 1990; Grantz et al., 1979; Grantz et al., 1990; Grantz et al., 1998; Taylor et al., 1981), although magnetic anomalies are not robustly expressed owing to the thick sediment cover (Baggeroer & Falconer, 1982; Grantz et al., 1990; Grantz et al., 1998). Recent Extended Continental Shelf (ECS) multichannel seismic imaging in the central part of Canada Basin also inferred the presence of a spreading center (Chian et al., 2016; Hutchinson et al., 2015, 2017), and seismic velocity models suggest oceanic crust distribution with maximum dimensions of  $\sim 340$  km by 590 km in the center of the Canada Basin (Chian et al., 2016).

Existing tectonic reconstructions of Amerasia Basin invoke different explanations for the features observed in and around the basin (for reviews of published reconstruction models see Chian et al., 2016; Doré

et al., 2016; Oakey & Saltus, 2016; Miller et al., 2018; Pease et al., 2014; Petrov et al., 2016). The model that has stood the test of time for opening of the basin is the “rotational model,” which invokes an ~60–90° counterclockwise rotation of a continental mass known as the Arctic Alaska/Chukotka microplate from its original position along Arctic Canada during the late Jurassic into the Cretaceous, about a pole of rotation located near the Mackenzie River Delta in Arctic Canada (Carey, 1955; Embry & Dixon, 1990; Freeland & Dietz, 1973; Grantz et al., 1979; Grantz et al., 2011; Grantz et al., 1998; Gurevich et al., 2006; Kuzmichev, 2009; Miller et al., 2018; Pease et al., 2014; Sweeney, 1985; Tailleux & Brosge, 1970). Although there are variations on this theme (e.g., Grantz et al., 2011; Miller et al., 2018; Pease et al., 2014), the Lomonosov Ridge serves as a transform boundary with over 2,600 km displacement (Dixon & Dietrich, 1990; Embry, 1990; Grantz, 2006; Grantz et al., 1990; Grantz et al., 2011; Harbert et al., 1990; Lawver et al., 2002; Rowley & Lottes, 1988).

The origins and crustal structure of the enigmatic Alpha-Mendeleev Ridge system (Figures 1 and 2) have also been highly disputed. The Alpha-Mendeleev Ridge complex is a 200–400 km wide arcuate system of bathymetric highs with up to 2,000 m of relief, which extends across Amerasia Basin from north of the Canadian margin to the Siberian Shelf (Figure 1). The exact mechanism and timing for their development are unclear, though most models have tied the ridges to the High Arctic Large Igneous Province (HALIP) thought by some to have originated from a plume (e.g., Døssing et al., 2013; Lawver et al., 2002). The Alpha-Mendeleev Ridge system has been interpreted as a time-transgressive hotspot track, possibly built on oceanic crust formed previously by seafloor spreading (Forsyth et al., 1986; Grantz et al., 1998, 2011; Lawver et al., 2002). However, it has also been interpreted as an intraplate oceanic volcanic edifice like the Ontong Java or Kerguelen plateaus (Asudeh et al., 1988; Forsyth et al., 1986; Jackson et al., 1986). Still other studies have argued that the Alpha and Mendeleev ridge system may have continental crust at its core even if now blanketed by submarine lavas and possibly underplated by basaltic magmas (e.g., Døssing et al., 2013; Lebedeva-Ivanova et al., 2006; Miller et al., 2006; Oakey & Saltus, 2016; Petrov et al., 2016).

Links between large igneous provinces (LIPs) and continental breakup have been suggested in several other settings (e.g., Buiter & Torsvik, 2014; Campbell & Griffiths, 1990; Coffin & Eldholm, 1994; Fromm et al., 2015; Hill, 1991; Sheth, 1999; Storey, 1995). The HALIP, invoked for the continental breakup that opened the Arctic Ocean, is an extensive magmatic province emplaced in the Early Cretaceous over landmasses now widely separated in the circum-Arctic Ocean region, including Arctic Canada, Greenland, Svalbard, Franz Josef Land, and the DeLong Islands (Figure 1). Subaerial occurrences of HALIP volcanism are in the form of dike swarms, sills, and multiple layers of flood basalts (Døssing et al., 2017; Evenchick et al., 2015; Golonka & Bocharova, 2000; Lawver et al., 2002; Nejbort et al., 2011). Despite the impressive areal extent and voluminous stacks of lava, the HALIP is one of the least studied LIPs in the world—its remoteness and inaccessibility certainly contributing to that fact. The isotopic ages published so far, mainly on materials from circum-Arctic landmasses, suggest that three large magmatic events formed the HALIP between circa 133–128, 128–112, and circa 106–80 Ma. (Buchan & Ernst, 2006; Corfu et al., 2013; Drachev & Saunders, 2006; Jokat et al., 2013; Maher, 2001; Polteau et al., 2016; Villeneuve & Williamson, 2006). This is consistent with magnetic anomalies (Vogt et al., 1979) suggesting Cretaceous generation of the Alpha and Mendeleev Ridges during an interval of sustained positive polarity between circa 120 and 80 Ma. However, this wide range in ages is atypical of other LIPs such as Deccan in India and Ferrar in Antarctica, which were formed in a narrow time interval of just  $\sim 1 \times 10^6$  years (Burgess et al., 2015; Encarnación et al., 1996; Minor & Mukasa, 1997; Schoene et al., 2015, 2019; Sprain et al., 2019).

Another prominent feature of Amerasia Basin—the Chukchi Borderland (Figures 1 and 2)—is a continental fragment composed of gently rounded plateau and a series of parallel linear basins bounded on one side by the Northwind Escarpment, which has very steep slopes and almost 3,000 m of relief. Lawver et al. (2011) suggested that the Chukchi Borderland was once part of the East Russian Arctic Shelf, while Grantz et al. (1998, 2011) argued for a restored position abutting the Canadian Arctic margin, between the Mackenzie Delta and Prince Patrick Island. Basement rocks dredged from fault scarps in the interior of the Chukchi Borderland indicate that it was once part of a Paleozoic arc terrane that may be related to the Pearya terrane of northern Ellesmere Island (Brumley, 2014; Brumley et al., 2015).

Until now, the only solid basaltic rock fragments from the Amerasia Basin sea floor were recovered during the 1998 cruise of the Russian ice breaker “Arktika” and German research vessel “Polarstern” when only

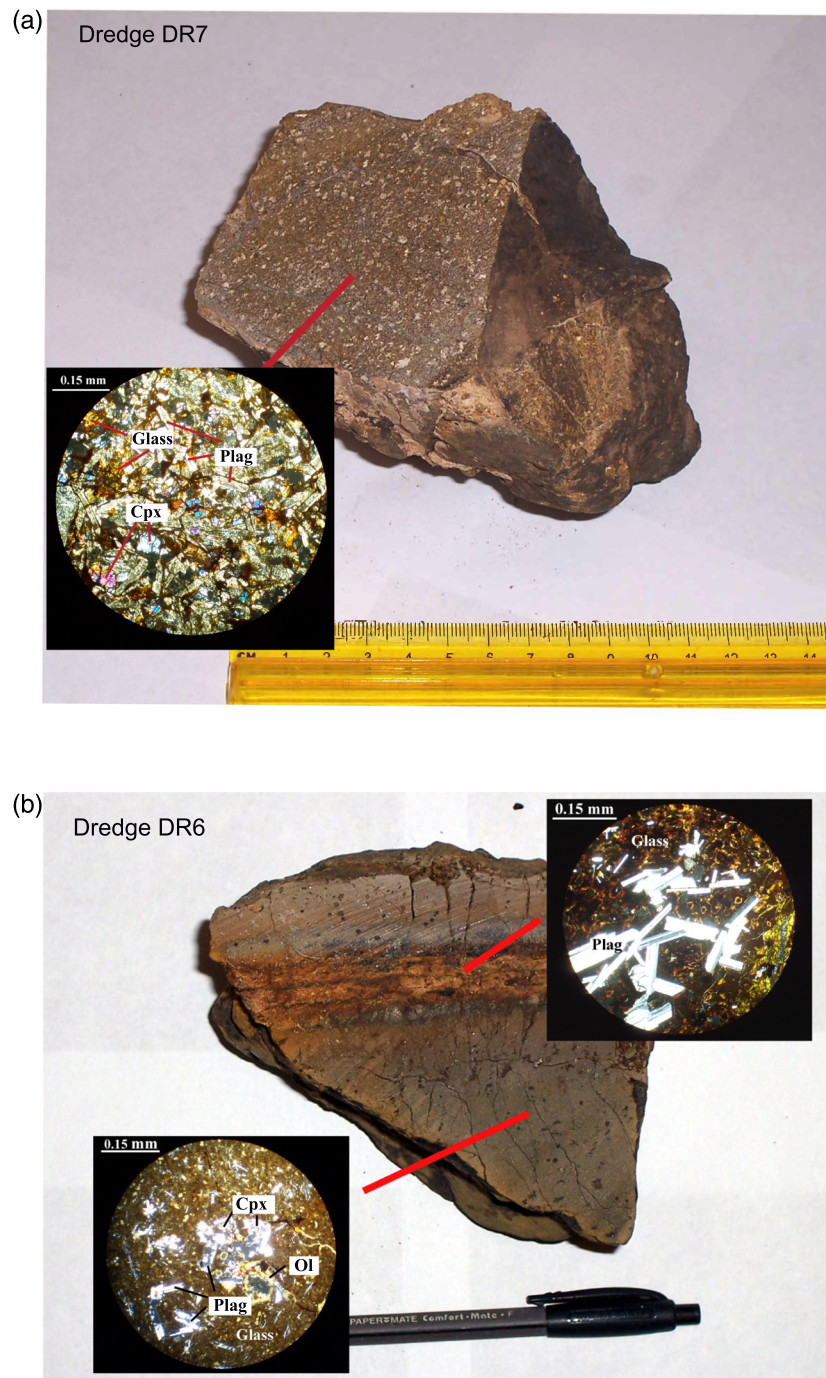


**Figure 3.** Hand-sample and polished thin-section images for submarine volcanic rocks from Amerasia Basin. Panel (a) shows a representative basaltic lava flow from Northwind Ridge (Dredge DR7), and panel (b) shows a typical pillow basalt structure from Healy Spur with phenocrysts of plagioclase, clinopyroxene, and olivine in a glassy matrix (Dredge DR6). In spite of the evident hydrothermal alteration, some plagioclase and portions of the matrix are reasonably well preserved.

about 1 kg of material was collected using a gravity coring technique (Jokat et al., 1999; Jokat et al., 2013; Mühe & Jokat, 1999). Jokat (2003) reported a  $^{40}\text{Ar}/^{39}\text{Ar}$  whole-rock age of  $82 \pm 1$  Ma for a sample of highly altered groundmass from the western sector of Alpha Ridge, initially assumed to be alkali basalt in composition. This was later refined to  $89 \pm 1$  Ma when the dating was repeated on acid-leached plagioclase groundmass laths (Jokat et al., 2013), and more robust major and trace element measurements showed that the sample is actually tholeiitic basalt (Figure 3).

### 3. Analytical Techniques

Our  $^{40}\text{Ar}/^{39}\text{Ar}$  age determinations were carried out on rock pieces with the least amount of alteration following painstaking sample preparation. We gently crushed the lavas in a titanium mortar and pestle and, using a binocular microscope, handpicked the freshest pieces from the 0.8–1.0 mm sieve fraction. These were then washed in superdeionized water and leached in a weak mixture of HCl-HNO<sub>3</sub> for a few hours, in order to get rid of any secondary alteration products. Sample chips (approximately 10 mg) were packaged in duplicate for each sample in pure Al foil, and then the foil packets were placed in evacuated quartz tubes and irradiated in Location 5C of the McMaster University Nuclear Reactor for a duration of 15 hr at a power level of 3 MW. Samples and standards were analyzed using a VH1200S mass spectrometer that is equipped with a Bauer-Signer source, operated at 150  $\mu\text{A}$  total emission current. The mass spectrometer is equipped with a Faraday detector and a Daly detector operated in analog mode with a gain of approximately  $10^4$ . All samples were analyzed with the Daly detector. Mass discrimination (source + detector) was monitored daily with  $\sim 4 \times 10^{-9}$  ccSTP of atmospheric Ar. Typically, the measured atmospheric  $^{40}\text{Ar}/^{36}\text{Ar}$  ratio has been about 290 for the past several years. All measured isotope measurements were corrected for a standard  $^{40}\text{Ar}/^{36}\text{Ar}$  value of 295.5. Isotope measurements were fitted to a signal decay plus memory effect function and extrapolated back to inlet time. Error estimates for each isotope were based upon the fit of individual measurements to the signal decay function, and these five isotope error estimates were propagated through all isotope ratios,  $J$  value calculations (i.e., accounting for neutron flux variation), and age estimates. Isotope concentration values for  $^{37}\text{Ar}$  and  $^{39}\text{Ar}$  were corrected for decay since the samples were irradiated. Corrections were made for interference reactions from Ca and K and for the buildup of  $^{36}\text{Ar}$  from the decay of  $^{36}\text{Cl}$ .

Within the irradiation packages, samples were interspersed with standards packets and  $J$  was calculated for samples by interpolating a fitted cosine function for  $J$  as a function of vertical position within the can.  $J$  value error estimates include the uncertainties in the isotope measurements for the standards plus any scatter of measured  $J$  about the fitted interpolating function. However, they do not include uncertainty in the assumed K-Ar age nor the decay constant uncertainties.  $J$  values were measured using the standard mineral Fish Canyon Tuff biotite (Split 3) and the age used for this standard was calibrated earlier using the MMhb-1 hornblende standard. The error-weighted mean of five analyses at an age of 520.4 Ma for MMhb-1 was  $27.99 \pm 0.04$  Ma ( $2\sigma$ ) for the Fish Canyon Tuff biotite. This value is in very good agreement with the age of 28.294 Ma for a Fish Canyon Tuff sanidine (Renne et al., 2010). Following irradiation, the whole-rock chips were placed in 2 mm diameter wells of a copper disk and step heated at increasing levels of laser power. Details about the  $^{40}\text{Ar}/^{39}\text{Ar}$  analytical procedures followed are given in Rooney et al. (2013).

Major oxide concentrations in the rocks were determined by XRF spectrometry on fused glass disks of samples mixed with lithium tetraborate flux at Michigan State University. Trace element concentrations were determined on the same fused glass disks using an Inductively Coupled Plasma-Mass Spectrometer (ICP-MS) with a hexapole collision cell (Micromass Platform ICP-MS) coupled with a UV laser ablation system Cetac LSX200+, also at Michigan State University. Details of the analytical techniques and procedures are given in Hannah et al. (2002). A few of the samples were analyzed in the Geoanalytical Laboratory of Washington State University using XRF spectrometry for major oxides and an HP-4500 Quadrupole ICP-MS for trace elements, both following methods outlined in Knaak et al. (1994) and Johnson et al. (1999).

Isotopic ratios for Sr, Nd, and Pb were determined on 100 mg rock powders dissolved in HF/HNO<sub>3</sub> acid solutions and processed through elemental separations by column chromatographic methods described in Mukasa et al. (1991). Each sample was loaded on an appropriate filament and then was run on a multicollector TIMS VG Sector at the University of Michigan. Lead ratios have been corrected for mass fractionation by 0.1% per a.m.u. based on replicate analyses of the NIST standard NBS-981. During the analytical work, the average value for the LaJolla Nd isotope standard was  $^{143}\text{Nd}/^{144}\text{Nd} = 0.511852 \pm 11$  ( $n = 5$ ) using  $^{144}\text{Nd}/^{146}\text{Nd} = 0.7219$  for normalization. The Sr isotopic ratios were corrected for mass fractionation using  $^{86}\text{Sr}/^{88}\text{Sr} = 0.1194$  and average  $^{87}\text{Sr}/^{86}\text{Sr}$  ratio for the NBS-987 standard of  $0.710252 \pm 10$  ( $n = 5$ ). Total blanks averaged 0.33 ng for Sr, 0.21 ng for Nd, and 0.06 ng for Pb, all of which are negligible. The procedure for determining the Hf isotopic compositions involved dissolution of 120 mg of pulverized sample in HF/HNO<sub>3</sub> acid solutions, followed by Hf separation from the sample matrix using the Ln resin procedure by Munker et al. (2001) before analysis on a Nu-Plasma High Resolution Multi Collector (HR MC)-ICP-MS at the University of Michigan. The JMC-475 standard yielded a mean  $^{176}\text{Hf}/^{178}\text{Hf}$  value of  $0.282142 \pm 6$  ( $n = 3$ ).

The values we report here for the unknown samples were normalized to the JMC-475 accepted  $^{176}\text{Hf}/^{178}\text{Hf}$  value of 0.282160. The total procedural blank level was less than 0.15 ng for Hf, which is also negligible.

## 4. Results

### 4.1. Eruption Ages Determined by the $^{40}\text{Ar}/^{39}\text{Ar}$ Method

Our  $^{40}\text{Ar}/^{39}\text{Ar}$  data for six bulk-rock samples from Healy Spur (site DR6) and one bulk-rock sample and one plagioclase mineral separate from Northwind Ridge (site DR7) provide new information about the eruption history of volcanism in Amerasia Basin. These being hydrothermal altered samples, careful handpicking of the cleanest rock chips with the aid of a binocular microscope was essential. It was not possible to demonstrate optically the complete elimination of alteration effects. However, we have assumed that hydrothermal alteration closely followed eruption and was short lived (i.e., rocks cooled off quickly in water environment and ceased to be readily reactive), implying that the ages reported here—though minimums—are not much younger than the eruption ages (e.g., Luttinen et al., 2015; Merle et al., 2018; Olierook et al., 2017). Extent of the hydrothermal alteration is discussed in another section below. Statistically determined plateau ages (i.e., fractions passing the chi-square null hypothesis test) were possible for a plagioclase sample and only two of the six whole-rock samples (ran in duplicates to assess reproducibility), but overall, there is good agreement with the ages of terrestrial volcanism in the Arctic region as described below.

Samples with disturbed Ar spectra exhibit profiles indicative of  $^{39}\text{Ar}$  recoil (i.e., the highest temperature fractions yield younger ages than the lower temperature fractions due to  $^{39}\text{Ar}$  migration induced by neutron bombardment during sample irradiation). We therefore adopted the reduced integrated age (RIA) concept described by Turner et al. (1978), Hall et al. (2004), and Rooney et al. (2013) in our calculations. The approach excludes the low-temperature fractions—which because of elevated Cl/K ratios are thought to be from fluid inclusions—and instead computes a  $^{40}\text{Ar}/^{39}\text{Ar}$  weighted mean age based on the remaining fractions in the spectrum. This is effectively a total gas age minus the low-temperature fractions originating from fluid inclusions. Moreover, though not reproduced here, we plotted inverse isochrons which show that initial  $^{40}\text{Ar}/^{36}\text{Ar}$  ratios are close to the atmospheric value of 295.5 and also that most of the Ar analyzed is radiogenic. This means that the samples have no excess Ar, possibly because of a high eruption temperature and magma fluidity, both facilitating degassing of any magmatic Ar.

The Ar data are illustrated on the diagrams in Figure 4 and summarized in Table 1. Detailed information about the Ar analytical data is provided in supporting information Table S1. A plagioclase separate from sample HLY0805 DR7-3 (Northwind Ridge; Figure 2) gives a  $^{40}\text{Ar}/^{39}\text{Ar}$  age of  $111.9 \pm 0.7$  Ma (plateau age; MSWD = 0.82), (Figure 4a). A basaltic whole-rock sample (HLY0805 DR7-4) from the same area of Northwind Ridge gives a  $^{40}\text{Ar}/^{39}\text{Ar}$  RIA of  $118.17 \pm 0.92$  Ma. Volcanic rocks of similar age are known in the circum-Arctic region, including 119–112 Ma lavas on the DeLong Islands in the Russian Arctic (Drachev & Saunders, 2006) and  $113 \pm 6$  Ma lavas on Axel Heiberg Island in the Canadian Arctic Archipelago (Muecke et al., 1990) (Figure 1).

Two aliquots of aphanitic basalt sample HLY0805 DR6-10/1 (Figures 4c and 4d) have yielded plateau ages of  $102.89 \pm 1.32$  Ma (MSWD = 0.59) and  $103.75 \pm 1.42$  Ma (MSWD = 1.73). Duplicates of the petrographically similar basaltic sample HLY0805 DR6-14 have yielded plateau ages of  $105.13 \pm 3.04$  Ma (MSWD = 1.11) and  $101.24 \pm 3.25$  Ma (MSWD = 1.13). Similar isotopic ages (103–92 Ma) are known for dikes from the Erlandsen Land of Northern Greenland (Lyberis & Manby, 2001) and also for basalts from Axel Heiberg and Ellesemere Islands of the Canadian Arctic Archipelago (97.2–92.3 Ma; Villeneuve & Williamson, 2006) (Figure 1).

Healy Spur lavas from site DR6 (Figure 2), characterized by a porphyritic texture and a thin glassy crust, have been the most challenging to date. In spite of aggressive leaching for these samples, it appears that we have not been able to eliminate all secondary alteration effects. As none of these four samples yielded plateaus, we report their RIAs and also observe that the duplicates ran for two of the four samples are not reproducible. Sample HLY0805 DR6-2—an aphanitic pillow basalt—has yielded  $^{40}\text{Ar}/^{39}\text{Ar}$  RIAs of  $79.10 \pm 0.71$  and  $88.98 \pm 1.37$  Ma (Figures 4g and 4h). A similar distribution of  $^{40}\text{Ar}/^{39}\text{Ar}$  RIAs is noted for duplicates of sample HLY0805 DR6-4, which are  $71.84 \pm 0.59$  and  $90.27 \pm 1.15$  Ma (Figures 4i and 4j). Samples HLY0805 DR6-3/5 and HLY0805 DR6-7/1, not analyzed in duplicates, have yielded  $^{40}\text{Ar}/^{39}\text{Ar}$  RIAs of  $81.10 \pm 0.85$  and  $82.30 \pm 1.00$  Ma (Figures 4k and 4l). Precision for these ages is poorest for



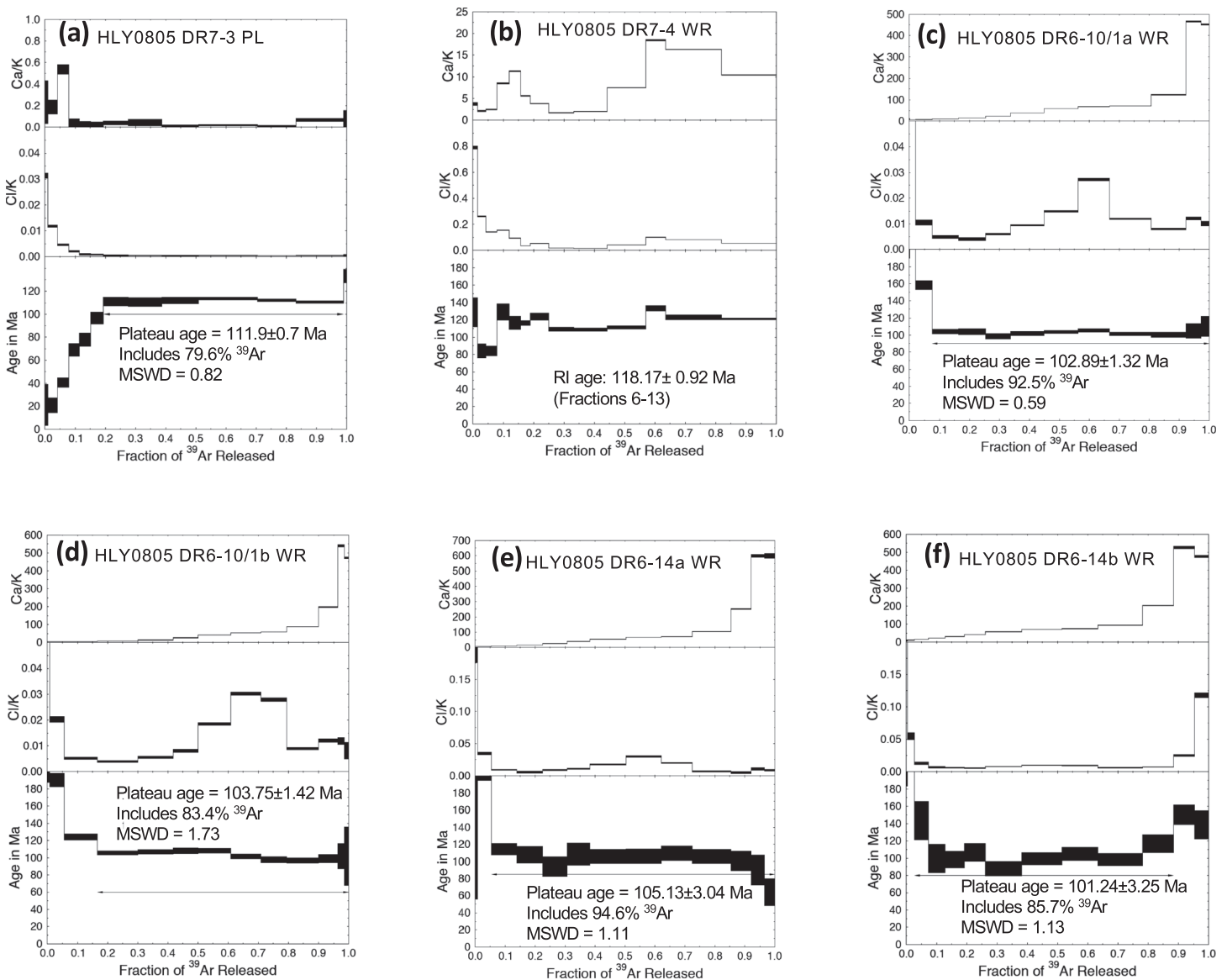


**Figure 4.** (a–f) Diagrams illustrating the step-heating spectra and Cl/K and Ca/K values for six whole-rock basaltic samples from Healy Spur (Dredge Site DR6) and one whole-rock basaltic sample and one plagioclase separate from Northwind Ridge of the Chukchi Borderland (Dredge Site DR7). Note that gas fractions from some of the samples meet the requirements for defining a plateau (i.e., fractions passing the chi-square null hypothesis test). Ages for spectra not meeting the plateau criteria are based on calculations of weighted means for all gas fractions, excluding those with high Cl/K, which are inferred to be from fluid inclusions. These are referred to as reduced integrated ages (RIAs), after Rooney et al. (2013), and justified by evidence of  $^{39}\text{Ar}$  recoil, such as low ages at the highest-temperature gas fractions.

samples with significant amounts of atmospheric Ar, underscoring the impact of seafloor alteration. These ages are therefore also minimum values for the time of eruption.

It is of interest to note that in spite of the hydrothermal alteration challenges in these four Healy Spur lavas, their calculated  $^{40}\text{Ar}/^{39}\text{Ar}$  RIAs broadly overlap with ages for basalts in the now widely separated areas of Northern Greenland (86–82 Ma; Estrada & Henjes-Kunst, 2004), Axel Heiberg Island of the Canada Arctic Archipelago (83.8–80.7 Ma; Villeneuve & Williamson, 2006), and the western sector of Alpha Ridge ( $89 \pm 1$  Ma; Jokát et al., 2013) (Figure 1). In summary, plateau ages have been produced for one plagioclase separate and two whole-rock samples (each with reproducible duplicates); all other samples were heavily impacted by hydrothermal alteration, and as such provide only minimum ages for eruption of these submarine lavas. In as much as hydrothermal alteration is closely tied in time to rocks that are still hot and highly

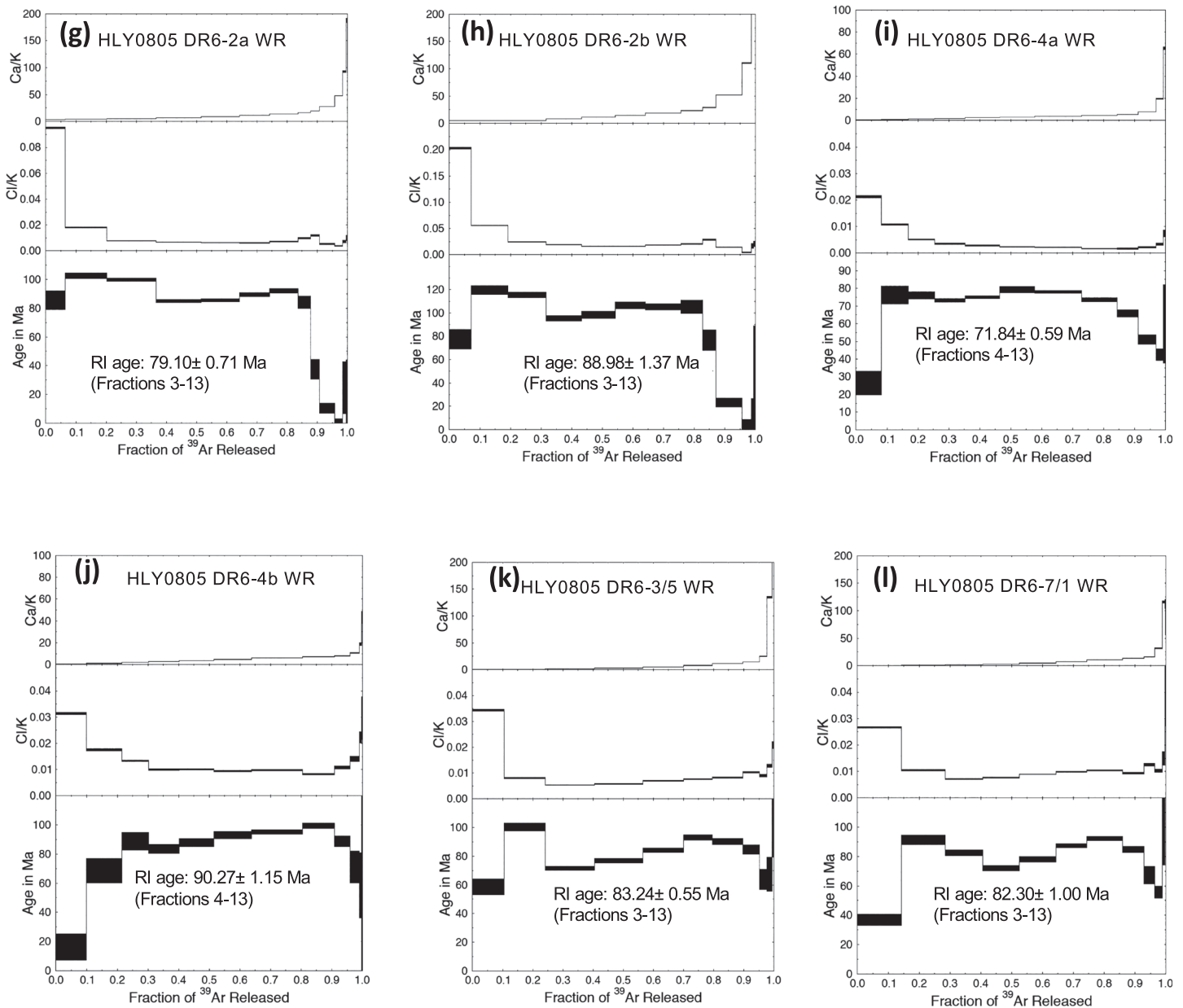


Figure 4. (continued)

reactive, we infer that Amerasia Basin experienced at least three episodes of volcanic activity during the Cretaceous falling at circa 118–112, circa 105–100, and circa 90–70 Ma.

#### 4.2. Major Oxide and Trace Element Compositions

While our lava samples from Amerasia Basin display somewhat elevated losses on ignition or LOI, mostly in the range of 3–6% (Table 2), this is much lower than the 23% reported by Van Wagoner et al. (1986) for acoustic basement rocks recovered from Alpha Ridge during the 1983 CESAR Expedition. A few samples have LOI of <1% suggesting only minor low-temperature seawater-rock interaction. Additionally, neither  $\text{Na}_2\text{O}$  nor  $\text{K}_2\text{O}$  correlates with oxides or elements that they normally correlate with in fresh samples (e.g.,  $\text{P}_2\text{O}_5$ ,  $\text{TiO}_2$ , and Nb). On the other hand,  $\text{TiO}_2$  and  $\text{P}_2\text{O}_5$  are well correlated with trace elements such as most REE, Zr, and Hf, indicating that these elements were immobile during the post eruption secondary processes. Therefore, because of the alteration-compromised alkali concentrations, we have classified the lavas using the diagram by Winchester and Floyd (1977), which is based on the immobile element ratios  $\text{Zr}/\text{TiO}_2$  versus  $\text{Nb}/\text{Y}$  (Figure 5). All analyzed samples fall in the field for subalkaline basalt and can be divided in

**Table 1**  
 $^{40}\text{Ar}/^{39}\text{Ar}$  Ages ( $\pm 1\sigma$ ) for Amerasia Basin Volcanic Rocks

Sample	Location	Rock or mineral	Plateau age (Ma)	Plateau MSWD	Plateau % $^{39}\text{Ar}$	Isochron age (Ma)	MSWD	$(^{40}\text{Ar}/^{36}\text{Ar})_i$	Points fitted
HLY0805 DR7-3	Northwind Ridge	Basalt (Plagioclase)	111.9 $\pm$ 0.7	0.82	80	112.0 $\pm$ 1.1	1.02	295.3 $\pm$ 1.7	7–12
HLY0805 DR6-10/1a	Healy Spur	Basalt (bulk rock)	102.89 $\pm$ 1.32	0.59	93	102.6 $\pm$ 1.7	2.68	351.5 $\pm$ 9.4	3–13
HLY0805 DR6-10/1b	Healy Spur	Basalt (bulk rock)	103.75 $\pm$ 1.42	1.73	83	104.8 $\pm$ 12.7	4.44	349.1 $\pm$ 12.7	4–13
HLY0805 DR6-14a	Healy Spur	Basalt (bulk rock)	105.13 $\pm$ .3.04	1.11	95	105.9 $\pm$ 5.2	2.66	325.5 $\pm$ 9.5	3–12
HLY0805 DR6-14b	Healy Spur	Basalt (bulk rock)	101.24 $\pm$ 3.25	1.13	86	105.1 $\pm$ 10.7	2.89	316.3 $\pm$ 10.7	4–11
Sample	Location	Rock	RI age (Ma)	RIA MSWD	RIA % $^{39}\text{Ar}$	Isochron age (Ma)	MSWD	$(^{40}\text{Ar}/^{36}\text{Ar})_i$	Points fitted
HLY0805 DR7-4	Northwind Ridge	Basalt (bulk rock)	118.17 $\pm$ 0.92	—	80	111.3 $\pm$ 4.6	11.12	312.2 $\pm$ 11.5	6–13
HLY0805 DR6-2a	Healy Spur	Basalt (bulk rock)	79.10 $\pm$ 0.71	—	78	102.9 $\pm$ 5.4	25.6	296.3 $\pm$ 10.4	3–13
HLY0805 DR6-2b	Healy Spur	Basalt (bulk rock)	88.98 $\pm$ 1.37	—	78	103.5 $\pm$ 5.8	24.1	297.8 $\pm$ 11.8	3–13
HLY0805 DR6-4a	Healy Spur	Basalt (bulk rock)	71.84 $\pm$ 0.59	—	75	76.0 $\pm$ 2.8	17.6	294.1 $\pm$ 10.2	4–13
HLY0805 DR6-4b	Healy Spur	Basalt (bulk rock)	90.27 $\pm$ 1.15	—	70	89.1 $\pm$ 2.8	20.8	282.0 $\pm$ 14.8	4–13
HLY0805 DR6-3/5	Healy Spur	Basalt (bulk rock)	83.24 $\pm$ 0.55	—	75	82.2 $\pm$ 3.3	21.6	294.0 $\pm$ 12.3	3–13
HLY0805 DR6-7/1	Healy Spur	Basalt (bulk rock)	82.30 $\pm$ 1.00	—	70	82.3 $\pm$ 2.6	7.8	299.6 $\pm$ 7.3	3–13

*Note.* Plateaus are defined using the method of Rooney et al. (2013) three or more contiguous gas fractions representing  $\geq 50\%$  of the  $^{39}\text{Ar}$  released that would pass the null hypothesis on a chi-square test using  $1\sigma$  uncertainties. That is, the fractions are not distinguishable in terms of age. Gas fractions included in the plateau age calculations are shown on the diagrams in Figures 4a, 4c, 4d, 4e, and 4f. The plateau ages are error-weighted means with scatter included in the error estimate. For samples not meeting the plateau criteria, we adopted the reduced integrated age (RIA) concept described in Rooney et al. (2013). All age estimates include uncertainties in neutron flux variation ( $J$ ). The MSWD measures the quality of the line fit, and an MSWD of 1.0 correlates with a line perfectly defined by the data.

three populations: low-Ti tholeiite I (118–112 Ma), low-Ti tholeiite II (105–100 Ma), and high-Ti tholeiite (90–70 Ma). It is important to note that the relative differences between the three sample populations to emerge using immobile-element data are related to age and locality. Furthermore, compositional differences between the three sample groups identified in Figure 5 are also observed on other trace element diagrams and on some isotope covariation diagrams. Lead isotopes are an exception in this regard.

#### 4.3. Low-Ti Tholeiites I

Three analyzed samples from the Northwind Ridge (minimum eruption ages of ca. 118–112 Ma) have elevated  $\text{SiO}_2$  (45.7–47.3 wt%),  $\text{Al}_2\text{O}_3$  (15.0–16.2 wt%), and total alkalis (4.7–5.1 wt%) with sodium slightly over potassium ( $\text{Na}_2\text{O} = 2.75\text{--}4.30$  wt%,  $\text{K}_2\text{O} = 0.84\text{--}1.99$  wt %) and moderate  $\text{MgO}$  (6.84–7.28 wt%),  $\text{Fe}_2\text{O}_{3\text{tot}}$  (12.3–13.3 wt%),  $\text{TiO}_2$  (1.21–1.36 wt%), and  $\text{P}_2\text{O}_5$  (0.23–0.28 wt%) concentrations. The LOI values range from 3.9 to 4.6 wt % suggesting moderate to high degrees of alteration. In addition, these rocks have  $\text{Mg\#}$  ( $\text{Mg\#}$  values of 47.9–53.8 and concentrations for Cr in the range of 122–178 ppm and for Ni of 133–279 ppm, all suggesting some fractionation of the original primary basaltic magmas. For comparison, primitive mantle melts have Cr concentrations  $>1,000$  ppm and Ni concentrations  $>300$  ppm (e.g., Hart & Davis, 1978; Norman & Garcia, 1999; Sato, 1977; Sobolev et al., 2005).

#### 4.4. Low-Ti Tholeiites II

The lava samples dredged from Healy Spur not only fall into two different eruption age groups but also have two distinct compositions (Table 2 and Figure 5). One group represented by samples with pillow structures and  $^{40}\text{Ar}/^{39}\text{Ar}$  minimum eruption ages of circa 105–100 Ma is composed of low  $\text{TiO}_2$ , high- $\text{Fe}_2\text{O}_{3\text{tot}}$ , high- $\text{MgO}$ , and low-alkaline lavas, ( $\text{TiO}_2 = 2.01\text{--}2.67$  wt%;  $\text{Fe}_2\text{O}_{3\text{tot}} = 10.9\text{--}16.6$  wt%;  $\text{MgO} = 7.0\text{--}8.7$  wt% and  $\text{Mg\#} = 51.0\text{--}53.7$ ;  $\text{Na}_2\text{O} + \text{K}_2\text{O} = 2.6\text{--}3.2$  wt%) with sodium significantly more abundant than potassium, all characteristic of low-Ti tholeiitic basalts. Loss on ignition values for these lavas has a range of 0.98–2.32 wt% for the mildly altered samples and 4.27–6.13 wt% for the more strongly altered ones. The lavas' major oxide composition along with concentrations of Cr (140–253 ppm) and Ni (128–306 ppm) suggests only moderate differentiation of the magmas from the original primary composition.



**Table 2**  
(Continued)

Location sample	Northwind ridge										Healy								Spur															
	DR7-3		DR7-4		DR7-5		DR6-6		DR6-10/1		DR6-14		DR6-1		DR6-2		DR6-2/1		DR6-3/1		DR6-3/3		DR6-3/4		DR6-3/5		DR6-4		DR6-7/1		DR6-11/2			
	Low-Ti tholeiite I	Low-Ti tholeiite I	Low-Ti tholeiite I	Low-Ti tholeiite I	Low-Ti tholeiite I	Low-Ti tholeiite I	Low-Ti tholeiite I	Low-Ti tholeiite I	Low-Ti tholeiite II	Low-Ti tholeiite II	Low-Ti tholeiite II	Low-Ti tholeiite II	Low-Ti tholeiite II	Low-Ti tholeiite II	Low-Ti tholeiite II	Low-Ti tholeiite II	Low-Ti tholeiite II	High-Ti tholeiite	High-Ti tholeiite	High-Ti tholeiite	High-Ti tholeiite	High-Ti tholeiite	High-Ti tholeiite	High-Ti tholeiite	High-Ti tholeiite	High-Ti tholeiite	High-Ti tholeiite	High-Ti tholeiite	High-Ti tholeiite					
Dy	6.23	6.59	6.58	6.58	6.58	6.58	6.58	6.58	6.58	6.58	6.58	6.58	6.58	6.58	6.58	6.58	6.58	6.58	6.58	6.58	6.58	6.58	6.58	6.58	6.58	6.58	6.58	6.58	6.58	6.58	6.58	6.58		
Ho	1.23	1.35	1.34	1.34	1.34	1.34	1.34	1.34	1.34	1.34	1.34	1.34	1.34	1.34	1.34	1.34	1.34	1.34	1.34	1.34	1.34	1.34	1.34	1.34	1.34	1.34	1.34	1.34	1.34	1.34	1.34	1.34		
Er	3.83	3.99	3.60	3.60	3.60	3.60	3.60	3.60	3.60	3.60	3.60	3.60	3.60	3.60	3.60	3.60	3.60	3.60	3.60	3.60	3.60	3.60	3.60	3.60	3.60	3.60	3.60	3.60	3.60	3.60	3.60	3.60		
Yb	3.69	3.88	3.27	3.27	3.27	3.27	3.27	3.27	3.27	3.27	3.27	3.27	3.27	3.27	3.27	3.27	3.27	3.27	3.27	3.27	3.27	3.27	3.27	3.27	3.27	3.27	3.27	3.27	3.27	3.27	3.27	3.27		
Lu	0.59	0.56	0.50	0.50	0.50	0.50	0.50	0.50	0.50	0.50	0.50	0.50	0.50	0.50	0.50	0.50	0.50	0.50	0.50	0.50	0.50	0.50	0.50	0.50	0.50	0.50	0.50	0.50	0.50	0.50	0.50	0.50		
Hf	2.68	2.90	2.32	2.32	2.32	2.32	2.32	2.32	2.32	2.32	2.32	2.32	2.32	2.32	2.32	2.32	2.32	2.32	2.32	2.32	2.32	2.32	2.32	2.32	2.32	2.32	2.32	2.32	2.32	2.32	2.32	2.32	2.32	
Pd	5.53	5.22	12.8	12.8	12.8	12.8	12.8	12.8	12.8	12.8	12.8	12.8	12.8	12.8	12.8	12.8	12.8	12.8	12.8	12.8	12.8	12.8	12.8	12.8	12.8	12.8	12.8	12.8	12.8	12.8	12.8	12.8	12.8	
Th	2.14	1.91	2.71	2.71	2.71	2.71	2.71	2.71	2.71	2.71	2.71	2.71	2.71	2.71	2.71	2.71	2.71	2.71	2.71	2.71	2.71	2.71	2.71	2.71	2.71	2.71	2.71	2.71	2.71	2.71	2.71	2.71	2.71	
U	2.23	1.54	1.76	1.76	1.76	1.76	1.76	1.76	1.76	1.76	1.76	1.76	1.76	1.76	1.76	1.76	1.76	1.76	1.76	1.76	1.76	1.76	1.76	1.76	1.76	1.76	1.76	1.76	1.76	1.76	1.76	1.76	1.76	
Ni	279	133	189	189	189	189	189	189	189	189	189	189	189	189	189	189	189	189	189	189	189	189	189	189	189	189	189	189	189	189	189	189	189	
Cu	296	203	157	157	157	157	157	157	157	157	157	157	157	157	157	157	157	157	157	157	157	157	157	157	157	157	157	157	157	157	157	157	157	
Zn	132	118	123	123	123	123	123	123	123	123	123	123	123	123	123	123	123	123	123	123	123	123	123	123	123	123	123	123	123	123	123	123	123	123
V	338	364	352	352	352	352	352	352	352	352	352	352	352	352	352	352	352	352	352	352	352	352	352	352	352	352	352	352	352	352	352	352	352	352
Cr	178	122	132	132	132	132	132	132	132	132	132	132	132	132	132	132	132	132	132	132	132	132	132	132	132	132	132	132	132	132	132	132	132	132

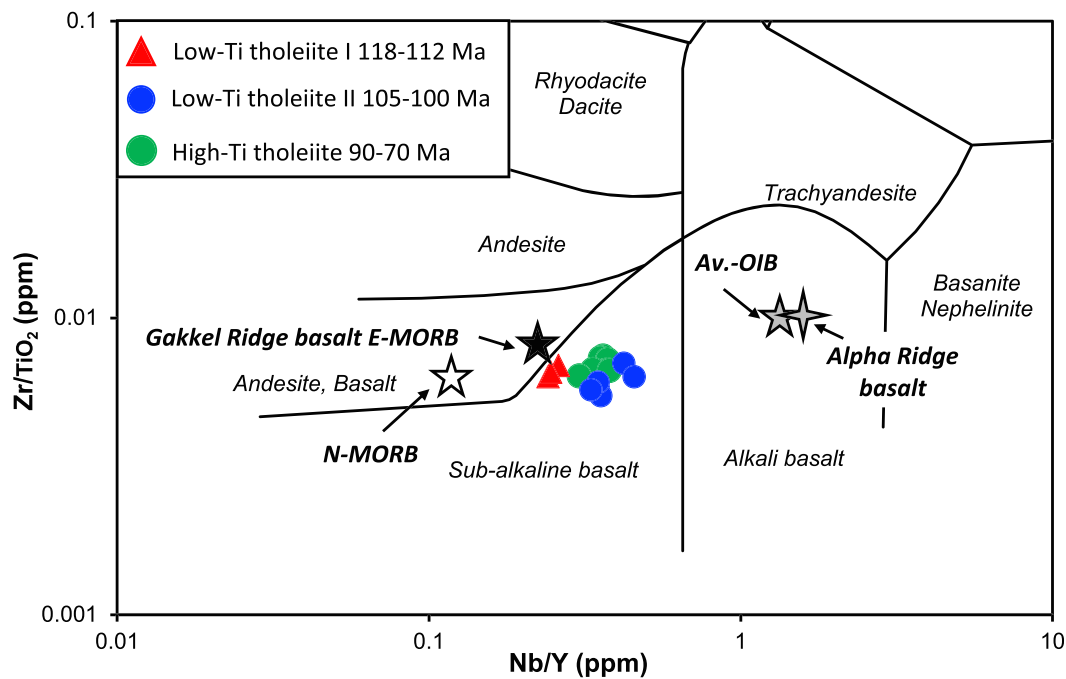


**Figure 5.** Classification diagram  $Zr/TiO_2$  versus  $Nb/Y$  for the volcanic rocks from Amerasia Basin. Thin black lines indicate the nomenclature of Winchester and Floyd (1977). Compositions for average ocean-island basalt (Av. OIB) and normal mid-ocean ridge basalt (N-MORB) are after Reiners (2002) and Gale et al. (2013), Alpha Ridge basalt is after Van Wagoner et al. (1986), and Gakkal ridge MORB is after Mühe et al. (1993; 1997).

#### 4.5. High-Ti Tholeiites

The second rock type dredged from Healy Spur has  $^{40}Ar/^{39}Ar$  minimum eruption ages of circa 90–70 Ma and displays the following chemical compositions:  $SiO_2 = 41.6\text{--}44.4\%$ ;  $TiO_2 = 3.98\text{--}4.32\text{ wt}\%$ ;  $Na_2O + K_2O = 4.3\text{--}4.9\text{ wt}\%$  with sodium over potassium,  $Fe_2O_{3\text{tot}} = 15.8\text{--}18.1\text{ wt}\%$ ;  $MgO = 4.4\text{--}4.8\text{ wt}\%$ , all characteristic of high-Ti tholeiitic basalts (Table 2 and Figure 5). Low concentrations of Ni (109–168 ppm), and especially Cr (40–50 ppm), along with low Mg# (33.8–37.5) indicate that the lavas underwent significant fractional crystallization, although high concentrations of  $Fe_2O_3$  at given MgO are observed in this rock type as well. However, in spite of spatial proximity, the age difference between this high-Ti tholeiite and the two low-Ti tholeiite II samples described above makes it clear that there is no genetic link between these two sets of Healy Spur lavas.

Trace element compositions plotted on the  $Zr/TiO_2$  versus  $Nb/Y$  classification diagram (Figure 5) show that these Amerasia Basin lavas fall in the field for subalkaline rock types, closely resembling Gakkal Ridge enriched mid-ocean ridge basalts (E-MORB) but less so for normal mid-ocean ridge basalts (N-MORB) (Gale et al., 2013; Mühe et al., 1993; 1997) and significantly different compared to Alpha Ridge basaltic lavas (Van Wagoner et al., 1986) and also compared to average OIB (Sun & McDonough, 1989).

Trace element abundance patterns for the studied samples display various degrees of enrichment in most large ion lithophile elements (LILE) relative to primitive mantle (Table 2 and Figure 6a). To avoid clutter on a single diagram, the comparator data from N-MORB, E-MORB, OIB, CFB, and back-arc basin basalts (BABB) are shown on the diagram in Figure 6b. The Northwind Ridge low-Ti tholeiites I identified as circa 118–112 Ma in Figure 6a display a relatively smooth pattern with a slightly negative slope (i.e., normalized LREE (light rare-earth element)/HREE (heavy rare-earth element)  $> 1$ ) but with sharp positive anomalies for K and Pb thought be due to seawater alteration. The normalized HREE abundance patterns for these Northwind Ridge low-Ti tholeiites I fall below 10 times primitive mantle, whereas the strongly incompatible elements can be 30 times more enriched than primitive mantle.

Both high-Ti tholeiite and low-Ti tholeiite II lavas from Healy Spur exhibit convex patterns on the primitive mantle-normalized trace element-distribution diagram—more enriched in every element compared to the circa 118–112 Ma low-Ti tholeiites I—but with notable troughs at Sr and Ba (Figure 6a). It is interesting to note that volcanic samples recovered by Van Wagoner et al. (1986) from the CESAR area of Alpha

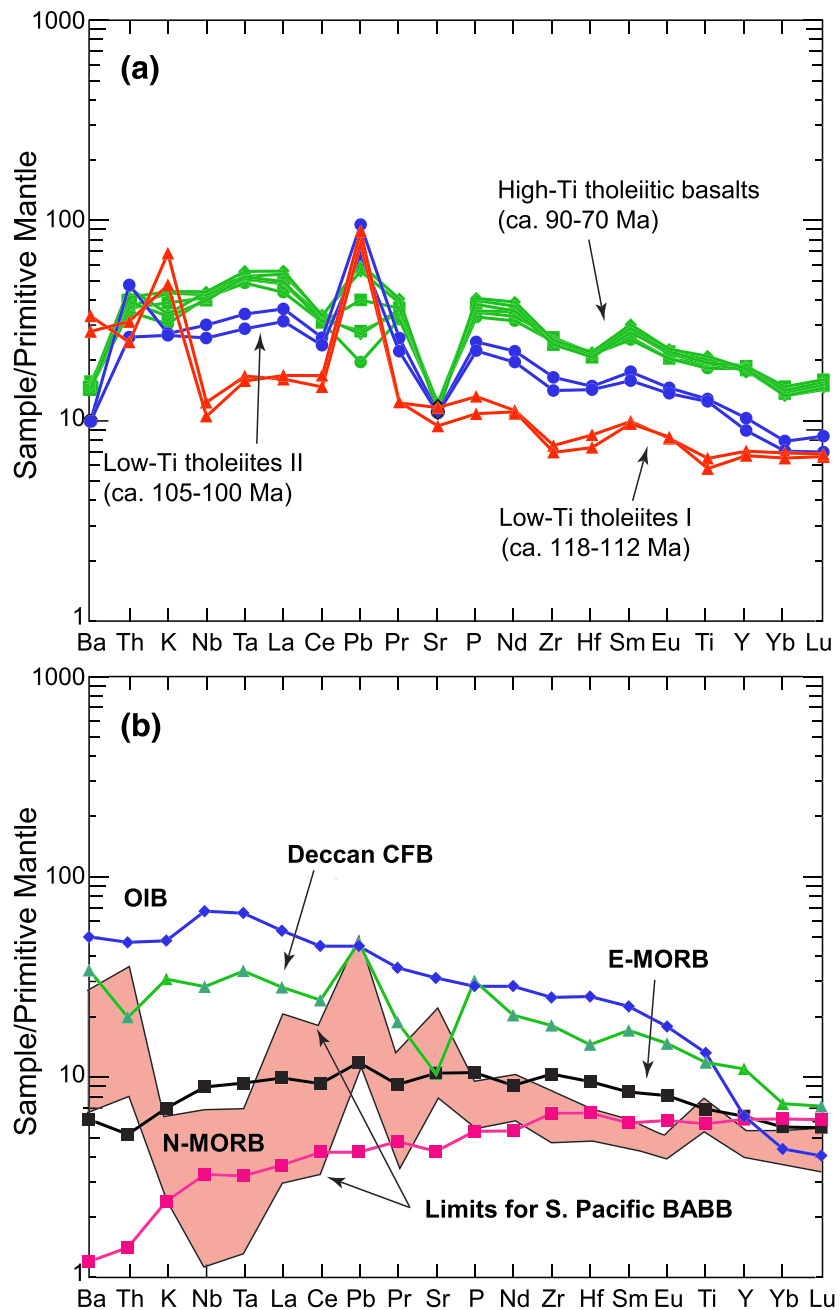


**Figure 6.** Primitive mantle-normalized trace element diagram (normalization values are after McDonough & Sun, 1995) showing a comparison of the dredged Arctic samples (a), with OIB, MORB, E-MORB (Gakkel Ridge), Deccan continental flood basalts (CFB), and S. Pacific back-arc basin basalts or BABB (b). Compositions of OIB and MORB are after Sun and McDonough (1989); enriched mid-ocean ridge basalt (E-MORB) of Gakkel Ridge is after Mühe et al. (1997); Deccan CFB is after Chandrasekharam et al. (1999); S. Pacific (BABB) is after Pearce and Stern (2006). Peaks for Pb on diagram (a) for some of the samples studied are likely due to seafloor alteration (see text for details).

Ridge display similarly low concentrations for Sr and Ba. It is also notable that the circa 105–100 Ma low-Ti tholeiites II display pronounced peaks at Pb, whereas the younger circa 90–70 Ma high-Ti tholeiites show only insignificant Pb peaks or none at all (Figure 6a). As explained below, this is likely the consequence of having suffered different levels of seawater alteration. Abundance patterns for the two groups of Healy Spur samples have no Nb or Ta depletions and have a pronounced trough at Sr ( $Sr_N/Nd_N = 0.28\text{--}0.45$ ), similar to the patterns displayed by CFB elsewhere, particularly by the Deccan Plateau basalts (Figure 6b) in India (e.g., Campbell & Griffiths, 1990; Chandrasekharam et al., 1999; Sheth et al., 2004).

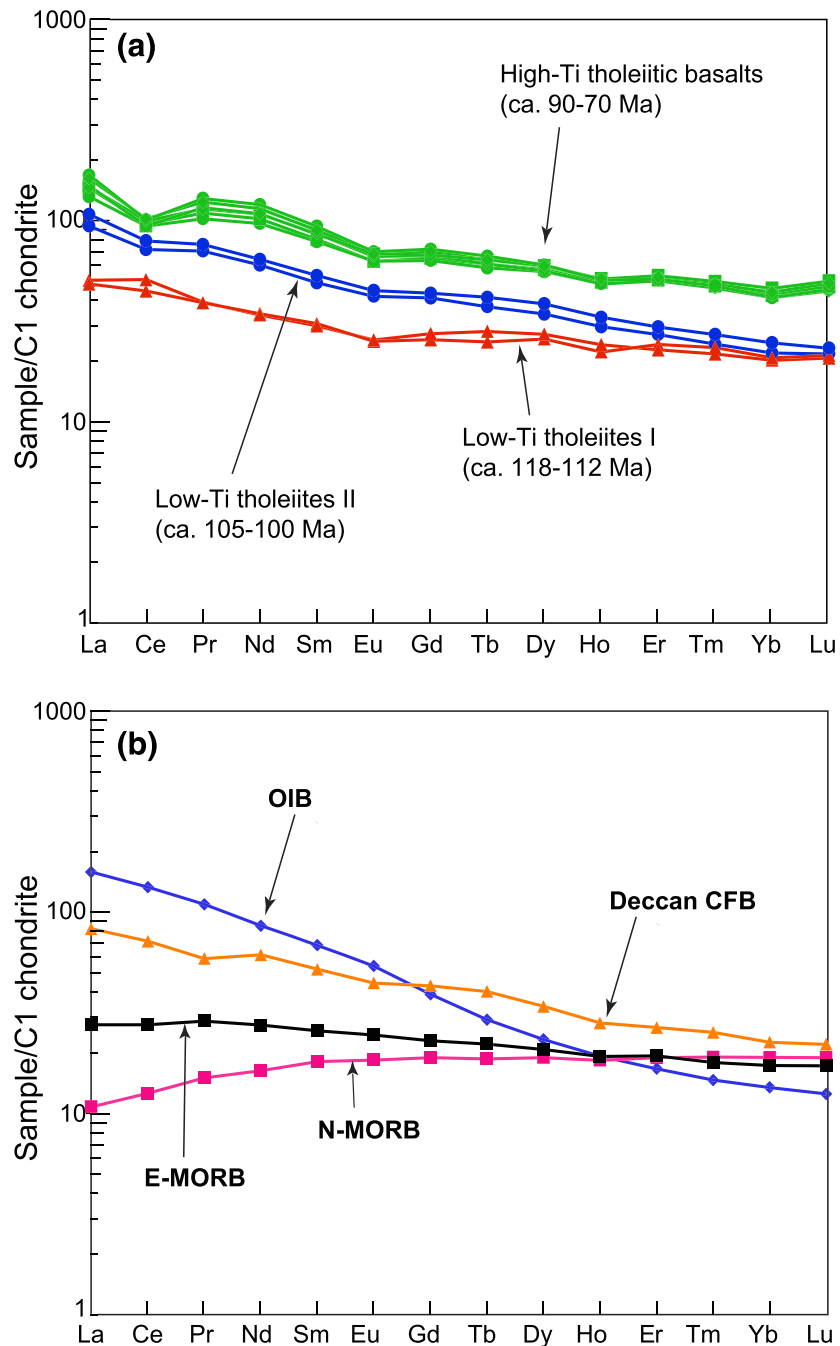


**Figure 7.** CI chondrite-normalized REE diagram (normalization values are after Anders & Grevesse, 1989) showing a comparison of the dredged Arctic samples (a), with OIB, MORB, E-MORB (Gakkel Ridge), and CFB (b). Compositions for OIB and MORB are after Sun and McDonough (1989); E-MORB of Gakkel Ridge is after Mühe et al. (1997); Deccan CFB is after Chandrasekharam et al. (1999).

Chondrite-normalized trace element abundance patterns are illustrated on the diagram in Figure 7a, with comparator data from various tectonic settings shown on the diagram in Figure 7b. The circa 118–112 Ma Northwind Ridge low-Ti tholeiites I define a smooth enrichment pattern from the HREE to the LREE ( $Ce_N/Yb_N = 1.7\text{--}2.5$ ). Similarly, both the circa 105–100 Ma low-Ti tholeiites II and circa 90–70 Ma high-Ti tholeiites from Healy Spur have chondrite-normalized REE patterns not significantly enriched in LREE over HREE ( $Ce_N/Yb_N = 2.0\text{--}3.3$ ). However, Healy Spur basalts have higher overall elemental abundances and more closely resemble the Deccan CFB pattern as shown on the diagrams in Figures 7a and 7b.



**Table 3**  
Isotope Compositions of Dredged Arctic Ocean Basalt Samples

Sample	Dredge region	Rock type	$^{206}\text{Pb}/^{204}\text{Pb}$	$^{207}\text{Pb}/^{204}\text{Pb}$	$^{208}\text{Pb}/^{204}\text{Pb}$	$^{143}\text{Nd}/^{144}\text{Nd}$	$\epsilon_{\text{Nd}(t)}$	$^{87}\text{Sr}/^{86}\text{Sr}$	$\pm 2\sigma$	$^{87}\text{Sr}/^{86}\text{Sr}(t)$	$\pm 2\sigma$	$^{176}\text{Hf}/^{177}\text{Hf}$	$\pm 2\sigma$	$\epsilon_{\text{Hf}(t)}$
DR7-3	Northwind Ridge	Low-Ti Tholeiite I	18.7475	15.5391	38.3123	0.512610 ± 19	0.51	0.709601 ± 12	± 12	0.708733	± 12	0.283224 ± 12	± 12	16.00
DR7-4	Northwind Ridge	Low-Ti Tholeiite I	18.7312	15.5564	38.2809	0.512662 ± 20	1.27	0.709458 ± 19	± 19	0.708424	± 19	0.283128 ± 6	± 6	12.64
DR7-5	Northwind Ridge	Low-Ti Tholeiite I	18.7866	15.5644	38.3505	0.512594 ± 17	0.19	0.709556 ± 12	± 12	0.708855	± 12	0.283163 ± 15	± 15	13.88
DR6-1	Healy Spur	Low-Ti Tholeiite II	18.5852	15.5595	38.3143	0.512877 ± 19	4.93	0.703841 ± 18	± 18	0.703502	± 18	0.283156 ± 12	± 12	13.62
DR6-2	Healy Spur	Low-Ti Tholeiite II	18.9618	15.5805	38.7572	0.512669 ± 18	1.20	0.704764 ± 10	± 10	0.703895	± 10	0.283191 ± 31	± 31	14.88
DR6-2/1	Healy Spur	Low-Ti Tholeiite II	18.7194	15.5463	38.4322	0.512749 ± 16	1.85	0.704629 ± 10	± 10	0.703778	± 10	0.283140 ± 22	± 22	13.06
DR6-3/1	Healy Spur	High-Ti Tholeiite	19.1996	15.5962	38.9509	0.512912 ± 18	5.78	0.704097 ± 9	± 9	0.703744	± 9	0.283128 ± 6	± 6	12.64
DR6-3/3	Healy Spur	High-Ti Tholeiite	19.3679	15.5797	38.9889	0.512919 ± 20	5.93	0.703894 ± 13	± 13	0.703620	± 13	0.283163 ± 15	± 15	13.88
DR6-3/4	Healy Spur	High-Ti Tholeiite	19.2486	15.5793	38.8230	0.512836 ± 20	4.30	0.704036 ± 10	± 10	0.703438	± 10	0.283156 ± 12	± 12	13.62
DR6-3/5	Healy Spur	High-Ti Tholeiite	19.1344	15.5834	38.7662	0.512816 ± 11	3.93	0.704000 ± 10	± 10	0.703679	± 10	0.283139 ± 11	± 11	13.01
DR6-4	Healy Spur	High-Ti Tholeiite	18.8163	15.5606	38.3568	0.512866 ± 19	4.86	0.703980 ± 12	± 12	0.703618	± 12	0.283138 ± 10	± 10	13.00
DR6-7/1	Healy Spur	High-Ti Tholeiite	18.8208	15.5827	38.6283	0.512790 ± 19	3.45	0.704198 ± 13	± 13	0.703237	± 13	0.283138 ± 10	± 10	13.00
DR6-11/2	Healy Spur	High-Ti Tholeiite	18.9149	15.5733	38.4498	0.512855 ± 18	4.63	0.704226 ± 20	± 20	0.703439	± 20	0.283138 ± 10	± 10	13.00
DR6-14	Healy Spur	High-Ti Tholeiite	18.6194	15.5889	38.3809	0.512855 ± 16	4.52	0.703849 ± 15	± 15	0.703726	± 15	0.283138 ± 10	± 10	13.00

#### 4.6. Isotope Compositions

The Pb-Sr-Nd-Hf isotope systematics for volcanic rocks from Amerasia Basin are characterized by significant variability (Table 3). Measured Pb-isotopic ratios (Figure 8) are quite radiogenic and fall mostly along or above the Northern Hemisphere Reference Line (NHRL; Hart, 1984), forming a cluster at the most radiogenic end of the MORB field ( $^{206}\text{Pb}/^{204}\text{Pb} = 18.59\text{--}19.37$ ;  $^{207}\text{Pb}/^{204}\text{Pb} = 15.54\text{--}15.60$ ;  $^{208}\text{Pb}/^{204}\text{Pb} = 38.29\text{--}38.99$ ) and overlapping slightly in  $^{207}\text{Pb}/^{204}\text{Pb}$  versus  $^{206}\text{Pb}/^{204}\text{Pb}$  space (Figure 8a) with values for the Iceland plume (e.g., Shorttle et al., 2013; Thirlwall, 1995) and also potentially trending toward the seawater values of Paul et al. (2015) as we discuss below.

The 118–112 Ma low-Ti tholeiites I from the Northwind Ridge exhibit decay-corrected Nd isotopic compositions close to the chondritic uniform reservoir (CHUR) ( $^{143}\text{Nd}/^{144}\text{Nd} = 0.512594\text{--}0.512610$ ) but have decay-corrected Sr isotopic ratios that are strongly radiogenic and considerably displaced to the right of the mantle array ( $^{87}\text{Sr}/^{86}\text{Sr} = 0.709556\text{--}0.709601$ ). Healy Spur high-Ti tholeiites on the other hand are depleted in terms of both Nd and Sr isotope ratios relative to the bulk silicate Earth (BSE); their measured  $^{143}\text{Nd}/^{144}\text{Nd}$  ratios vary from 0.512669 to 0.512950, and measured  $^{87}\text{Sr}/^{86}\text{Sr}$  ratios fall between 0.703820 and 0.704764, both covering narrow ranges and straddling the mantle array (Figure 9).

None of the samples, however, has the time-integrated record of source depletion exhibited by lavas recovered from the Gakkel Ridge or the Iceland plume by previous studies. Healy Spur low-Ti tholeiites II erupted at circa 105–100 Ma display less radiogenic Nd isotopic compositions ( $^{143}\text{Nd}/^{144}\text{Nd} = 0.512669\text{--}0.512749$ ) and slightly more radiogenic Sr isotope ratios ( $^{87}\text{Sr}/^{86}\text{Sr} = 0.704629\text{--}0.704764$ ) than the younger (circa 90–70 Ma) high-Ti tholeiitic lavas ( $^{143}\text{Nd}/^{144}\text{Nd} = 0.512790\text{--}0.512919$ ;  $^{87}\text{Sr}/^{86}\text{Sr} = 0.703894\text{--}0.704198$ ). It is worth emphasizing that none of the Healy Spur samples display elevated  $^{87}\text{Sr}/^{86}\text{Sr}$  ratios at any given  $^{143}\text{Nd}/^{144}\text{Nd}$  ratios, which implies no or only minimal modification of these ratios with seawater-derived Sr. A subset of the basalt samples studied exhibits small variations in decay-corrected  $^{176}\text{Hf}/^{177}\text{Hf}$  ratios between 0.283128 and 0.283224, corresponding to about 5  $\epsilon$  units. On the  $\epsilon_{\text{Nd}(t)}$  versus  $\epsilon_{\text{Hf}(t)}$  diagram (Figure 10), the data points form an elongated cluster stretching diagonally from the OIB field toward less radiogenic  $\epsilon_{\text{Nd}}$  and more radiogenic  $\epsilon_{\text{Hf}}$ .

## 5. Discussion

### 5.1. Submarine Alteration of Volcanic Rocks From Amerasia Basin

Seawater-rock interaction commonly results in the loss or gain of elements by both mediums depending on several factors, including rock composition and temperature at the exchange interface. Staudigel and Hart (1983) and Sofade (2018) showed that immobile elements, such as Ti or Zr, can be used as reference in calculations of the elemental losses and gains by the two mediums during hydrothermal alteration of submarine lavas. Following the approach of Sofade (2018), we have used Ti as a reference element to calculate two parameters crucial to quantifying the elemental exchange. The passive enrichment factor (PEF) is defined as the ratio ( $\text{Ti}_{\text{altered sample}}/\text{Ti}_{\text{fresh rocks}}$ ) and the gain-to-loss factor (GLF) of a certain element (E) by the ratio ( $E_{\text{altered sample}}/E_{\text{fresh rocks}}/(\text{Ti}_{\text{altered sample}}/\text{Ti}_{\text{fresh rock}})$ ). The lava's elemental loss or gain relative to the Ti concentration is determined by the magnitude of deviation from unity—positively or negatively—as illustrated on the diagrams in Figures 11 and 12. We have based our gain/loss mass balance calculations on the average composition of altered submarine lava samples in each suite, identified on the basis of spatial, temporal, and compositional connections. Low-Ti tholeiite from Franz Josef Land (Levskii

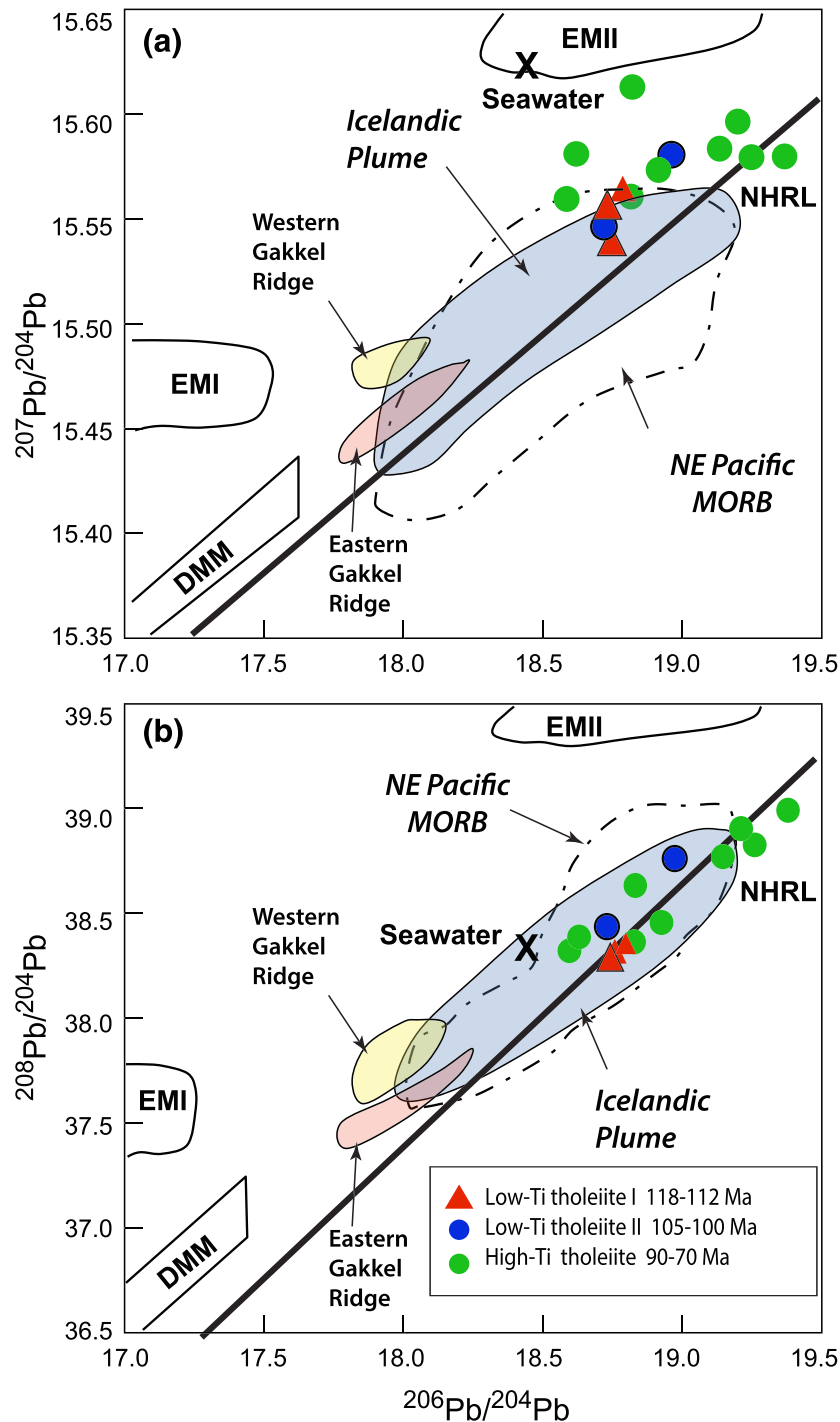


**Figure 8.** The  $^{207}\text{Pb}/^{204}\text{Pb}$  versus  $^{206}\text{Pb}/^{204}\text{Pb}$  (a) and  $^{208}\text{Pb}/^{204}\text{Pb}$  versus  $^{206}\text{Pb}/^{204}\text{Pb}$  (b) diagrams for Amerasia Basin submarine lavas. The Northern Hemisphere Reference Line (NHRL) and mantle components EMI, EMII (enriched mantle Types 1 and 2), and depleted MORB mantle (DMM), shown for comparison, are after Zindler and Hart (1986) and Hart (1988); fields for Gakkel Ridge basalts are after Mühe et al. (1997) and Goldstein et al. (2008); seawater values are from Paul et al. (2015).

et al., 2006; Ntaflou & Richter, 2003)—contemporaneous with other Arctic volcanism, including submarine lavas in Amerasia Basin—was used as an example of fresh rock in mass balance calculations for low-Ti tholeiite I from Northwind Ridge. The least altered (LOI = 0.98%) low-Ti tholeiite II from our dredged Healy Spur lavas was used as an example of fresh rock in mass balance calculations for all low-Ti tholeiite

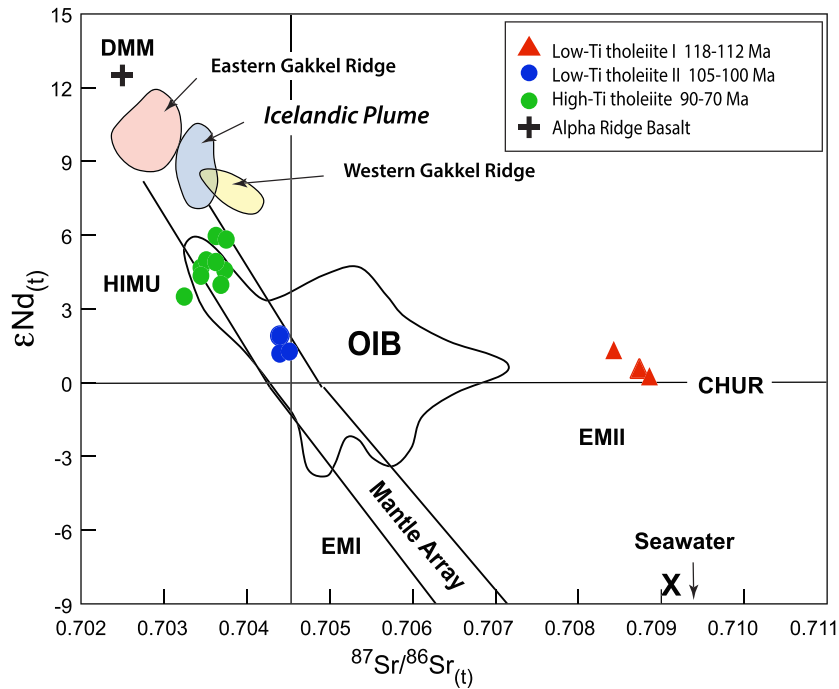


**Figure 9.** The  $^{143}\text{Nd}/^{144}\text{Nd}$  versus  $^{87}\text{Sr}/^{86}\text{Sr}$  isotope diagram for Amerasia Basin submarine lavas compared to the fields for OIB, DMM, HIMU, EMI, EMII, eastern and western Gakkel Ridge basalts, and Icelandic plume basalts. The mantle endmembers and bulk silicate Earth (BSE) are after Hart (1988), and fields for Gakkel Ridge basalts are after Mühe et al. (1997) and Goldstein, Soffer, Langmuir, Cai, et al. (2008) and for the Icelandic plume, after Hemond et al. (1993); seawater values are from Pieprgas and Wasserburg (1980), Veizer (1989), Martin and Scher (2004), and Elmore et al. (2011).

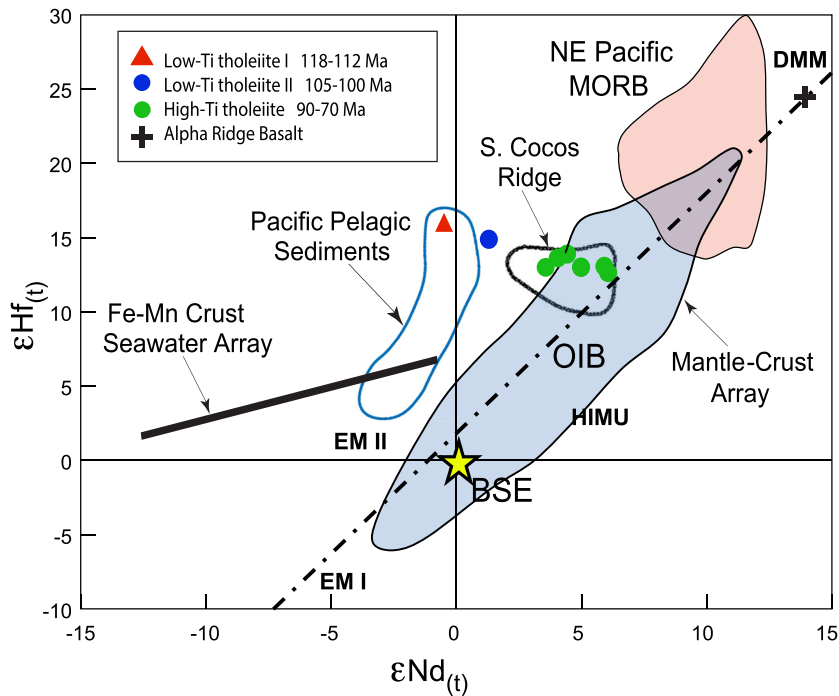


**Figure 10.** The  $\epsilon_{\text{Hf}(t)}$  versus  $\epsilon_{\text{Nd}(t)}$  diagram for volcanic rocks from Amerasia Basin in comparison with OIB, NE Pacific MORB, DMM, and BSE. Mantle-crust array, OIB, EMI, EMII, and BSE after Blichert-Toft et al. (1999); NE Pacific MORB after Jicha et al. (2004); DMM after Salters and Stracke (2004); seawater array and Pacific pelagic sediments after Greene et al. (2008); and southern Cocos Ridge after Geldmacher et al. (2003).

II samples. High-Ti tholeiite from Faroe Islands (Millett et al., 2017) was used as an example of fresh rock in mass balance calculations for high-Ti tholeiite samples dredged from Healy Spur.

In the absence of direct information about temperature at the interface during alteration of the rocks by seawater, we have assumed fairly rapid quenching based on the abundance of glass and pillow structures for some of the samples, implying relatively low temperature conditions for the alteration. Figure 11 shows that most major oxides have either been gained or lost depending on rock composition. In all cases,  $K_2O$  and  $P_2O_5$  were significantly gained during the alteration, and the magnitude is directly correlated with the degree of alteration (judging from the LOI values). In nearly all cases (slightly altered low-Ti tholeiites II; Figure 11b, being the exception),  $CaO$  was lost during the alteration, and this has been observed elsewhere (cf. Bednarz & Schminke, 1989; Seyfried & Mottl, 1982). Silica was lost in all samples, except for low-Ti tholeiite (Figure 11a). In fact, this process may explain the low  $SiO_2$  concentrations of some samples (down to 41.8 wt% for sample DR6-2 of strongly altered low-Ti tholeiite II; Table 2 and Figure 11c). The rest of the major oxides behaved inconsistently and were either lost or gained during alteration, but only to small and minor degrees.

Mass balance calculations show that most trace elements were gained during alteration, some to much greater degrees than others. Gains are directly correlated with the degree of alteration based on LOI. The elements Rb, Th, and U exhibit the largest gains (Figure 12); Pb was gained in all low-Ti tholeiite samples but not in the high-Ti tholeiite which experienced a small loss (Figure 12d). It is notable that the HFSE Zr and Hf were neither gained nor lost appreciably, no matter the degree of alteration, and as such can be viewed as reliably immobile. For all samples, REE were gained proportionately as a function of the degree of alteration, though in all cases the gains are quite small.

The important elements Ba and Sr exhibit some interesting contrasts. In most cases, Ba seems to be unaffected by the alteration, except for low-Ti tholeiites I which show significant gain (Figure 12a). It is not clear why this compositional suite has such a large discrepancy for Ba compared to the other suites, though the choice of reference sample used in the mass balance calculations could very well be a factor in this case. The element Sr, important because of the significance of its isotopic compositions to our understanding of magma-source characteristics, was largely immobile, showing only minor gain or loss due to alteration. These observations are consistent with the findings by Utzmann et al. (2002) and Sofade (2018) that transition metals and REE are only slightly enriched in basaltic lavas during low-temperature submarine hydrothermal alteration.

## 5.2. Implications From Major Oxide, Trace Element, and Radiogenic-Isotope Compositions

Until the study presented here, Van Wagoner et al. (1986) had provided the only mineralogical descriptions and interpretations of major oxide and trace element compositions for eruptive volcanic products from Amerasia Basin. They concluded that Alpha Ridge, where the samples were collected, is an aseismic ridge similar to the Walvis Rise, formed by hotspot activity during opening of Canada Basin, which is one section of Amerasia Basin. Our new chemical and isotopic data indicate that there are at least three distinct groups of lavas distinguished on the basis of eruption age and composition: Low-Ti tholeiites I of the Northwind Ridge erupted at circa 118–112 Ma, and at Healy Spur, low-Ti tholeiites II erupted at circa 105–100 Ma and high-Ti tholeiites erupted at circa 90–70 Ma.

All of the samples we have studied experienced a certain amount of crystal fractionation. Although the circa 105–100 Ma low-Ti tholeiites II from Healy Spur have major oxide compositions not far removed from those of primary melts (e.g., MgO up to 8.7%), we are invoking olivine fractionation because of the evident decrease in Ni, down to 128 ppm, compared to typical primary melts which fall in the range of ~300–600 ppm (e.g., Hart & Davis, 1978; Sato, 1977; Sobolev et al., 2005). Moreover, for the circa 90–70 Ma high-Ti tholeiites from the same locality, low concentrations of MgO (4.4–4.8%), as well as Ni and Cr (108–168 ppm and 40–50 ppm, respectively), indicate that significant olivine and Cr-spinel fractionation occurred. The presence of deep troughs at Sr on the elemental abundance distribution diagram (Figure 6a) suggests that clinopyroxene is also one of the main fractionating phases. This is a robust observation having demonstrated in the previous section that Sr was not adversely affected by submarine hydrothermal alteration in any of the lavas studied. Strontium partitions well into clinopyroxene at pressures from 15 up to 30 kbar (Ntaflos & Richter, 2003), and therefore, fractionation of this phase at high pressure could account for the negative

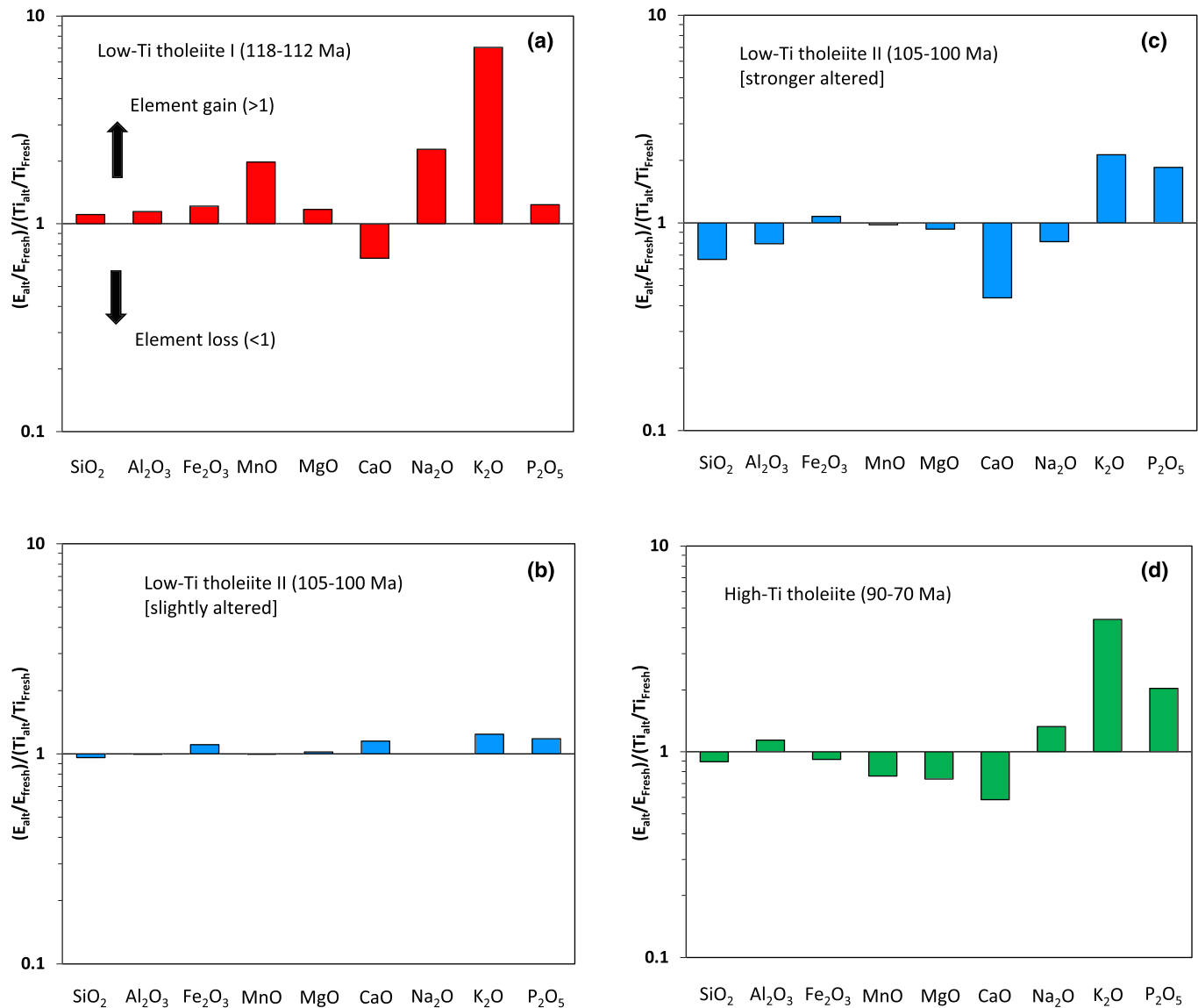


**Figure 11.** (a–d) Mass balance plots for major oxides in altered submarine volcanic rocks from Amerasia Basin (see text for the details). Loss or gain of elements due to seafloor hydrothermal alteration is indicated by deviation from unity by the mobile elements using fresh basalt of comparable Ti concentration as reference material (Sofade, 2018).

Sr anomaly. Plagioclase—another phase with Sr compatibility—may have also fractionated but only to a small extent judging from the limited negative Eu anomalies, with  $\text{Eu}/\text{Eu}^* = 0.93\text{--}0.94$  (Figure 7a). Immediately below, we examine the differences in lava compositions between the two localities and offer some possible explanations.

### 5.3. Northwind Ridge (Low-Ti Tholeiites I)

Northwind Ridge tholeiites with relatively high Mg#, Cr, and Ni concentrations, all summarized in Table 2, experienced only minor differentiation—most likely olivine fractionation—when compared to estimated primitive melt concentrations for Ni of 700–800 ppm and Mg# of ~70 (e.g., Nielsen et al., 2006). In addition, the very small negative Eu anomaly ( $\text{Eu}/\text{Eu}^* = 0.89\text{--}0.90$ ) exhibited by samples from this locality on the REE distribution diagram (Figure 7a) suggests that plagioclase fractionation was minor. In fact, the gentle increases in REE normalized abundances on either side of this slight negative Eu anomaly might reflect a complex history of initial depletion of the source rocks followed by minor crystal fractionation in the magmas.

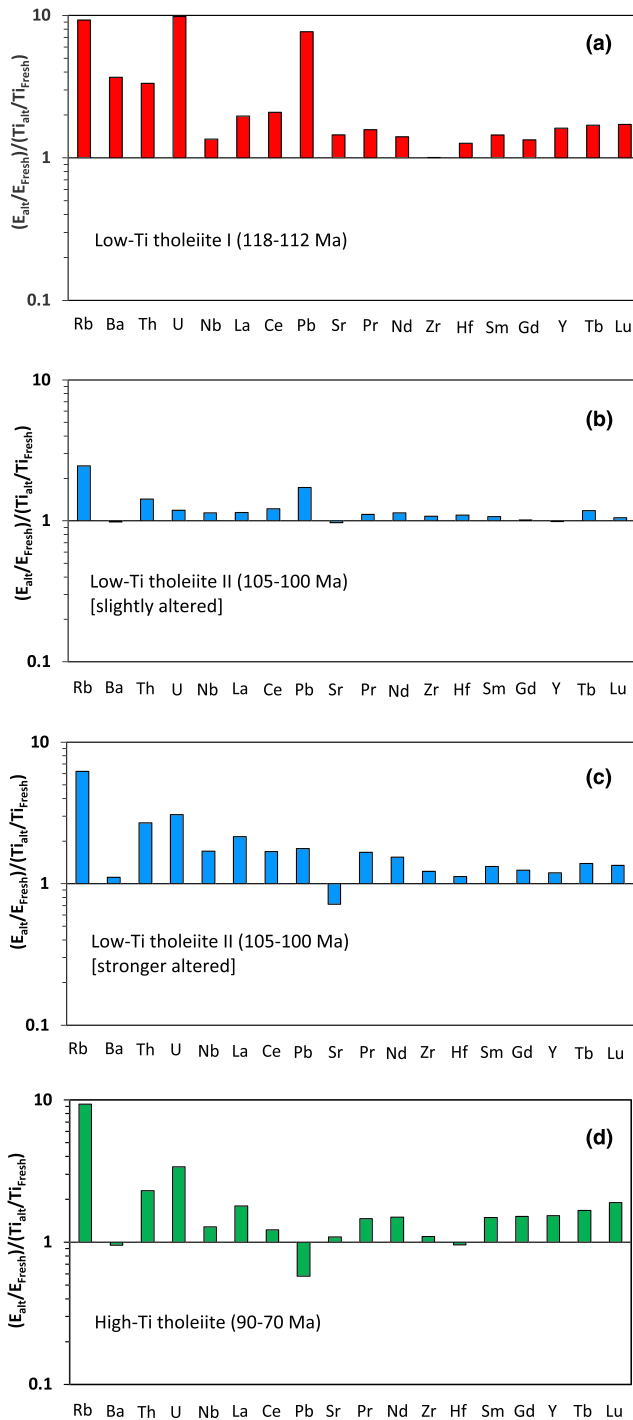


**Figure 12.** (a–d) Mass balance plots for trace elements in altered submarine volcanic rocks from Amerasia Basin illustrating loss or gain of elements relative to a fresh basalt sample of comparable Ti concentration used as reference material (Sofade, 2018).

differentiated tholeiitic lavas containing 2.01–2.67% TiO<sub>2</sub> and circa 90–70 Ma high-Ti evolved tholeiites containing 3.85–4.32% TiO<sub>2</sub>. Geochemical characteristics for these two rock types resemble those of CFB provinces elsewhere (e.g., Arndt et al., 1993; Beccaluva et al., 2009; Jourdan et al., 2007; Marzoli et al., 2019; Ntaflou & Richter, 2003).

Furthermore, the low degree of REE fractionation ( $Ce_N/Yb_N = 1.7\text{--}2.5$ ;  $Gd_N/Lu_N = 1.0\text{--}1.3$ ) and high overall and unfractionated HREE concentrations (20–24 times CI chondrite) suggest melt derivation from a garnet-free source in the shallow mantle. Otherwise, HREE being moderately compatible elements would preferentially have been retained by garnet and not gone into the melt. This implies that melts for the Northwind Ridge low-Ti tholeiites I were generated in the spinel stability field within the upper mantle. A number of studies (e.g., Saunders et al., 1988; Saunders et al., 1991) have shown that involvement of the lithosphere in melt generation is convincingly displayed by Ce/Nb versus Th/Nb plots as illustrated in Figure 13 for which Nb is used as denominator because of its insensitivity to fractional crystallization. However, we can suggest strong involvement of a lithospheric component during melt generation on the basis of the small enrichment observed in the highly incompatible trace elements relative to moderately compatible elements ( $Ba/Y \sim 6$ ) and elevated ratios of some highly incompatible trace elements (e.g.,  $Th/Ce = 0.09\text{--}0.11$ ;  $Ce/Nb = 2.58\text{--}3.09$ ;  $Th/Nb = 0.24\text{--}0.33$ ). Furthermore, Northwind Ridge low-Ti tholeiite I compositions deviate strongly from the OIB-like Th/Ce ratio of 0.05 toward higher ratios which typify lithospheric compositions.

The circa 118–112 Ma Northwind Ridge low-Ti tholeiites I display the most radiogenic Sr ( $^{87}Sr/^{86}Sr$  up to 0.709601 or  $^{87}Sr/^{86}Sr_{(t)}$  up to 0.708855) and the least radiogenic Nd ( $^{143}Nd/^{144}Nd$  down to 0.512594 or  $\epsilon_{Nd(t)}$  down to  $-0.58$ ) among the rocks studied (Table 3; Figure 9). Major seawater contribution to radiogenic  $^{87}Sr$  in the Northwind Ridge basalts can be ruled out because Sr behaved as an immobile element during the seawater/rock interaction illustrated in Figure 12 and because the  $^{143}Nd/^{144}Nd$  ratios, which are not sensitive to contamination by seawater, are low enough to support a lithospheric origin for the melts. Furthermore, because of the clear secondary U enrichment in all studied samples and Pb in the low-Ti tholeiite I lavas (Table 2 and Figure 12), we did not use decay-corrected Pb isotopic ratios as this would introduce an error that is difficult to quantify. Radiogenically produced Pb from the secondary U enrichment and seawater contamination may explain the slight deviation of most data points from the NHRL toward the EMII compositions on the  $^{207}Pb/^{204}Pb$  versus  $^{206}Pb/^{204}Pb$  covariation diagram (Figure 8a). Crustal contamination of the ascending magmas is another potential complicating factor difficult to tease out from this data set. However, note that virtually all data points plot along the NHRL on the  $^{208}Pb/^{204}Pb$  versus  $^{206}Pb/^{204}Pb$  covariation diagram (Figure 8b), which favors seawater contamination over crustal contamination. Plots of Mg# versus  $^{207}Pb/^{204}Pb$  and Mg# versus  $^{87}Sr/^{86}Sr$  (supporting information Figure S2) show no correlations that would be attributable to crustal contamination, supporting the seawater contamination assertion.

#### 5.4. Healy Spur (Low-Ti Tholeiites II and High-Ti Tholeiites)

Volcanic rocks recovered from Healy Spur are distinct when compared to the Northwind Ridge lavas, both chemically and isotopically. Healy Spur tholeiites are composed of two groups: circa 105–100 Ma low-Ti slightly

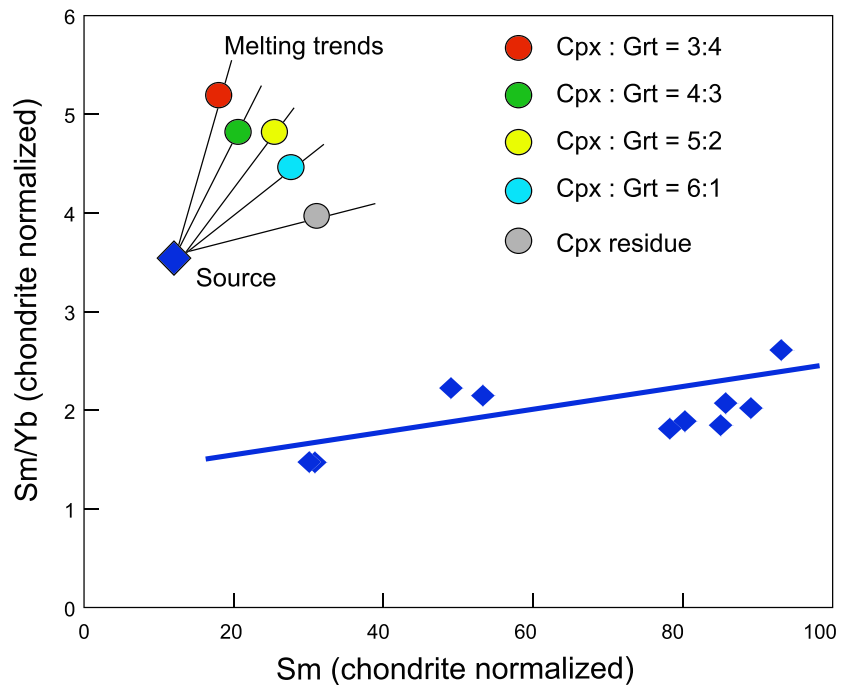


**Figure 13.** The Ce/Nb versus Th/Nb diagram showing the field for MORB, the Th/Ce line for OIB, and shifts in composition for Amerasia Basin as magmas derived from the asthenosphere are contaminated by lithospheric components. Derivation exclusively within the subcontinental lithospheric mantle (SCLM) is also proposed for the 118–112 Ma Northwind Ridge low-Ti tholeiitic basalts. Lines for OIB and field for MORB are after Ntaflos and Richter (2003).

Trace element compositions for the circa 105–100 Ma low-Ti tholeiites II (Figure 6) are similar to those typical of CFB elsewhere and especially the Deccan basalts of India (Campbell & Griffiths, 1990; Chandrasekharam et al., 1999; Krishnamurthy & Cox, 1977) (Figure 7). Minor REE fractionation in these tholeiites ( $Ce_N/Yb_N = 2.8\text{--}3.3$ , and  $Gd_N/Lu_N = 1.4\text{--}1.9$ ) points to a garnet-free source and suggests magma derivation largely in the spinel stability field within the upper mantle. While the high-Mg concentrations (7.02–8.69% MgO) may suggest limited melt fractionation, low Mg# (51.0–53.7) resulted from high Fe concentrations ( $Fe_2O_{3tot} = 10.9\text{--}15.3\%$ ) point to significant crystal fractionation in the primary melts.

Compositional characteristics of the circa 90–70 Ma high-Ti tholeiites include low Mg# and low concentrations of Mg, Ni, and Cr (Table 2), which together suggest significant differentiation of the original primary melt. Low degrees of REE fractionation with  $(Ce/Yb)_N = 2.0\text{--}2.4$  and  $(Gd/Lu)_N = 1.3\text{--}1.6$  suggest melt generation in a garnet-free source in the upper mantle. Minimal fractionation of the highly incompatible to more compatible trace elements suggests higher degrees of melting to produce these high-Ti tholeiites than for the circa 105–100 Ma low-Ti tholeiites II. Higher overall concentrations of compatible trace elements such as Ti for the 90–70 Ma tholeiites suggest increasing degrees of melting in the source materials between circa 105 and circa 70 Ma, assuming magma derivation from the same depths within the upper mantle. This is counterintuitive without source refertilization by metasomatic processes. In the absence of strong evidence for metasomatism, the data are best explained by variance in the depth of melting.

While there is a wide range and some scatter in the Pb isotopic compositions for Healy Spur lavas (Figures 8a and 8b), a trend between depleted and enriched components is discernable, especially on the thoriumgenic Pb diagram. One interpretation is that the endmember compositions producing the mixing array are both in the mantle. However, the circa 90–70 Ma high-Ti tholeiites fall at the most radiogenic end of the Pb isotopic trends yet also have the least radiogenic Sr and most radiogenic Nd in the sample suite (Figure 9). Thus, the Sr and Nd isotopic systems are decoupled from the Pb isotopic systems, especially when one notes the scatter and displacement from the NHRL of most data points on the  $^{207}Pb/^{204}Pb$  versus  $^{206}Pb/^{204}Pb$  diagram toward the seawater Pb isotopic composition measured by Paul et al. (2015) (Figure 8a). A possible explanation for this—particularly in light of elevated  $^{207}Pb/^{204}Pb$  (but not  $^{208}Pb/^{204}Pb$ ) for any  $^{206}Pb/^{204}Pb$  value—is that the

Pb isotopic ratios have been affected by seafloor alteration (i.e., Pb was added to the lavas as they were altered by seawater and also radiogenically from U added to the lavas by seawater during the Cretaceous opening of Amerasia Basin). On the other hand, the Nd and Sr isotopes are buffered by higher elemental concentrations in the initial mantle melts and are therefore not substantially affected. The covariation in  $\epsilon_{\text{Nd}(t)}$  and  $\epsilon_{\text{Hf}(t)}$  illustrated in Figure 10 shows a diminishment through time of source or contamination components with a time-integrated record of superchondritic Lu/Hf, most likely in the lithosphere (e.g., Blichert-Toft et al., 1999; Vervoort et al., 2000).

Rare-earth element characteristics of the studied lavas from both Northwind Ridge and Healy Spur (Table 2) suggest generation of the primary melts in garnet-free sources within the upper mantle (at pressures <20 kbar). To conclusively illustrate this point, we compared the chondrite-normalized Amerasia Basin lava Sm concentrations and Sm/Yb values to the experimental melts generated by Takahashi et al. (1998) for various proportions of garnet and clinopyroxene in the source (Figure 13). All Amerasia Basin basalts plot along a line with the shallowest slope, corresponding to a mantle source with only clinopyroxene in the residuum, and no garnet.

In order to estimate the proportions of different source components in Healy Spur basalts, we have plotted on the diagrams in Figures 13–15 the elemental ratios of some highly incompatible elements, using Nb or Yb as the denominator because these elements are not fractionated during melting (e.g., Ntafos & Richter, 2003; Pearce & Stern, 2006) and behave similarly during seafloor alteration (Figure 12). The low-Ti tholeiites of both Types I and II plot along the line connecting OIB and continental lithosphere compositions on the Ce/Nb versus Th/Nb diagram (Figure 14), which suggests a mixture of at least two components. Figure 12 shows that seafloor alteration added Th to some of these submarine lavas but not in significant enough quantities to impact the trend shown on the logarithmic scale Ce/Nb versus Th/Nb diagram in Figure 14.

Furthermore, on the Ta/Nd versus Th/Nb diagram (Figure 15a)—with endmember compositions from Willbold and Stracke (2006) and Aldanmaz et al. (2008)—we see that the 90–70 Ma high-Ti tholeiites fall close to the line between a depleted upper mantle source (e.g., source for Gakkel Ridge lavas) and a plume component—with no evidence for presence of a lithospheric component—whereas the circa 118–112 Ma low-Ti tholeiites I from Northwind Ridge, and to a smaller extent the 105–100 Ma low-Ti tholeiites II from Healy Spur, define a trend (nearly horizontal line in Figure 15a) toward the subcontinental lithospheric mantle (SCLM). On the Th/Yb versus Nb/Yb diagram (Figure 15b), the 105–100 Ma low-Ti tholeiites II and 90–70 Ma high-Ti tholeiites straddle the line between E-MORB (e.g., Gakkel Ridge) and the plume component, indicating that these lavas are largely two-component mixtures, whereas the circa 118–112 Ma low-Ti tholeiites I from Northwind Ridge fall substantially off this trend, underscoring the importance of lithospheric components in these lavas.

We attempted to estimate the inputs of different components to the original melts using geochemical abundance pattern for various trace elements (Figure 16). Elements such as Zr, Hf, and HREE generally form the baseline corresponding to the depleted endmember—in this case, a MORB-like mantle here represented by Gakkel Ridge E-MORB compositions of the eastern Arctic Ocean. Other elements such as Nb, Ta, Ce, Ti, and MREE—referred to by Pearce and Stern (2006) as “deep subduction elements”—are likely to be introduced into the melts from deeper mantle levels of a convecting asthenosphere or upwelling plume. Barium and Sr, both important in elemental balance, are strongly depleted relative to the adjacent elements on the abundance pattern diagrams and also relative to typical OIB and flood basalts, most likely because of significant fractional crystallization. In addition, Pb is susceptible to seawater contamination owing to the low concentrations in basaltic magmas. Nevertheless, at least three components contributing to the melts can be recognized: shallow mantle MORB-like component, deep asthenospheric or plume component, and SCLM component.

It is worth noting also that both Healy Spur rock types have Ba negative anomalies, whereas other highly incompatible LILE exhibit a history of enrichment (Figure 6). Van Wagoner et al. (1986) observed similar characteristics for some highly altered basaltic hyaloclastites from Alpha Ridge and attributed them to secondary alteration effects. Our samples on the other hand do not display such severe degrees of secondary alteration, and as such we suggest that the negative Ba and Sr anomalies are not the results of secondary effects but are rather intrinsic properties of the magmas. This conclusion is borne out by the Ba and Sr



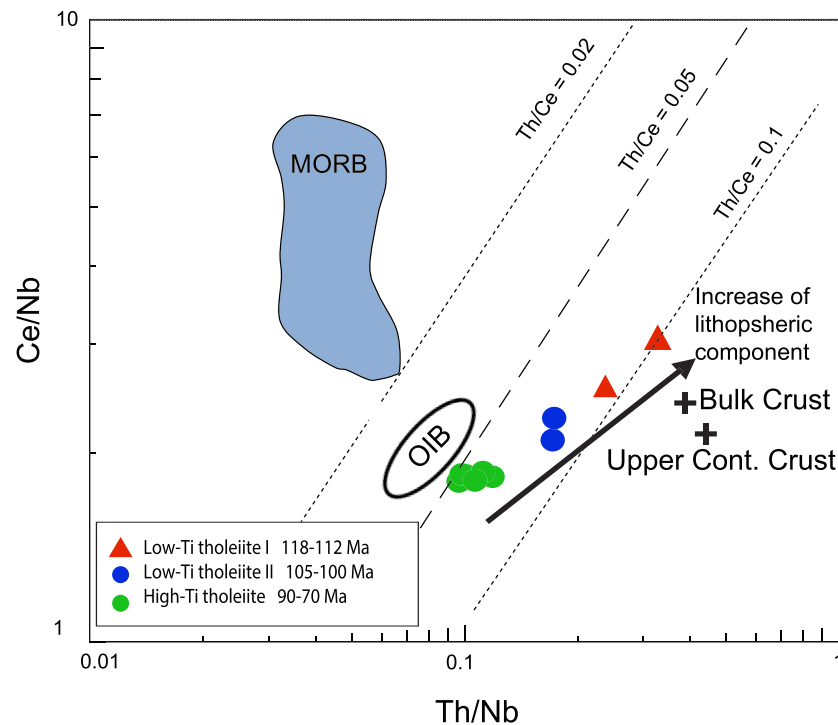


**Figure 14.** CI chondrite-normalized Sm/Yb values versus Sm concentrations in Amerasia Basin basalts. Also shown are the compositional trends for partial melts leaving various proportions of clinopyroxene and garnet in the residues, after Takahashi et al. (1998).

patterns in Figures 12b to 12d, which show only minor gains or losses of these elements during seafloor alteration in Amerasia Basin.

Here, we try to estimate through modeling the extent of fractional crystallization in these Amerasia Basin lavas and then compare results with the observed volcanic rock compositions. Assumptions have to be made about the primary melt compositions and hypothesized fractionating phases. For this modeling, the hypothesized parental melt compositions, fractionating phases, product magmas following crystal fractionation, and actual rock compositions observed in Amerasia Basin are summarized in Table 4. Generally, the earliest and most primitive melts produced at shallow levels during plume ascent are high-Mg picrites (e.g., Arndt et al., 1993; Beccaluva et al., 2009; Campbell & Griffiths, 1990; Krishnamurthy & Cox, 1977). We have therefore based the primary melt composition in our modeling on a typical picrite composition (e.g., Beccaluva et al., 2009, and references therein). We applied the least squares approximation of Bryan et al. (1969) and the program by R.H. Naslund (<http://bingweb.binghamton.edu/~naslund>) to calculate compositions produced by fractional crystallization of the hypothesized parental liquids. As argued above, we considered olivine, clinopyroxene, chrome spinel, plagioclase, and amphibole as the potential fractionating phases.

As a start, we considered fractionation that would remove phases with the proportions of 22% olivine, 6% clinopyroxene, and 3% plagioclase from a picrite melt with 16 wt% MgO. This produces an evolved magma, “Daughter liquid 1,” with 9.6% MgO (Table 4), which is compositionally similar to the circa 105–100 Ma low-Ti tholeiites II from dredge HLY0805 DR6-2. It is entirely possible, therefore, that these circa 105–100 Ma tholeiites in Amerasia Basin are fractional crystallization products of a parental picritic melt.

### 5.5. Lithospheric Contamination—Source of the Hf-Nd Isotope Decoupling?

In regions where basaltic magmas ascend through continental lithosphere, numerous studies have demonstrated ample evidence for magma-crustal rock interaction (e.g., Brandon et al., 1993; McDonough, 1990; Meshesha & Shinjo, 2007; Rudnick & Presper, 1990). The oldest basaltic magmas in Amerasia Basin

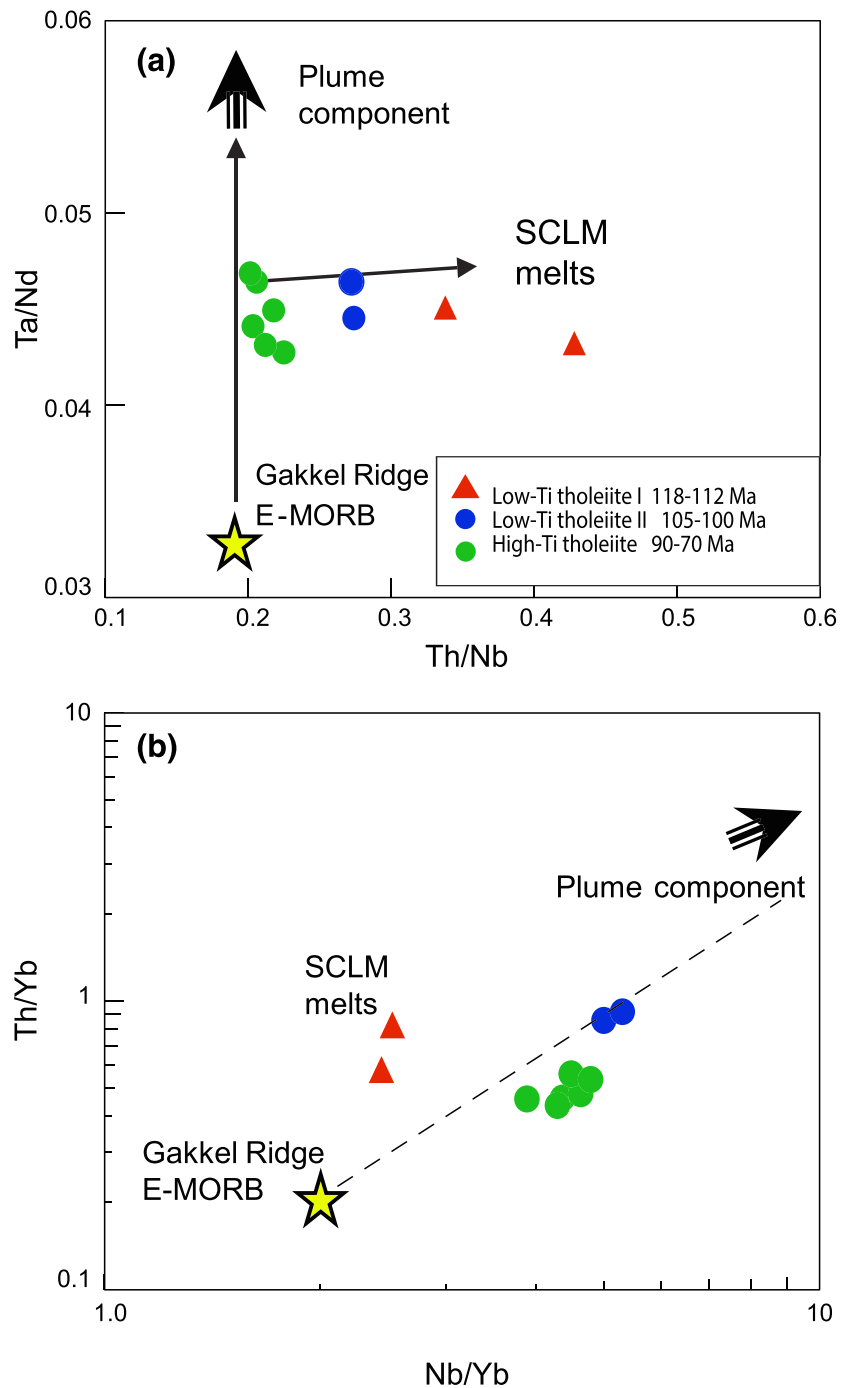


**Figure 15.** The Ta/Nd versus Th/Nb (a) and Th/Yb versus Nb/Yb (b) diagrams illustrating possible involvement of several components in generation of Amerasia Basin melts. Endmember compositions are from Willbold and Stracke (2006) and Aldanmaz et al. (2008). The Gakkel Ridge E-MORB compositions are from Mühe et al. (1997) and D'Errico et al. (2016).

ascended through continental lithosphere being thinned by extension but nevertheless conducive to magma-rock interaction even if neither mantle nor crustal xenoliths have ever been observed in the dredged samples.

In general, several geochemical characteristics may fingerprint the digestion of continental lithospheric materials by basaltic magmas. Negative Nb, Ta, and Ti anomalies—all well documented in CFB

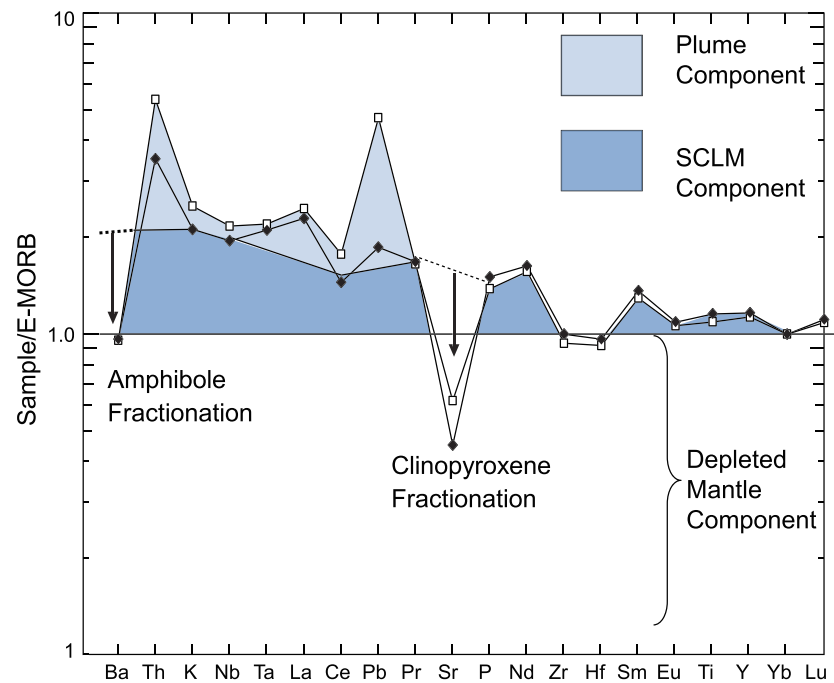


**Figure 16.** Trace element geochemical abundance patterns demonstrating the progressive changes incurred with input of different components (after Pearce & Stern, 2006) to form the more trace element enriched lavas (e.g., Sample HLY0805 DR6-2) and less enriched lavas (e.g., HLY0805 DR6-3/5). In a given system, the SCLM component is characterized by elements such as Th, LREE, and Pb. The plume component is characterized by input of the elements mentioned immediately above for SCLM (except Pb which in this case may be elevated by alteration), plus K, Nb, Ta, and MREE. The patterns are normalized to E-MORB (Gakkel Ridge basalts, the closest available representative of a MORB-like mantle in the region (Mühe et al., 1997; D'Errico et al., 2016) and then to  $Yb_N = 1$  as denominator, which is only minimally affected by fractional crystallization and as the least mobile element in the entire spectrum.

worldwide—are often invoked as unmistakable signs of lithospheric assimilation by basaltic magmas (Brandon et al., 1993; McDonough, 1990; Rudnick & Presper, 1990). Evidence for lithospheric ingestion by basaltic magmas has also come from steep trends on Nd-Sr isotopic covariation diagrams (e.g., Halama et al., 2004; Paces & Bell, 1989; Stevenson et al., 1997). These trends are thought to develop in basaltic magmas due to assimilation of ancient lower crust or metasomatized SCLM typified by very low initial  $^{143}\text{Nd}/^{144}\text{Nd}$  at given  $^{87}\text{Sr}/^{86}\text{Sr}$  values (Halama et al., 2004).

The circa 118–112 Ma tholeiites I from Northwind Ridge exhibit features that could be attributed to ingestion of lithospheric materials. For example, all Sr isotope ratios at given  $^{143}\text{Nd}/^{144}\text{Nd}$  ratios in this area (Table 3) are too high to be completely attributed to seawater contamination, especially in light of the Sr patterns shown on the diagrams in Figure 12. More likely, besides adding radiogenic Sr to the basaltic magmas, lithospheric assimilation and seawater interaction at the time of eruption both introduced “excess” Rb that promoted the ingrowth of radiogenic Sr. Additional evidence for lithospheric contamination includes negative Ti and Nb anomalies (Figure 6a). Therefore, in the absence of xenoliths of any kind from these lavas, the indirect geochemical signatures presented here are the best evidence for the nature of the lithosphere that was assimilated.

In contrast, none of the Healy Spur lavas (i.e., 105–100 Ma low-Ti tholeiites II and 90–70 Ma high-Ti tholeiites) exhibit negative Nb, Ta, or Ti anomalies (Figure 6a) and all fall within the mantle array on the  $\epsilon\text{Nd}_{(t)}$  versus  $^{87}\text{Sr}/^{86}\text{Sr}_{(t)}$  diagram (Figure 9). Therefore, although a small amount of lithospheric contamination cannot be ruled out entirely, evidence suggests that lithospheric influences decreased with time from eruption of the circa 105–100 Ma low-Ti tholeiites II to the circa 90–70 Ma high-Ti tholeiites.

Supporting this assertion is the observed decoupling of  $^{176}\text{Hf}/^{177}\text{Hf}$  and  $^{143}\text{Nd}/^{144}\text{Nd}$  values as a function of approximate eruption age (Figure 10). Commonly, Hf and Nd isotopes have a positive covariation in oceanic basalts (MORB and OIB), which defines the mantle array (e.g., Blichert-Toft & Arndt, 1999;

**Table 4**  
*Compositions of Parental Melts and Their Daughter Products in Comparison With the Observed Compositions and Mineral Analyses Used for Modeling*

Ol%	22			13		
Cpx%	6			6		
Plag%	3					
Pl%				8		
	Parental	Daughter	Sample	Parental	Daughter	Sample
	picrite	liquid 1	DR6-2	basalt	liquid 2	DR6-3/1
			Lo-Ti	Lo-Ti		Hi-Ti
			Tholeiite	Tholeiite		Tholeiite
SiO <sub>2</sub>	45.01	45.75	45.49	45.49	45.69	46.30
TiO <sub>2</sub>	2.10	2.53	2.84	2.84	3.52	4.22
Al <sub>2</sub> O <sub>3</sub>	12.38	15.70	15.68	15.68	17.16	16.46
FeO <sub>tot</sub>	13.87	14.25	14.92	14.92	16.68	15.85
MnO	0.20	0.22	0.34	0.34	0.43	0.17
MgO	15.97	9.63	9.24	9.24	4.81	4.85
CaO	7.39	8.03	7.54	7.54	6.83	6.51
Na <sub>2</sub> O	2.00	2.50	2.56	2.56	3.10	3.67
K <sub>2</sub> O	0.65	0.82	0.84	0.84	1.07	1.19
P <sub>2</sub> O <sub>5</sub>	0.45	0.59	0.55	0.55	0.70	0.77
Total	100.00	100.00	100.00	100.00	100.00	100.00
Mg#	67.2	54.6	52.5	52.5	34.0	35.3
	Ol	Cpx	Amph	Pl		
SiO <sub>2</sub>	40.24	52.02	40.57	46.75		
TiO <sub>2</sub>	0.04	1.44	4.33			
Al <sub>2</sub> O <sub>3</sub>	0.05	1.44	14.40	33.47		
FeO <sub>tot</sub>	14.56	5.85	11.93	0.18		
MnO	0.05		0.12			
MgO	44.77	17.13	11.74	0.25		
CaO	0.29	21.70	9.79	17.82		
Na <sub>2</sub> O		0.43	3.22	1.53		
K <sub>2</sub> O			0.90			
Total	100	100	97	99.68		
Mg#	84.6	83.9	63.7	71.2		

*Note.* The rows above the liquid compositions represent the mineral proportions removed in order to form a daughter liquid. Compositions of fractionating minerals are after Ionov et al. (2002) and Beccaluva et al. (2009).

Salters & Hart, 1991; Vervoort & Blichert-Toft, 1999). It is therefore unusual but not unprecedented to have the two isotopic systems decoupled from each other as observed in this suite of samples. Decoupling of the Hf and Nd isotopic systems has been documented in Hawaiian and Korean Peninsula mantle xenoliths (Bizimis et al., 2004, 2007; Choi & Mukasa, 2012), in South African Archean to Proterozoic lower-crustal xenoliths (Schmitz et al., 2004), and in sedimentary systems undergoing recycling into the mantle (Patchett et al., 1984). Choi and Mukasa (2012) explained the Hf-Nd decoupling in the Korean Peninsula mantle xenoliths in terms of late-stage metasomatism overprinting the source in the lithospheric mantle.

### 5.6. Melting Events Beneath Amerasia Basin

Despite the limited number of samples recovered by dredging volcanic edifices in Amerasia Basin, age and geochemical patterns allow the deduction of mantle melting processes through time. Arguments in the above sections are consistent with the idea that Northwind Ridge low-Ti tholeiites I were generated largely by melting in the lithospheric upper mantle, within the spinel stability field. The lithospheric mantle forms part of the cold boundary layer at the top of the mantle and can only be melted by rapid uplift and stretching if it gains sufficient heat from an upwelling asthenospheric mantle, with or without the influence of a hot plume. Addition of significant amounts of volatiles also helps to lower the melting temperature of peridotites and consequently facilitates magma production. Anhydrous melting, largely by conductive heat transfer, must be restricted to a zone just above the central hot axis of the upwelling material, and therefore, no melting will occur in the mantle lithosphere toward the peripheries of the upwelling material (Campbell & Griffiths, 1990).

Judging from the geochemical characteristics of the circa 118–112 Ma low-Ti tholeiites I at Northwind Ridge—that is time-integrated record of low Th/Pb ratios manifested by the Pb isotopic diagram in Figure 8b and low overall abundances on the element distribution

diagrams, compared to the circa 105–100 Ma low-Ti tholeiites II and the circa 90–70 Ma high-Ti tholeiites—we have deduced that source peridotites were highly depleted. Moreover, the lack of a negative Ba anomaly in the trace element-abundance patterns for the circa 118–112 Ma low-Ti tholeiites I (Figure 6a) suggests the absence of amphibole either in the residuum or as a fractionating phase. An anhydrous source is therefore invoked. The dry peridotite solidus temperature at a pressure of 20 kbar (roughly the boundary between the spinel and garnet stability fields) is ~1400°C (Takahashi, 1986; Takahashi et al., 1998). Melt temperature for the circa 118–112 Ma low-Ti tholeiites I, estimated with use of the Sugawara (2000) thermometer, is ~1180°C. The discrepancy of >200°C may simply reflect cooling of the magmas en route to the surface. Such a temperature drop suggests slow ascent—allowing fractionation and crystallization—which is consistent with the phyric and compositional characteristics of the Northwind Ridge basalts. This melting event at circa 118–112 Ma was the precursor to later and more voluminous CFB volcanism.

Subsequent melting in Amerasia Basin—as expressed at Healy Spur and in the contiguous Alpha Ridge and Mendeleev Ridge—is consistent with decreasing importance of lithospheric components in the magma and increasing importance of asthenospheric components, possibly in upwelling cells. This magmatism is coeval and may be cogenetic with the HALIP, described at various circum-Arctic landmasses by others (e.g., Buchan & Ernst, 2006; Corfu et al., 2013; Drachev & Saunders, 2006; Døssing et al., 2013; Embry & Osadetz, 1988; Evenchick et al., 2015; Jowitt et al., 2014; Maher Jr., 2001; Polteau et al., 2016; Villeneuve & Williamson, 2006).

The first lavas to erupt following extensive thinning of the mantle lithosphere were the circa 105–100 Ma low-Ti tholeiites II. We suggested above on the basis of their trace element abundance patterns that the asthenospheric source these basalts were derived from likely contained some volatiles. Multiple melting experiments (e.g., Falloon & Green, 1989; Green, 1973; Millhollen et al., 1974; Olafsson & Eggler, 1983) showed that introduction of volatiles to peridotite sources in the mantle significantly reduces the solidus temperature. If we assume the pressure at the zone of melting not to have exceeded 20 kbar (i.e., within the spinel stability field), then a low-Ti tholeiite II magma, like the one from Healy Spur, is produced adiabatically corresponding to the CO<sub>2</sub>-saturated peridotite solidus of Falloon and Green (1989). Because there is little evidence for an ambient temperature in the source regions of 1500°C—which would produce a picritic magma and perhaps even definitively implicate a plume (e.g., Beccaluva et al., 2009; Campbell & Griffiths, 1990)—we can deduce that melting occurred in an upwelling asthenospheric mantle. Increase in some compatible element concentrations (such as Ti) from older to younger lavas in Amerasia Basin requires an increase through time of the degree of melting in the source, best facilitated by rapid asthenospheric upwelling accompanying lithospheric thinning.

### 5.7. Evaluation of Tectonic Models for Amerasia Basin Based on <sup>40</sup>Ar/<sup>39</sup>Ar Ages and Lava Geochemistry

Our newly obtained <sup>40</sup>Ar/<sup>39</sup>Ar spectra were impacted by alteration and should therefore be viewed as recording age minimums for the three submarine volcanic events described. Nevertheless, the data suggest that there was active volcanism in the submarine sections of the HALIP continuously or intermittently for at least 30 Myr, from circa 118–112 to circa 90–70 Ma. Absence of older volcanic rocks in our limited number of dredges does not preclude their potential presence in the region as is suggested by lava exposures on some circum-Arctic landmasses falling in the age range of circa 130 to 120 Ma (e.g., Corfu et al., 2013; Dockman et al., 2018; Evenchick et al., 2015; Maher, 2001; Polteau et al., 2016; Villeneuve & Williamson, 2006). Also, models for Canada Basin opening beginning in the Late Jurassic to Early Cretaceous (e.g., TAILLEUR et al., 1973; Grantz et al., 1979; Grantz & May, 1983; Lawver et al., 2002; Miller et al., 2018) support the presence of volcanism that is older than our samples. All of the age determinations in the above studies combined demonstrate presence of active magmatism in the HALIP for some 50 Myr—between circa 130 and 80 Ma, making it difficult to attribute this protracted mantle melting to a single mechanism (Dockman et al., 2018). A number of tectonic and mantle melting models therefore require evaluation before converging toward the most likely scenarios.

#### 5.7.1. The Back-Arc Model

Before and during breakup of the Paleo-Arctic Continent, the Pacific subduction zone—now located just south of the Aleutian Islands—was much closer to the paleogeographic location of Amerasia Basin. Spatially and temporally associated ophiolites and continental arcs (130–115 Ma) have been documented throughout Arctic Alaska and northeastern Siberia (Akinin et al., 2009; Kuzmichev, 2009; Miller et al., 2002, 2010, 2018; Pease & Coakley, 2018, and references therein). The tectonic and magmatic evolution of these terranes no doubt influenced the lithospheric mantle beneath Amerasia Basin by addition of transient basaltic melts and possibly even volatiles (e.g., Baggeroer & Falconer, 1982; Grantz et al., 1990; Grantz et al., 1998; Miller et al., 2018).

Therefore, back-arc spreading behind the Pacific subduction zone is one of the mechanisms to consider in development of Amerasia Basin. There is general consensus that one of the distinctive features of BABB is the presence of a shallow subduction geochemical components mobile in low-temperature aqueous fluids, for example, Rb, Ba, Sr, and Pb (Pearce & Stern, 2006, and references therein). As such, BABB are transitional between MORB and island arc tholeiitic basalts in their trace element characteristics, sharing with the latter high concentrations of subduction-mobile components (e.g., Rb, Ba, LREE, Sr, P, Pb, and radiogenic Sr), as well as low concentrations of subduction-immobile components (e.g., Nb, Ta, Ti, Zr, Hf, and HREE) (Fretzdorff et al., 2002; Gill, 1976; Gribble et al., 1998; Pearce & Stern, 2006; Sinton et al., 2003; Woodhead et al., 1993). While the basaltic samples in our study display enrichment in some of the subduction-mobile elements, most of those elements are recognized to be recyclable, with extended residence times in the deep mantle (Pearce & Stern, 2006). Deep-mantle recycled components are thought to originate in enriched mantle plumes and are not related to active, shallow subduction processes. No shallow subduction characteristics (i.e., aqueous fluids released at low temperatures from subducted crust or

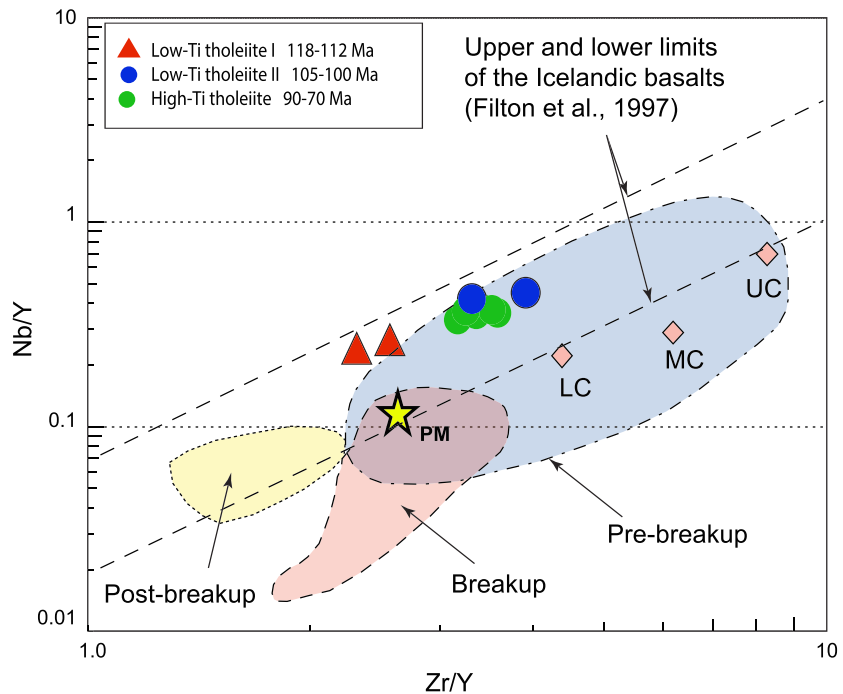


**Figure 17.** The Nb/Y versus Zr/Y diagram showing the compositional fields for prebreakup, breakup, and postbreakup lavas formed at the locus of disaggregating supercontinents (after Kempton et al., 2000). The upper and lower limits for Icelandic basalts are after Fitton et al. (1997). Note that all of the Amerasia Basin samples analyzed plot in the prebreakup field. LC, MC, and UC are compositions of lower, middle, and upper crust (Kempton et al., 2000).

sediments and LILE enrichment) have been observed in the basalts we have studied (see Figures 6a and 16). A back-arc environment can therefore be ruled out.

### 5.7.2. The Plume Model

The observed pattern of eruption ages (ours on submarine lavas and those of others on circum-Arctic landmasses), geochemical characteristics, and isotopic compositions are not inconsistent with a plume origin—particularly using arguments and observations first made by Campbell and Griffiths (1990). However, other studies have been inconclusive in definitively tying these geochemical characteristics and protracted magmatism to a plume (e.g., Ivanov et al., 2018; Kamenetsky et al., 2017). Deep-seated mantle plumes have been invoked for much of the global flux of intraplate volcanism even though careful seismic tomography has definitively identified only 28 in number (French & Romanowicz, 2015; Montelli et al., 2004). None of the lavas defining the Canada Basin medial magnetic anomalies have ever been sampled owing to the thick sediment cover (Gaina et al., 2014; Mosher et al., 2012; Saltus et al., 2011) but are thought to be the result of seafloor spreading, a natural culmination of the rifting that formed Amerasia Basin (Chian et al., 2016; Grantz et al., 2011; Hutchinson et al., 2017; Taylor et al., 1981; Vogt et al., 1982). The extent and duration of that seafloor spreading remain unknown but are subjects of ongoing studies. However, the lavas defining the magnetic anomalies probably have MORB-like geochemical characteristics—rather different compared to the Northwind Ridge and Healy Spur lavas described in this study.

Combining our study with various others is beginning to clarify the tectonic and magmatic history of the western Arctic Basin region. Villeneuve and Williamson (2006) showed that the oldest eruptive products in the HALIP were emplaced at circa 130 Ma. It is presumed that this volcanic activity coincided with a hot plume head rising through the asthenospheric mantle and impinging the bottom of the lithosphere, beneath a now disaggregated Arctic Continent. This plume may be responsible for uplift and doming leading to geodetic anomalies and therefore continental destabilization and faulting with triple-junction geometry (e.g., Forsyth et al., 1986; Figure 18a). The suggested doming of the Arctic Continent lithosphere is consistent with the wide regression and a stratigraphic disconformity documented in the high Arctic for the duration

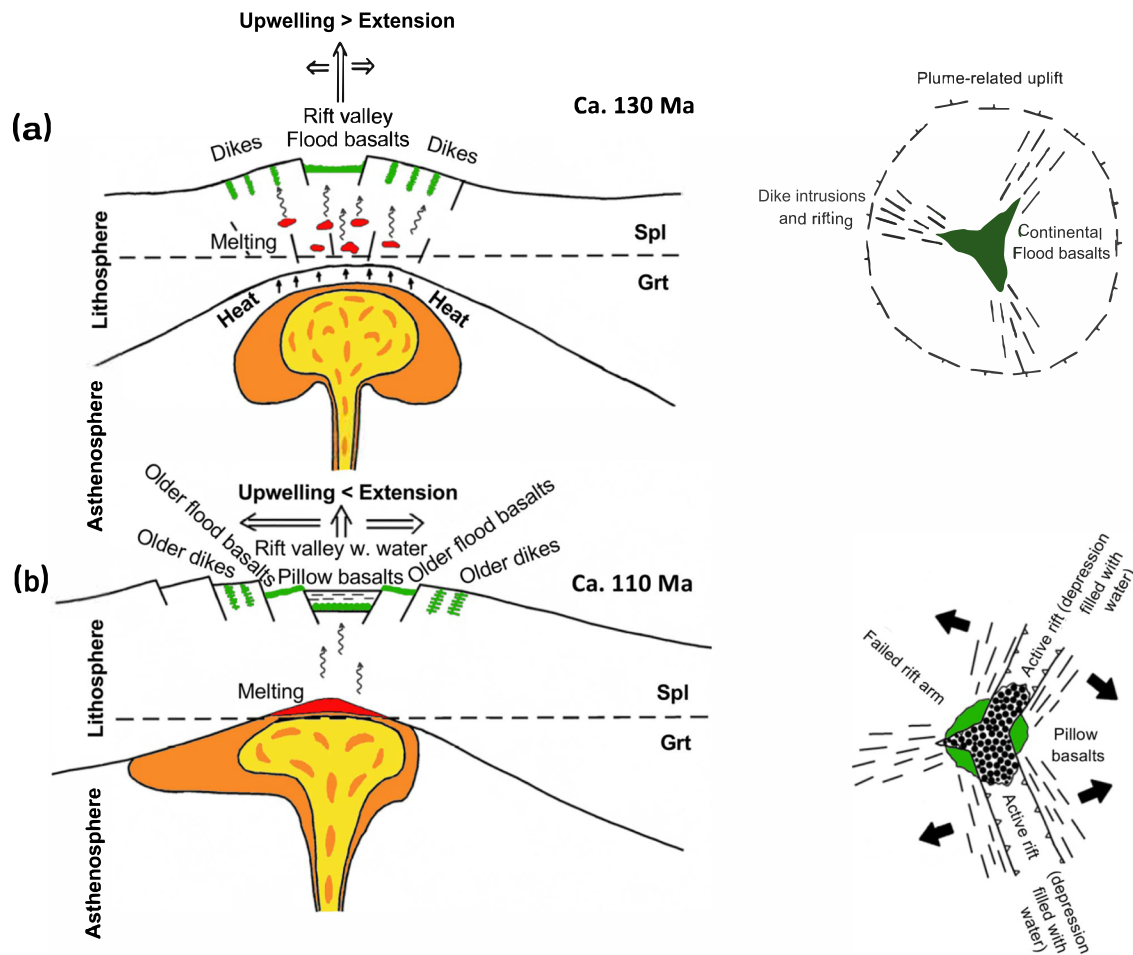


**Figure 18.** Proposed model for development of Amerasia Basin during the Cretaceous (cross-section and planar view). (a) Circa 130 Ma: heat anomaly introduced by the ascending plume head (recorded in circum-Arctic terrestrial HALIP lavas) causing melting in the SCLM and eruption of subaerial tholeiitic basalts. Through uplift, the ascending plume created dynamic topography and a domal structure in the overlying lithosphere causing geotectonic instabilities and breakup of the Arctic Continent with triple point geometry. (b) Circa 110 Ma: Upon impinging the bottom of the lithosphere, the ascending plume head was deflected to the west; plume interacted with lithospheric materials in the spinel stability field producing melts carrying mixed asthenospheric and lithospheric geochemical signatures; crustal thinning resulted from the continued extensional deformation along normal faults that defined horsts and grabens; submarine volcanism occurred at this time creating pillow basalts. (c) Circa 100 Ma: High-Ti tholeiitic basalts were produced by increasing degrees of partial melting. (d) Circa 80 Ma: Continued rifting and lithospheric thinning eventually generated genuine ocean crust with magnetic anomalies orthogonal to the long axis for Canada Basin.

between the Hauterivian to Aptian in the Early Cretaceous (Embry & Dixon, 1990; Maher, 2001; Midtkandal & Nystuen, 2009). The onset of regional surface uplift by dynamic topography has commonly preceded magmatism in many continental LIPs all over the Earth (e.g., Cox, 1989; Kent, 1991; Saunders et al., 2007; White & McKenzie, 1989). Also, the inception of a plume in the Arctic Basin is thought to have created a thermal anomaly leading to melting of the SCLM, resulting in the emplacement of some radial dike swarm and basalt flows reported throughout the Arctic region (Buchan & Ernst, 2006; Døssing et al., 2013; Drachev & Saunders, 2006; Evenchick et al., 2015; Golonka & Bocharova, 2000; Lawver et al., 2002; Minakov et al., 2018; Nejbort et al., 2011). The oldest known plume-related volcanic rocks in the region are located in Franz Josef Land, Svalbard, northern Greenland, and on Ellesemere Island in Arctic Canada (Corfu et al., 2013; Maher, 2001; Polteau et al., 2016; Villeneuve & Williamson, 2006). Palinspastic reconstructions show that though now separated by large distances, these regions were once located close to each other, and likely not far from the axial region of the hypothesized plume head (Miller et al., 2018).

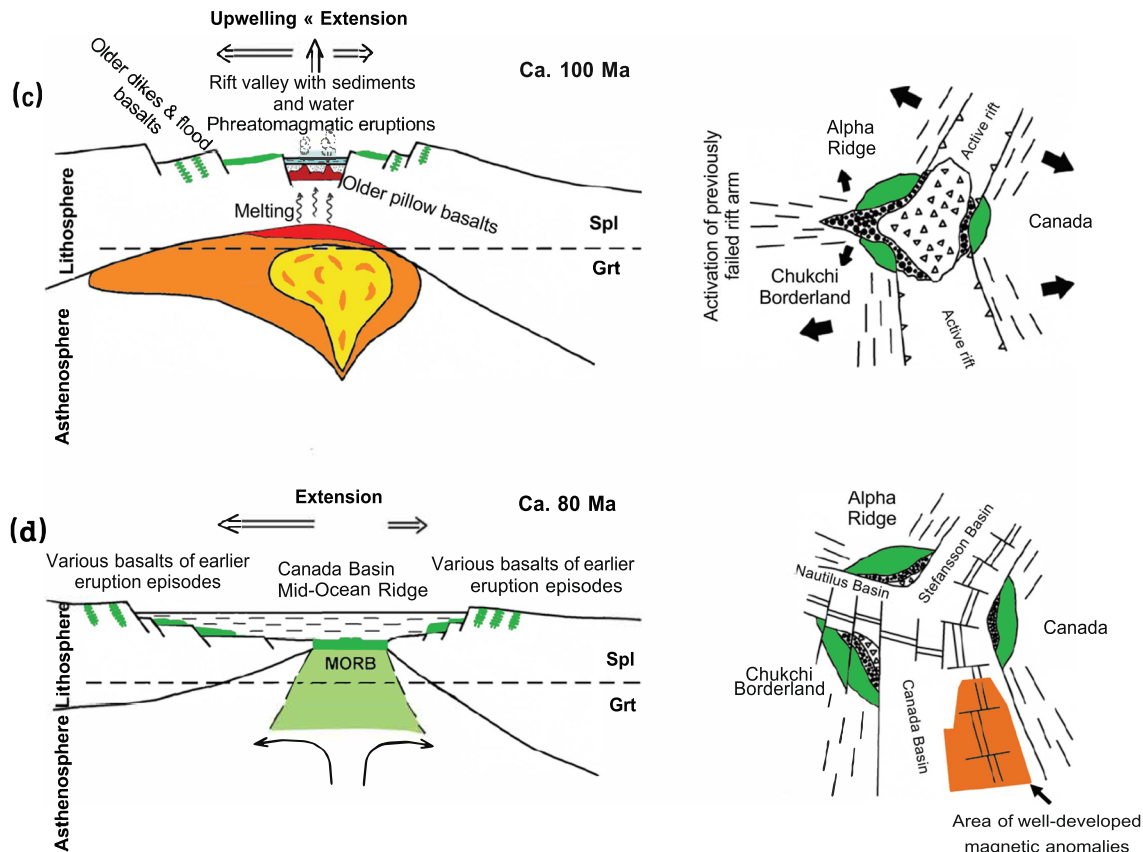


Figure 18. (continued)

It is possible that the later stages of plume impingement, regional doming, continental break up and rifting are recorded in the eruption of subaerial low-Ti tholeiites I of the Northwind Ridge represented by site DR7 (circa 118–112 Ma), basaltic rocks in the DeLong Islands (119–112 Ma; Drachev and Saunders, 2006), and Axel Heiberg Island of the Canada Arctic Archipelago (113 ± 6 Ma; Muecke et al., 1990). However, Dockman et al. (2018) have argued in favor of limiting plume-related magmatism to 128–120 Ma during which only tholeiitic basalts were erupted. Not much is known about the geochemical characteristic of volcanism on the DeLong and Axel Heiberg islands, but our study suggests that tholeiites from our dredge site DR7 were generated in a SCLM source, most likely at high temperatures under the influence of a thermal anomaly introduced by the hypothesized plume head.

### 5.7.3. Development of a Continental Rift

Our data suggest that the geochemical and isotopic characteristics of Amerasia Basin lavas analyzed so far closely resemble those of CFB provinces associated with the prebreakup stages of rifting continents. Following the approach by Kempton et al. (2000) who divided North Atlantic Tertiary basalts into three main groups (prebreakup, breakup and post breakup) based on their Nb-Zr-Y systematics, we have plotted Amerasia Basin lavas in our study on a similar diagram in Figure 17. All of our samples plot in the field for prebreakup basaltic lavas, which along with other geochemical characteristics discussed above, allows us to suggest an intraplate origin and spatial and temporal associations with other lavas in the Arctic region defining the HALIP, which has been linked to a plume by a number of studies (e.g., Buchan & Ernst, 2006; Dockman et al., 2018; Døssing et al., 2013; Drachev & Saunders, 2006; Embry & Osadetz, 1988; Maher Jr., 2001).

We argue that after reaching the bottom of the lithosphere, the ascending plume head was most likely deflected to the west because old, resistant, deep-rooted rocks of the Canadian Shield in the east would not have allowed the plume head to spread evenly in all directions (Figures 18a and 18b). Cooler



peripheral parts of the plume head should then have developed under the present-day Arctic region. We have proposed that in the early stages the plume interacted with the lithospheric mantle within the spinel stability field, producing melts carrying mixed asthenospheric and lithospheric signatures. That is to say, the bottom of the lithosphere to which the plume head became attached was located at a depth not exceeding 65–70 km—this being the boundary between spinel and garnet stability fields in the upper mantle, corresponding to pressures between ~18 and ~22 kbar, depending on the thermal gradient (Beccaluva et al., 2009; Foley et al., 2006). Crustal thinning resulting from the extensional regime induced by the plume was accompanied by deep faulting and development of horsts and grabens that characterize Amerasia Basin and the immediately surrounding areas. Some of the melts may have erupted at this stage of lithospheric attenuation, producing the circa 118–112 Ma low-Ti tholeiites I dredged from Northwind Ridge (Figure 18b).

The low-Ti tholeiites II and high-Ti tholeiites, both erupted at Healy Spur at 105–100 and 90–70 Ma, respectively (Figures 18c and 18d), were produced in a magma source at increasing degrees of partial melting. Lithospheric attenuation continued after eruption of the circa 105–100 Ma lavas such that by the eruption of the 90–70 Ma lavas, the lithospheric geochemical signature was no longer discernable in the mantle beneath Healy Spur. Expression of predominantly asthenospheric geochemical signatures in the high-Ti tholeiites, with hardly any signs of even upper crustal contamination, is interpreted to represent complete removal of the lithosphere beneath Healy Spur by circa 90–70 Ma (Figure 18d). All the melting during at least 30 Myr of volcanic activity in the recovered dredges on Northwind Ridge and Healy Spur—two localities that flank Canada Basin—took place within a narrow depth range: between the garnet-out/spinel-in and spinel-out/plagioclase-in boundaries. That is to say, the pressures in the mantle source(s) were limited to a range between 22 and 9 kbar, corresponding to a mantle column some 40 km thick, at depths between ~30 and ~70 km.

While little is known about late Cretaceous submarine volcanism in the western Arctic, we know from terrestrial lavas around Amerasia Basin that following the widespread eruptions at circa 85–80 Ma, there was dramatic decrease in melt volumes (e.g., Buchan & Ernst, 2006; Villeneuve & Williamson, 2006). Mudie et al. (1986) argued that no significant tectonic activity took place in the eastern part of Alpha Ridge after ~73 Ma. However, there is growing evidence, based on seismic, gravity, and magnetics data that prior to cessation of active rifting in Amerasia Basin, oceanic lithosphere formed. A gravity low reported by Taylor et al. (1981), Forsyth et al. (1986), Grantz et al. (1990), and Coles and Taylor (1990) has been interpreted as a fossilized spreading center. Moreover, geophysical profiles across Canada Basin (Chian et al., 2016; Hutchinson et al., 2009; 2017) have documented layer three refraction velocities and lineated paired magnetic anomalies, consistent with an inactive spreading center of unspecified age in a limited area of Canada Basin (Figure 18d). Discovery by a joint United States-Canada expedition of the USCGC Healy and CCGS Louis S. St-Laurent (August–September 2009) of a seamount in the north-central part of Canada Basin also favors existence of oceanic lithosphere at least in the central part of Canada Basin. It seems, nevertheless, that most tectonic models for the region today still seriously underestimate the importance of vertical motions while overestimating the importance of extensional deformation.

Finally, opening of the Central Atlantic Ocean might serve as an important analog for the tectonic development of Canada Basin and is consistent with the ages we have obtained on the three suites of submarine lavas we have studied. It also helps to provide some boundary conditions for the age of the Canada Basin magnetic anomalies, which as of now have not been dated. Basaltic dikes and sills in the eastern United States, Canada, French Guyana, and Surinam emplaced as Central Atlantic rifting started were dated at circa 205–201 Ma (Deckart et al., 1997; Jourdan et al., 2009; Marzoli et al., 1999; Marzoli et al., 2019; Merle et al., 2011; Sebai et al., 1991; Sutter & Smith, 1979), and oceanic crust with well-developed lineated magnetic anomalies along the eastern seaboard of North America did not appear until circa 175 Ma according to Klitgord and Schouten (1986) and Schouten and Klitgord (1986) or 168.5 Ma according to Greene et al. (2017), some 30–36 Myr later. This history is documented for an Atlantic spreading center characterized as slow (i.e., 1–2 cm/year), similar to what is hypothesized for the now-inactive Canada Basin spreading center based on the morphology of its central valley deep. Faster Central Atlantic opening has been suggested by Jourdan et al. (2007), and references therein, but this was before recognition by Greene et al. (2017) that the oldest magnetic anomalies are as young as 168.5 Ma. Therefore, if Arctic

Continent doming and rifting commenced at circa 130 Ma, we suggest that the oldest magnetic anomalies in Canada Basin are circa 100 Ma or younger. This conclusion is supported by independent evidence presented by Chian et al. (2016) based on magnetic anomaly polarities and oceanic crust thickness in Canada Basin. They argue that positive and negative magnetic anomaly pairs identified in Canada Basin could not have been emplaced during the Cretaceous quiet period, between circa 124 and circa 83 Ma. Yet to invoke an age older than 124 Ma for the anomalies following plume-induced doming of the Arctic Continent at 130 Ma requires unreasonably fast rifting and spreading rates in the range of 3.5–7.5 cm/year, inconsistent with the observed morphology of the central valley deep. Also, such high spreading rates would produce oceanic crust much thicker than the observed 4–7 km. Therefore, earlier assertions by Grantz et al. (2011) for the Canada Basin magnetic anomalies to be no younger than 124 Ma are not supported by these two independent lines of reasoning.

## 6. Conclusions

The following conclusions may be drawn from the study summarized here:

1. Three main episodes of volcanic activity have been identified on the basis of  $^{40}\text{Ar}/^{39}\text{Ar}$  age determinations of submarine basaltic rocks dredged from Amerasia Basin: circa 118–112 Ma low-Ti tholeiites I of the Northwind Ridge and circa 105–100 Ma low-Ti tholeiites II and circa 90–70 Ma high-Ti tholeiites—both from Healy Spur. Our limited number of dredges does not preclude potential for the presence of older submarine lavas, as suggested by exposures on some circum-Arctic landmasses falling in the age range of circa 130 to 120 Ma.
2. The circa 118–112 Ma low-Ti tholeiites I at Northwind Ridge resulted from melting of the SCLM source within the spinel stability field of the upper mantle and were precursory to melting and eruption of magmas from isotopically more depleted sources, including the asthenosphere. Melting events that produced circa 105–100 Ma low-Ti tholeiites II and circa 90–70 Ma high-Ti tholeiites at Healy Spur may be related to ascent of a plume head, and the concomitant melting yielding bimodal distribution of basaltic compositions, typical of plume-related CFB provinces elsewhere.
3. Basalts of the two younger magmatic pulses display progressively increasing asthenospheric signatures from the older circa 105–100 Ma low-Ti tholeiites II to the younger circa 90–70 Ma high-Ti tholeiites, indicating lithospheric attenuation through time, concomitant upwelling, and increased degree of partial melting.
4. All studied volcanic rocks belong to the intraplate volcanic associations whose petrological, geochemical, and isotopic characteristics are consistent with emplacement in a continental setting with thinning lithosphere. Tectonically, the submarine lavas we have studied are likely to be part of the voluminous basaltic lavas of the HALIP, which affected the Arctic region during the onset of rifting that produced Amerasia Basin.
5. All plume-related volcanic activity appears to have stopped after circa 70 Ma in the Amerasia Basin region and perhaps elsewhere in the HALIP, indicating a change in tectonic regime from a continental hot spot environment to an active intraplate rift zone.
6. Occurrence of basaltic volcanism in the same region for the period of at least 50 Myr illustrates the complexity of tectonomagmatic events initiated by plume impingement on the lithosphere and sustained by further rifting, related to far-field changes in stress regimes.
7. Using Central Atlantic Ocean opening at slow spreading rates as an analog, and the documented doming and inception of rifting in the Arctic Continent at 130 Ma, we have deduced that Canada Basin lineated magmatic anomalies associated with a now-inactive spreading center are 100 Ma or younger.

## Data Availability Statement

The data supporting the conclusions presented in this manuscript are provided in the data tables and figures herein and are compared to data fields from some of the references cited. The new data have also been archived by the EarthChem Library at this URL (<https://doi.org/10.1594/IEDA/100555>).

## Acknowledgments

We are indebted to the USCGC Icebreaker HEALY crew and Captain F. Sommer who made the fieldwork possible and also to the whole science team of the HLY0805 mission. C. Hall is thanked for  $^{40}\text{Ar}/^{39}\text{Ar}$  age determinations and C. Knaak and T. Vogel for assistance with the XRF and ICP-MS analyses. This manuscript benefited from discussions with L. A. Lawver, H. R. Jackson, E. L. Miller, C. M. Hall, D. R. Hutchinson, D. C. Mosher, and J. Childs. S.-H. Choi is thanked for critical reading of an earlier version of the manuscript. Invaluable reviews were provided by the Journal Editor Stephen Parman, Associate Editor John Lassiter, external reviewers Fred Jourdan and Renaud Merle, and an anonymous reviewer, to whom we are grateful. This study was supported by NSF Grant NSF OPP-1025513 to S. B. Mukasa and by NOAA Grants NA10NOS4000074 and NA15NOS4000200.

## References

- Akinin, V. V., Prokopiev, A. V., Toro, J., Miller, E. L., Wooden, J., Goryachev, N. A., et al. (2009). U-Pb SHRIMP ages of granitoides from the main batholith belt (North East Asia). *Doklady Earth Sciences*, *426*, 605–610. <https://doi.org/10.1134/S1028334x09040217>
- Aldanmaz, E., Yaliniz, M. K., Guctekin, A., & Goncuoglu, M. C. (2008). Geochemical characteristics of mafic lavas from the Neotethyan ophiolites in western Turkey: Implications for heterogeneous source contribution during variable stages of ocean crust generation. *Geological Magazine*, *145*, 37–54. <https://doi.org/10.1017/S0016756807003986>
- Anders, E., & Grevesse, N. (1989). Abundances of the elements—Meteoritic and solar. *Geochimica et Cosmochimica Acta*, *53*(1), 197–214. [https://doi.org/10.1016/0016-7037\(89\)90286-X](https://doi.org/10.1016/0016-7037(89)90286-X)
- Andronikov, A. V., Mukasa, S. B., Mayer, L. A., & Brumley, K. (2008). First recovery of submarine basalts from the Chukchi Borderland and Alpha/Mendeleev Ridge, Arctic Ocean. *EOS Transactions AGU*, *89*, 53.
- Arndt, N. T., Czamanske, G. K., Wooden, J. L., & Fedorenko, V. A. (1993). Mantle and crustal contributions to continental flood volcanism. *Tectonophysics*, *223*(1–2), 39–52. [https://doi.org/10.1016/0040-1951\(93\)90156-E](https://doi.org/10.1016/0040-1951(93)90156-E)
- Asudeh, I., Green, A. G., & Forsyth, D. A. (1988). Canadian expedition to study the Alpha Ridge complex: Results of the seismic refraction survey. *Geophysical Journal International*, *92*(2), 283–301. <https://doi.org/10.1111/j.1365-246X.1988.tb01140.x>
- Baggeroer, A. B., & Falconer, R. (1982). Array refraction profiles and crustal models of the Canada Basin. *Journal of Geophysical Research*, *87*(N6), 5461–5476. <https://doi.org/10.1029/JB087iB07p05461>
- Beccaluva, L., Bianchini, G., Natali, C., & Siena, F. (2009). Continental flood basalts and mantle plumes: A case study of the northern Ethiopian plateau. *Journal of Petrology*, *73*, A99–A99. <https://doi.org/10.1093/petrology/egp024>
- Bednarz, U., & Schminke, H.-U. (1989). Mass transfer during sub seafloor alteration of the upper Troodos crust (Cyprus). *Contributions to Mineralogy and Petrology*, *102*(1), 93–101. <https://doi.org/10.1007/BF01160193>
- Bizimis, M., Griselin, M., Lassiter, J. C., Salters, V. J. M., & Sen, G. (2007). Ancient recycled mantle lithosphere in the Hawaiian plume: Osmium-hafnium isotopic evidence from peridotite mantle xenoliths. *Earth and Planetary Science Letters*, *257*, 259–273. <https://doi.org/10.1016/j.epsl.2007.02.036>
- Bizimis, M., Sen, G., & Salters, V. J. M. (2004). Hf-Nd isotope decoupling in the oceanic lithosphere: Constraints from spinel peridotites from Oahu, Hawaii. *Earth and Planetary Science Letters*, *217*, 43–58. [https://doi.org/10.1016/S0012-821x\(03\)00598-3](https://doi.org/10.1016/S0012-821x(03)00598-3)
- Blichert-Toft, J., & Arndt, N. T. (1999). Hf isotope compositions of komatiites. *Earth and Planetary Science Letters*, *171*(3), 439–451. [https://doi.org/10.1016/S0012-821x\(99\)00151-X](https://doi.org/10.1016/S0012-821x(99)00151-X)
- Blichert-Toft, J., Frey, F. A., & Albarede, F. (1999). Hf isotope evidence for pelagic sediments in the source of Hawaiian basalts. *Science*, *285*(5429), 879–882. <https://doi.org/10.1126/science.285.5429.879>
- Brandon, A. D., Hooper, P. R., Goles, G. G., & Lambert, R. S. (1993). Evaluating crustal contamination in continental basalts—The isotopic composition of the Picture Gorge Basalt of the Columbia River Basalt Group. *Contributions to Mineralogy and Petrology*, *114*(4), 452–464. <https://doi.org/10.1007/Bf00321750>
- Brumley, K. (2009). *Tectonic geomorphology of the Chukchi Borderland: Constraint for tectonic reconstruction models*. M.Sc. thesis. Fairbanks AK: University of Alaska Fairbanks. 116 p.
- Brumley, K. (2014). *Geologic history of the Chukchi Borderland, Arctic Ocean*. Stanford, California: Stanford University. Ph. D. Thesis, 242 p.
- Brumley, K., Mayer, L., Miller, E. L., & Coakley, B. (2008). Dredged rock samples from the Alpha Ridge, Arctic Ocean: Implications for the tectonic history and origin of the Amerasia Basin. *EOS Transactions AGU*, *89*, Abst.
- Brumley, K., Miller, E. L., Konstantinou, A., Grove, M., Meisling, K. E., & Mayer, L. A. (2015). First bedrock samples dredged from submarine outcrops in the Chukchi borderland, Arctic Ocean. *Geosphere*, *11*, 76–92. <https://doi.org/10.1130/Ges01044.1>
- Brumley, K. J., Mukasa, S. B., O'Brien, T. M., Mayer, L. A., & Chayes, D. N. (2013). Dredged bedrock samples from the Amerasia Basin, Arctic Ocean. In *AGU Fall Meeting Abstracts*, 2013AGUFMOS13B1703B.
- Bryan, W. B., Finger, L. W., & Chayes, F. (1969). Estimating proportions in petrographic mixing equations by least-squares approximation. *Science*, *163*(3870), 926. <https://doi.org/10.1126/science.163.3870.926>
- Buchan, K. L., & Ernst, R. (2006). Giant dyke swarms and the reconstruction of the Canadian Arctic islands, Greenland, Svalbard and Franz Josef Land. *Proceedings of the Monograph in Engineering Waters*, *27*. <https://doi.org/10.1201/NOE0415398992.ch2>
- Buiter, S. J. H., & Torsvik, T. H. (2014). A review of Wilson cycle plate margins: A role for mantle plumes in continental break-up along sutures? *Gondwana Research*, *26*, 627–653. <https://doi.org/10.1016/j.gr.2014.02.007>
- Burgess, S. D., Bowring, S. A., Fleming, T. H., & Elliot, D. H. (2015). High-precision geochronology links the Ferrar large igneous province with early-Jurassic Ocean anoxia and biotic crisis. *Earth and Planetary Science Letters*, *415*, 90–99. <https://doi.org/10.1016/j.epsl.2015.01.037>
- Campbell, I. H., & Griffiths, R. W. (1990). Implications of mantle plume structure for the evolution of flood basalts. *Earth and Planetary Science Letters*, *99*(1–2), 79–93. [https://doi.org/10.1016/0012-821x\(90\)90072-6](https://doi.org/10.1016/0012-821x(90)90072-6)
- Carey, S. W. (1955). The orocline concept in geotectonics. *Royal Society of Tasmania*, *89*, 255–288.
- Chandrasekharam, D., Mahoney, J. J., Sheth, H. C., & Duncan, R. A. (1999). Elemental and Nd-Sr-Pb isotope geochemistry of flows and dikes from the Tapi rift, Deccan flood basalt province, India. *Journal of Volcanology and Geothermal Research*, *93*(1–2), 111–123. [https://doi.org/10.1016/S0377-0273\(99\)00081-5](https://doi.org/10.1016/S0377-0273(99)00081-5)
- Chian, D., Jackson, H. R., Hutchinson, D. R., Shimeld, J. W., Oakey, G. N., Lebedeva-Ivanova, N., et al. (2016). Distribution of crustal types in Canada Basin, Arctic Ocean. *Tectonophysics*, *691*, 8–30. <https://doi.org/10.1016/j.tecto.2016.01.038>
- Choi, S. H., & Mukasa, S. B. (2012). Lu-Hf and Sm-Nd isotope systematics of Korean spinel peridotites: A case for metasomatically induced Nd-Hf decoupling. *Lithos*, *154*, 263–276. <https://doi.org/10.1016/j.lithos.2012.07.017>
- Coffin, M. F., & Eldholm, O. (1994). Large igneous provinces—Crustal structure, dimensions, and external consequences. *Reviews of Geophysics*, *32*(1), 1–36. <https://doi.org/10.1029/93rg02508>
- Coles, R. L., & Taylor, P. (1990). Magnetic anomalies. In A. Grantz, L. Johnson, & J. F. Sweeney (Eds.), *The Arctic Ocean Region* (pp. 119–132). Boulder: Geological Society of America.
- Corfu, F., Polteau, S., Planke, S., Faleide, J. I., Svensen, H., Zayoncheck, A., & Stolbov, N. (2013). U-Pb geochronology of cretaceous magmatism on Svalbard and Franz Josef Land, Barents Sea large Igneous Province. *Geological Magazine*, *150*(6), 1127–1135. <https://doi.org/10.1017/S0016756813000162>
- Cox, K. G. (1989). The role of mantle plumes in the development of continental drainage patterns. *Nature*, *342*(6252), 873–877. <https://doi.org/10.1038/342873a0>

- Deckart, K., Feraud, G., & Bertrand, H. (1997). Age of Jurassic continental tholeiites of French Guyana, Surinam and Guinea: Implications for the initial opening of the Central Atlantic Ocean. *Earth and Planetary Science Letters*, *150*(3–4), 205–220. [https://doi.org/10.1016/S0012-821x\(97\)00102-7](https://doi.org/10.1016/S0012-821x(97)00102-7)
- D'Errico, M. E., Warren, J. M., & Godard, M. (2016). Evidence for chemically heterogeneous Arctic mantle beneath the Gakkel Ridge. *Geochimica et Cosmochimica Acta*, *174*, 291–312. <https://doi.org/10.1016/j.gca.2015.11.017>
- Dietz, R. S., & Shumway, G. (1961). Arctic basin geomorphology. *Geological Society of America Bulletin*, *72*(9), 1319. [https://doi.org/10.1130/0016-7606\(1961\)72\[1319:Abg\]2.0.Co;2](https://doi.org/10.1130/0016-7606(1961)72[1319:Abg]2.0.Co;2)
- Dixon, J., & Dietrich, J. R. (1990). Canadian Beaufort Sea and adjacent land areas. In A. Grantz, L. Johnson, & J. F. Sweeney (Eds.), *The Arctic Ocean Region* (pp. 239–256). Boulder: Geological Society of America.
- Dockman, D. M., Pearson, D. G., Heaman, L. M., Gibson, S. A., & Sarkar, C. (2018). Timing and origin of magmatism in the Sverdrup Basin, northern Canada—implications for lithospheric evolution in the high Arctic large Igneous Province (HALIP). *Tectonophysics*, *742–743*, 50–65. <https://doi.org/10.1016/j.tecto.2018.05.010>
- Dössing, A., Gaina, C., & Brozena, J. M. (2017). Building and breaking a large igneous province: An example from the High Arctic. *Geophysical Research Letters*, *44*(12), 6011–6019. <https://doi.org/10.1002/2016gl072420>
- Doré, A. G., Lundin, E. R., Gibbons, A., Somme, T. O., & Torudbakken, B. O. (2016). Transform margins of the Arctic: A synthesis and re-evaluation. *Transform Margins: Development, Controls and Petroleum Systems*, *431*, 63–94. <https://doi.org/10.1144/Sp431.8>
- Dössing, A., Jackson, H. R., Matzka, J., Einarsson, I., Rasmussen, T. M., Olesen, A. V., & Brozena, J. M. (2013). On the origin of the Amerasia Basin and the high Arctic large Igneous Province—Results of new aeromagnetic data. *Earth and Planetary Science Letters*, *363*, 219–230. <https://doi.org/10.1016/j.epsl.2012.12.013>
- Drachev, S., & Saunders, A. (2006). *The early cretaceous Arctic LIP: Its geodynamic setting and implications for Canada Basin opening*. In *Proceedings of the Fourth International Conference on Arctic Margins* (pp. 216–223). Anchorage, USA: U.S. Department of the Interior Minerals Management Service Alaska Outer Continental Shelf Region.
- Elmore, A. C., Piotrowski, A. M., Wright, J. D., & Scrivner, A. E. (2011). Testing the extraction of past seawater Nd isotopic composition from North Atlantic deep sea sediments and foraminifera. *Geochemistry, Geophysics, Geosystems*, *12*, Q09008. <https://doi.org/10.1029/2011gc003741>
- Embry, A. F. (1990). Geological and geophysical evidence in support of the hypothesis of anticlockwise rotation of Northern Alaska. *Marine Geology*, *93*(1–4), 317–329. [https://doi.org/10.1016/0025-3227\(90\)90090-7](https://doi.org/10.1016/0025-3227(90)90090-7)
- Embry, A. F., & Dixon, J. (1990). The breakup unconformity of the Amerasia Basin, Arctic-Ocean—Evidence from Arctic Canada. *Geological Society of America Bulletin*, *102*(11), 1526–1534. [https://doi.org/10.1130/0016-7606\(1990\)102%3C1526:Tbuota%3E2.3.Co;2](https://doi.org/10.1130/0016-7606(1990)102%3C1526:Tbuota%3E2.3.Co;2)
- Embry, A. F., & Osadetz, K. G. (1988). Stratigraphy and tectonic significance of cretaceous volcanism in the queen Elizabeth Islands, Canadian Arctic archipelago. *Canadian Journal of Earth Sciences*, *25*(8), 1209–1219. <https://doi.org/10.1139/e88-118>
- Encarnación, J., Fleming, T. H., Elliot, D. H., & Eales, H. V. (1996). Synchronous emplacement of Ferrar and Karoo dolerites and the early breakup of Gondwana. *Geology*, *24*(6), 535–538. [https://doi.org/10.1130/0091-7613\(1996\)024%3C0535:Seofak%3E2.3.Co;2](https://doi.org/10.1130/0091-7613(1996)024%3C0535:Seofak%3E2.3.Co;2)
- Estrada, S., & Henjes-Kunst, F. (2004). Volcanism in the Canadian high Arctic related to the opening of the Arctic Ocean. *Zeitschrift der Deutschen Geologischen Gesellschaft*, *154*, 579–603. <https://doi.org/10.1127/zdgg/154/2004/579>
- Evangelatos, J., Funck, T., & Mosher, D. C. (2017). The sedimentary and crustal velocity structure of Makarov Basin and adjacent Alpha Ridge. *Tectonophysics*, *696–697*, 99–114. <https://doi.org/10.1016/j.tecto.2016.12.026>
- Evenchick, C. A., Davis, W. J., Bedard, J. H., Hayward, N., & Friedman, R. M. (2015). Evidence for protracted high Arctic large igneous province magmatism in the Central Sverdrup Basin from stratigraphy, geochronology, and paleodepths of saucer-shaped sills. *Geological Society of America Bulletin*, *127*, 1366–1390. <https://doi.org/10.1130/B31190.1>
- Falloon, T. J., & Green, D. H. (1989). The solidus of carbonated, fertile peridotite. *Earth and Planetary Science Letters*, *94*(3–4), 364–370. [https://doi.org/10.1016/0012-821x\(89\)90153-2](https://doi.org/10.1016/0012-821x(89)90153-2)
- Fitton, J. G., Saunders, A. D., Norry, M. J., Hardarson, B. S., & Taylor, R. N. (1997). Thermal and chemical structure of the Iceland plume. *Earth and Planetary Science Letters*, *153*(3–4), 197–208. [https://doi.org/10.1016/S0012-821x\(97\)00170-2](https://doi.org/10.1016/S0012-821x(97)00170-2)
- Flinders, A. F., Mayer, L. A., Calder, B. A., & Armstrong, A. A. (2014). Evaluation of Arctic multibeam sonar data quality using nadir crossover error analysis and compilation of a full-resolution data product. *Computer and Geosciences-UK*, *66*, 228–236. <https://doi.org/10.1016/j.cageo.2014.02.003>
- Foley, S. F., Andronikov, A. V., Jacob, D. E., & Melzer, S. (2006). Evidence from Antarctic mantle peridotite xenoliths for changes in mineralogy, geochemistry and geothermal gradients beneath a developing rift. *Geochimica et Cosmochimica Acta*, *70*, 3096–3120. <https://doi.org/10.1016/j.gca.2006.03.010>
- Forsyth, D. A., Morelhuissier, P., Asudeh, I., & Green, A. G. (1986). Alpha-Ridge and Iceland—Products of the same plume. *Journal of Geodynamics*, *6*(1–4), 197–214. [https://doi.org/10.1016/0264-3707\(86\)90039-6](https://doi.org/10.1016/0264-3707(86)90039-6)
- Freeland, G. L., & Dietz, R. S. (1973). Rotation history of Alaskan tectonic blocks. *Tectonophysics*, *18*(3–4), 379–389. [https://doi.org/10.1016/0040-1951\(73\)90054-1](https://doi.org/10.1016/0040-1951(73)90054-1)
- French, S. W., & Romanowicz, B. (2015). Broad plumes rooted at the base of the Earth's mantle beneath major hotspots. *Nature*, *525*(7567), 95–99. <https://doi.org/10.1038/nature14876>
- Fretzdorff, S., Livermore, R. A., Devey, C. W., Leat, P. T., & Stoffers, P. (2002). Petrogenesis of the back-arc east Scotia Ridge, South Atlantic Ocean. *Journal of Petrology*, *43*(8), 1435–1467. <https://doi.org/10.1093/petrology/43.8.1435>
- Fromm, T., Planert, L., Jokat, W., Ryberg, T., Behrmann, J. H., Weber, M. H., & Haberland, C. (2015). South Atlantic opening: A plume-induced breakup? *Geology*, *43*, 931–934. <https://doi.org/10.1130/G36936.1>
- Gaina, C., Medvedev, S., Torsvik, T. H., Koulakov, I., & Werner, S. C. (2014). 4D Arctic: A glimpse into the structure and evolution of the Arctic in the light of new geophysical maps, plate tectonics and tomographic models. *Surveys in Geophysics*, *35*, 1095–1122. <https://doi.org/10.1007/s10712-013-9254-y>
- Gaina, C., Werner, S., Saltus, R., Maus, S., & the CAMP-GM Group (2011). Circum-Arctic mapping project—New magnetic and gravity anomaly maps of the Arctic. In A. M. Spencer (Ed.), *Arctic Petroleum Geology* (Vol. 35, pp. 39–48). London: Geological Society of London Memoir. <https://doi.org/10.1144/M35.3>
- Gale, A., Dalton, C. A., Langmuir, C. H., Su, Y. J., & Schilling, J. G. (2013). The mean composition of ocean ridge basalts. *Geochemistry, Geophysics, Geosystems*, *14*, 489–518. <https://doi.org/10.1029/2012gc004334>
- Geldmacher, J., Hanan, B. B., Blichert-Toft, J., Harpp, K., Hoernle, K., Hauff, F., et al. (2003). Hafnium isotopic variations in volcanic rocks from the Caribbean Large Igneous Province and Galapagos hot spot tracks. *Geochemistry, Geophysics, Geosystems*, *4*, 1062. <https://doi.org/10.1029/2002gc000477>

- Gill, J. B. (1976). Composition and Age of Lau Basin and ridge volcanic-rocks—Implications for evolution of an interarc basin and remnant arc. *Geological Society of America Bulletin*, 87(10), 1384–1395. [https://doi.org/10.1130/0016-7606\(1976\)87%3C1384:Caaolb%3E2.0.Co;2](https://doi.org/10.1130/0016-7606(1976)87%3C1384:Caaolb%3E2.0.Co;2)
- Goldstein, S. L., Soffer, G., Langmuir, C. H., Cai, Y., Lehnert, K. A., Graham, D. W., & Michael, P. J. (2008). The Gakkel Ridge—A smoking gun for an origin of DUPAL mantle. *Geochimica et Cosmochimica Acta*, 72, A316–A316.
- Golonka, J., & Bocharova, N. Y. (2000). Hot spot activity and the break-up of Pangea. *Palaeogeography, Palaeoclimatology, Palaeoecology*, 161, 49–69. [https://doi.org/10.1016/S0031-0182\(00\)00117-6](https://doi.org/10.1016/S0031-0182(00)00117-6)
- Grantz, A. (2006). Geophysical and geological evidence that Amerasia Basin, Arctic Ocean was created by two phases of anti-clockwise rotation. In *GSA, 81 Ann Meeting Pacific Section AAPG*. Paper No 42-4. Oxnard, CA: Pacific Section AAPG.
- Grantz, A., Clark, D. L., Phillips, R. L., Srivastava, S. P., Blome, C. D., Gray, L. B., et al. (1998). Phanerozoic stratigraphy of Northwind Ridge, magnetic anomalies in the Canada Basin, and the geometry and timing of rifting in the Amerasia Basin, Arctic Ocean. *Geological Society of America Bulletin*, 110(6), 801–820. [https://doi.org/10.1130/0016-7606\(1998\)110%3C0801:Psonrm%3E2.3.Co;2](https://doi.org/10.1130/0016-7606(1998)110%3C0801:Psonrm%3E2.3.Co;2)
- Grantz, A., Eitrem, S., & Dinter, D. A. (1979). Geology and tectonic development of the continental-margin north of Alaska. *Tectonophysics*, 59(1–4), 263–291. [https://doi.org/10.1016/0040-1951\(79\)90050-7](https://doi.org/10.1016/0040-1951(79)90050-7)
- Grantz, A., Hart, P. E., & Childers, V. A. (2011). Geology and tectonic development of the Amerasia and Canada basins, Arctic Ocean. *Geological Society Memoir*, 35(1), 771–799. <https://doi.org/10.1144/M35.50>
- Grantz, A., Johnson, G. L., Sweeney, J. F. G., May, S. D., & Hart, P. E. (1990). Geology of the Arctic continental margin of Alaska. In A. Grantz, L. Johnson, & J. F. Sweeney (Eds.), *The Arctic Ocean Region* (pp. 257–288). Boulder: Geological Society of America.
- Grantz, A., & May, S. D. (1983). Geologic framework and petroleum potential of United-States Chukchi shelf north of point-Hope, Alaska. *AAPG Bulletin*, 67(3), 474–474. <https://doi.org/10.1306/03b5b0b5-16d1-11d7-8645000102c1865d>
- Green, D. H. (1973). Experimental melting studies on a model upper mantle composition at high-pressure under water-saturated and water-undersaturated conditions. *Earth and Planetary Science Letters*, 19, (1), 37–53. [https://doi.org/10.1016/0012-821x\(73\)90176-3](https://doi.org/10.1016/0012-821x(73)90176-3)
- Greene, A. R., Scoates, J. S., & Weis, D. (2008). Wrangellia flood basalts in Alaska: A record of plume-lithosphere interaction in a Late Triassic accreted oceanic plateau. *Geochemistry, Geophysics, Geosystems*, 9, Q12004. <https://doi.org/10.1029/2008gc002092>
- Greene, J. A., Tominaga, M., Miller, N. C., Hutchinson, D. R., & Karl, M. R. (2017). Refining the formation and early evolution of the eastern north American margin: New insights from multiscale magnetic anomaly analyses. *Journal of Geophysical Research: Solid Earth*, 122, 8724–8748. <https://doi.org/10.1002/2017jb014308>
- Gribble, R. F., Stern, R. J., Newman, S., Bloomer, S. H., & O'Hearn, T. (1998). Chemical and isotopic composition of lavas from the Northern Mariana Trough: Implications for magmagenesis in back-arc basins. *Journal of Petrology*, 39(1), 125–154. <https://doi.org/10.1093/ptrology/39.1.125>
- Gurevich, N. I., Merkur'ev, S. A., & Abel'skaya, A. A. (2006). Evolution of the southern part of the Canada Basin (Arctic Ocean) based on magnetometric data. *Doklady Earth Sciences*, 407, 308–311. <https://doi.org/10.1134/S1028334x06020358>
- Halama, R., Marks, M., Brüggemann, G., Siebel, W., Wenzel, T., & Markl, G. (2004). Crustal contamination of mafic magmas: Evidence from a petrological, geochemical and Sr-Nd-Os-O isotopic study of the Proterozoic Isortoq dike swarm, South Greenland. *Lithos*, 74(3–4), 199–232. <https://doi.org/10.1016/j.lithos.2004.03.004>
- Hall, C. M., Kesler, S. E., Russell, N., Piñero, E., Sánchez, R., Pérez, M., et al. (2004). Age and tectonic setting of the Camagüey volcanic-intrusive arc, Cuba: Late Cretaceous extension and uplift in the western Greater Antilles. *The Journal of Geology*, 112, 521–542. <https://doi.org/10.1086/422664>
- Hall, J. K. (1990). Chukchi Borderland. In A. Grantz, L. Johnson, & J. F. Sweeney (Eds.), *The Arctic Ocean Region* (pp. 593–616). Boulder: Geol. Soc. Amer.
- Hannah, R. S., Vogel, T. A., Patino, L. C., Alvarado, G. E., Perez, W., & Smith, D. R. (2002). Origin of silicic volcanic rocks in Central Costa Rica: A study of a chemically variable ash-flow sheet in the Tiribi tuff. *Bulletin of Volcanology*, 64(2), 117–133. <https://doi.org/10.1007/s00445-001-0188-8>
- Harbert, W., Frei, L., Jarrard, R., Halgedahl, S., & Engebretson, D. (1990). Paleomagnetic and plate-tectonic constraints on the evolution of the Alaskan-eastern Siberian Arctic. In A. Grantz, L. Johnson, & J. F. Sweeney (Eds.), *The Arctic Ocean Region* (pp. 567–593). Boulder, Colorado: Geological Society of America, geology of North America.
- Hart, S. R. (1984). A large-scale isotope anomaly in the Southern Hemisphere mantle. *Nature*, 309(5971), 753–757. <https://doi.org/10.1038/309753a0>
- Hart, S. R. (1988). Heterogeneous mantle domains—Signatures, genesis and mixing chronologies. *Earth and Planetary Science Letters*, 90(3), 273–296. [https://doi.org/10.1016/0012-821x\(88\)90131-8](https://doi.org/10.1016/0012-821x(88)90131-8)
- Hart, S. R., & Davis, K. E. (1978). Nickel partitioning between olivine and silicate melt. *Earth and Planetary Science Letters*, 40(2), 203–219. [https://doi.org/10.1016/0012-821x\(78\)90091-2](https://doi.org/10.1016/0012-821x(78)90091-2)
- Hemond, C., Arndt, N. T., Lichtenstein, U., Hofmann, A. W., Oskarsson, N., & Steinthorsson, S. (1993). The heterogeneous Iceland plume—Nd-Sr-O isotopes and trace-element constraints. *Journal of Geophysical Research*, 98(B9), 15833–15850. <https://doi.org/10.1029/93jb01093>
- Hill, J. D. (1991). Emplacement and Tectonic Implications of the Midproterozoic Peralkaline Flowers River Igneous Suite, North-Central Labrador. *Precambrian Research*, 49(3–4), 217–227. [https://doi.org/10.1016/0301-9268\(91\)90033-7](https://doi.org/10.1016/0301-9268(91)90033-7)
- Hutchinson D.R., D. Chian, H. R. Jackson, N. Lebedeva-Ivanova, J. Shimeld, Q. Li, et al. (2015). *Oceanic crust in the Canada Basin of the Arctic Ocean*. *Geophysical Research Abstracts* 17, EGU2015–5543, 2015 EGU General Assembly. Vienna, Austria: European Geosciences Union.
- Hutchinson, D. R., Jackson, H. R., Houseknecht, D. W., Li, Q., Shimeld, J. W., Mosher, D. C., et al. (2017). Significance of northeast-trending features in Canada Basin, Arctic Ocean. *Geochemistry, Geophysics, Geosystems*, 18, 4156–4178. <https://doi.org/10.1002/2017gc007099>
- Hutchinson, D. R., Jackson, H. R., Shimeld, J. W., Chapman, C. B., Childs, J. R., Funck, T., & Rowland, R. W. (2009). Acquiring marine data in Canada Basin, Arctic Ocean. *Eos*, 90, 197–198. <https://doi.org/10.1029/2009EO230001>
- Ionov, D. A., Bodinier, J. L., Mukasa, S. B., & Zanetti, A. (2002). Mechanisms and sources of mantle metasomatism: Major and trace element compositions of peridotite xenoliths from Spitsbergen in the context of numerical modelling. *Journal of Petrology*, 43, 2219–2259. <https://doi.org/10.1093/ptrology/43.12.2219>
- Ivanov, A. V., Mukasa, S. B., Kamenetsky, V. S., Ackerson, M., Demonterova, E. I., Pokrovsky, B. G., et al. (2018). Volatile concentrations in olivine-hosted melt inclusions from meimechite and melanephelinite lavas of the Siberian traps large Igneous Province: Evidence for flux-related high-Ti, high-mg magmatism. *Chemical Geology*, 483, 442–462. <https://doi.org/10.1016/j.chemgeo.2018.03.011>

- Jackson, H. R., Forsyth, D. A., & Johnson, G. L. (1986). Oceanic affinities of the Alpha Ridge, Arctic Ocean. *Marine Geology*, 73(3–4), 237–261. [https://doi.org/10.1016/0025-3227\(86\)90017-4](https://doi.org/10.1016/0025-3227(86)90017-4)
- Jicha, B. R., Singer, B. S., Brophy, J. G., Fournelle, J. H., Johnson, C. M., Beard, B. L., et al. (2004). Variable impact of the subducted slab on Aleutian island arc magma sources: Evidence from Sr, Nd, Pb, and Hf isotopes and trace element abundances. *Journal of Petrology*, 45(9), 1845–1875. <https://doi.org/10.1093/petrology/egh036>
- Johnson, D. M., Hooper, P. R., & Conrey, R. M. (1999). XRF analysis of rocks and minerals for major and trace elements on single dilution Li-tetraborate fused bead. *Advances in X-Ray Analysis*, 41, 843–867.
- Jokat, W. (2003). Seismic investigations along the western sector of Alpha Ridge, central Arctic Ocean. *Geophysical Journal International*, 152(1), 185–201. <https://doi.org/10.1046/j.1365-246X.2003.01839.x>
- Jokat, W., Ickrath, M., & O'Connor, J. (2013). Seismic transect across the Lomonosov and Mendeleev ridges: Constraints on the geological evolution of the Amerasia Basin, Arctic Ocean. *Geophysical Research Letters*, 40, 5047–5051. <https://doi.org/10.1002/grl.50975>
- Jokat, W., Stein, R., Rachor, E., & Schewe, I. (1999). Expedition gives fresh view of Central Arctic geology. *Eos, Transactions American Geophysical Union*, 80(465), 472–473. <https://doi.org/10.1029/eo080i040p00465-01>
- Jokat, W., Uenzelmannneben, G., Kristoffersen, Y., & Rasmussen, T. M. (1992). Lomonosov Ridge - a Double-Sided Continental-Margin. *Geology*, 20(10), 887–890. [https://doi.org/10.1130/0091-7613\(1992\)020%3C0887:Lradsce%3E2.3.Co;2](https://doi.org/10.1130/0091-7613(1992)020%3C0887:Lradsce%3E2.3.Co;2)
- Jourdan, F., Bertrand, H., Scharer, U., Blichert-Toft, J., Feraud, G., & Kampunzu, A. B. (2007). Major and trace element and Sr, Nd, Hf and Pb isotope compositions of the Karoo large igneous province, Botswana-Zimbabwe: Lithosphere vs mantle plume contribution. *Journal of Petrology*, 48, 1043–1077. <https://doi.org/10.1093/petrology/egm010>
- Jourdan, F., Feraud, G., Bertrand, H., & Watkeys, M. K. (2007). From flood basalts to the inception of oceanization: Example from the <sup>40</sup>Ar/<sup>39</sup>Ar high-resolution picture of the Karoo large igneous province. *Geochemistry, Geophysics, Geosystems*, 8, Q02002. <https://doi.org/10.1029/2006gc001392>
- Jourdan, F., Feraud, G., Bertrand, H., Watkeys, M., & Renne, P. R. (2007). Distinct brief major events in the Karoo large igneous province clarified by new Ar-40/Ar-39 ages on the Lesotho basalts. *Lithos*, 98(1–4), 195–209. <https://doi.org/10.1016/j.lithos.2007.03.002>
- Jourdan, F., Marzoli, A., Bertrand, H., Cirilli, S., Tanner, L. H., Kontak, D. J., et al. (2009). Ar-40/Ar-39 ages of CAMP in North America: Implications for the Triassic-Jurassic boundary and the K-40 decay constant bias. *Lithos*, 110, 167–180. <https://doi.org/10.1016/j.lithos.2008.12.011>
- Jowitz, S. M., Williamson, M. C., & Ernst, R. E. (2014, 307). Geochemistry of the 130 to 80 Ma Canadian High Arctic Large Igneous Province (HALIP) event and implications for Ni-Cu-PGE prospectivity. *Economic Geology*, 109, 281. <https://doi.org/10.2113/econgeo.109.2.281>
- Kamenetsky, V. S., Maas, R., Kamenetsky, M. B., Yaxley, G. M., Ehrig, K., Zellmer, G. F., et al. (2017). Multiple mantle sources of continental magmatism: Insights from "high-Ti" picrites of Karoo and other large igneous provinces. *Chemical Geology*, 455, 22–31. <https://doi.org/10.1016/j.chemgeo.2016.08.034>
- Kempton, P. D., Fitton, J. G., Saunders, A. D., Nowell, G. M., Taylor, R. N., Hardarson, B. S., & Pearson, G. (2000). The Iceland plume in space and time: A Sr-Nd-Pb-Hf study of the North Atlantic rifted margin. *Earth and Planetary Science Letters*, 177, 255–271. [https://doi.org/10.1016/S0012-821x\(00\)00047-9](https://doi.org/10.1016/S0012-821x(00)00047-9)
- Kent, R. (1991). Lithospheric uplift in Eastern Gondwana—Evidence for a long-lived mantle plume system. *Geology*, 19, (1), 19–23. [https://doi.org/10.1130/0091-7613\(1991\)019%3C0019:Luiage%3E2.3.Co;2](https://doi.org/10.1130/0091-7613(1991)019%3C0019:Luiage%3E2.3.Co;2)
- Klitgord, K. D., & Schouten, H. A. (1986). Plate kinematics of the central Atlantic. In P. R. Vogt, & B. E. Tucholke (Eds.), *The Western North Atlantic Region* (pp. 351–378). Boulder, Colorado: Geol Soc Amer, Geology of North America.
- Knaak, C., Cornelius, S. B., & Hooper, P. R. (1994). *Trace element analyses of rocks and minerals by ICP-MS*. Washington State University: Department of Geology. Open-File Report, 18p
- Krishnamurthy, P., & Cox, K. G. (1977). Picrite basalts and related lavas from Deccan Traps of western India. *Contributions to Mineralogy and Petrology*, 62(1), 53–75. <https://doi.org/10.1007/Bf00371027>
- Kuzmichev, A. B. (2009). Where does the south Anyui suture go in the new Siberian islands and Laptev Sea?: Implications for the Amerasia basin origin. *Tectonophysics*, 463, 86–108. <https://doi.org/10.1016/j.tecto.2008.09.017>
- Lawver, L. A., Gahagan, L. M., & Norton, I. (2011). Palaeogeographic and tectonic evolution of the Arctic region during the Palaeozoic. *Geological Society, London, Memoirs*, 35, <https://doi.org/10.1144/M35.5>
- Lawver, L. A., Grantz, A., & Gahagan, L. M. (2002). Plate kinematic evolution for the present Arctic region since the Ordovician. In *Tectonic evolution of the Bering Shelf-Chukchi Sea-Arctic margin and adjacent landmasses* (Vol. 360, pp. 333–358). Boulder, CO: Geological Society of America.
- Lebedeva-Ivanova, N. N., Zamansky, Y. Y., Langinen, A. E., & Sorokin, M. Y. (2006). Seismic profiling across the Mendeleev Ridge at 82°N: Evidence of continental crust. *Geophysical Journal International*, 165, 527–544. <https://doi.org/10.1111/j.1365-246X.2006.02859.x>
- Levskii, L. K., Stolbov, N. M., Bogomolov, E. S., Vasilieva, I. M., & Makarieva, E. M. (2006). Sr-Nd-Pb isotopic systems in basalts of the Franz Josef Land archipelago. *Geochemistry International*, 44, 327–337. <https://doi.org/10.1134/S0016702906040021>
- Luttinen, A. V., Heinonen, J. S., Kurhila, M., Jourdan, F., Manttari, I., Vuori, S. K., & Huhma, H. (2015). Depleted mantle-sourced CFB Magmatism in the Jurassic Africa-Antarctica rift: Petrology and <sup>40</sup>Ar/<sup>39</sup>Ar and U/Pb chronology of the Vestfjella dyke swarm, Dronning Maud land, Antarctica. *Journal of Petrology*, 56, 919–952. <https://doi.org/10.1093/petrology/egv022>
- Lyberis, N., & Manby, G. (2001). The Eureka deformation of north and eastern North Greenland. *Polarforschung*, 69, 95–106. <https://doi.org/10.1029/2001TC901040>
- Maher, H. D. (2001). Manifestations of the Cretaceous high Arctic large igneous province in Svalbard. *Journal of Geology*, 109, (1), 91–104, 104. <https://doi.org/10.1086/317960>
- Martin, E. E., & Scher, H. D. (2004). Preservation of seawater Sr and Nd isotopes in fossil fish teeth: Bad news and good news. *Earth and Planetary Science Letters*, 220, 25–39. [https://doi.org/10.1016/S0012-821x\(04\)00030-5](https://doi.org/10.1016/S0012-821x(04)00030-5)
- Marzoli, A., Bertrand, H., Youbi, N., Callegaro, S., Merle, R., Reischberg, L., et al. (2019). The Central Atlantic Magmatic Province (CAMP) in Morocco. *Journal of Petrology*, 60, 945–996. <https://doi.org/10.1093/petrology/egz021>
- Marzoli, A., Renne, R., Piccirillo, E. M., Ernesto, M., Bellieni, G., & De Min, A. (1999). Extensive 200-million-year-old continental flood basalts of the Central Atlantic magmatic province. *Science*, 284(5414), 616–618. <https://doi.org/10.1126/science.284.5414.616>
- Mayer, L. A., & Armstrong, A. A. (2008). U.S. law of the sea cruise to map the foot of the slope and 2500-m Isobath of the U.S. Arctic Ocean margin. In *Cruise report for 2008*. (pp. 1–179). Durham, NH: University of new Hampshire (UNH), Center for Coastal and Ocean Mapping (CCOM)/joint hydrographic center (JHC).
- Mayer, L. A., Brumley, K., Andronikov, A., Chayes, D. N., Armstrong, A. A., Calder, B., et al. (2008). Recent mapping and sampling on Chukchi Borderland and Alpha/Mendeleev Ridge complex. *Eos, Transactions of the American Geophysical Union*, 89.

- McDonough, W. F. (1990). Constraints on the composition of the continental lithospheric mantle. *Earth and Planetary Science Letters*, 101(1), 1–18. [https://doi.org/10.1016/0012-821x\(90\)90119-1](https://doi.org/10.1016/0012-821x(90)90119-1)
- McDonough, W. F., & Sun, S. S. (1995). The composition of the Earth. *Chemical Geology*, 120(3–4), 223–253. [https://doi.org/10.1016/0009-2541\(94\)00140-4](https://doi.org/10.1016/0009-2541(94)00140-4)
- Merle, R., Jourdan, F., & Girardeau, J. (2018). Geochronology of the Tore-Madeira Rise seamounts and surrounding areas: A review. *Australian Journal of Earth Sciences*, 65, 591–605. <https://doi.org/10.1080/08120099.2018.1471005>
- Merle, R., Marzoli, A., Bertrand, H., Reisberg, L., Verati, C., Zimmermann, C., et al. (2011). Ar-40/Ar-39 ages and Sr-Nd-Pb-Os geochemistry of CAMP tholeiites from Western Maranhao basin (NE Brazil). *Lithos*, 122, 137–151. <https://doi.org/10.1016/j.lithos.2010.12.010>
- Meshesha, D., & Shinjo, R. (2007). Crustal contamination and diversity of magma sources in the northwestern Ethiopian volcanic province. *Journal of Mineralogical and Petrological Sciences*, 102, 272–290. <https://doi.org/10.2465/jmps.061129>
- Midtkandal, I., & Nystuen, J. P. (2009). Depositional architecture of a low-gradient ramp shelf in an epicontinental sea: The lower cretaceous of Svalbard. *Basin Research*, 21, 655–675. <https://doi.org/10.1111/j.1365-2117.2009.00399.x>
- Miller, E. L., Gehrels, G. E., Pease, V., & Sokolov, S. (2010). Stratigraphy and U-Pb detrital zircon geochronology of Wrangel Island, Russia: Implications for Arctic paleogeography. *AAPG Bulletin*, 94, 665–692. <https://doi.org/10.1306/10200909036>
- Miller, E. L., Gelman, M., Parfenov, L., & Hourigan, J. (2002). Tectonic setting of Mesozoic magmatism: A comparison between north-eastern Russia and the north American cordillera. In E. L. Miller, A. Grantz, & S. L. Klemperer (Eds.), *Tectonic evolution of the Bering Shelf-Chukchi Sea Arctic Margin and Adjacent landmasses* (Vol. 360, pp. 333–358). Boulder, CO: Spec. Paper GSA.
- Miller, E. L., Meisling, K. E., Akinin, V. V., Brumley, K., Coakley, B. J., Gottlieb, E. S., et al. (2018). Circum-Arctic lithosphere evolution (CALE) transect C: Displacement of the Arctic Alaska-Chukotka microplate towards the Pacific during opening of the Amerasia Basin of the Arctic. *Circum-Arctic Lithosphere Evolution*, 460, 57–120. <https://doi.org/10.1144/Sp460.9>
- Miller, E. L., Toro, J., Gehrels, G., Amato, J. M., Prokopiev, A., Tuchkova, M. I., et al. (2006). New insights into Arctic paleogeography and tectonics from U-Pb detrital zircon geochronology. *Tectonics*, 25, TC3013. <https://doi.org/10.1029/2005TC001830>
- Millett, J. M., Hole, M. J., Jolley, D. W., & Passey, S. R. (2017). Geochemical stratigraphy and correlation within large igneous provinces: The final preserve stages of the Faroe Islands basalt group. *Lithos*, 286–287, 1–15. <https://doi.org/10.1016/j.lithos.2017.05.011>
- Millhollen, G. L., Irving, A. J., & Wyllie, P. J. (1974). Melting interval of peridotite with 5.7 per cent water to 30 kilobars. *Journal of Geology*, 82(5), 575–587. <https://doi.org/10.1086/628007>
- Minakov, A., Yarushina, V., Faleide, J. I., Krupnova, N., Sakoulina, T., Dergunov, N., & Glebovsky, V. (2018). Dyke emplacement and crustal structure within a continental large igneous province, northern Barents Sea. *Geological Society - Special Publications*, 460, 371–395. <https://doi.org/10.1144/Sp460.4>
- Minor, D. R., & Mukasa, S. B. (1997). Zircon U-Pb and hornblende Ar-40-Ar-39 ages for the Dufek layered mafic intrusion, Antarctica: Implications for the age of the Ferrar large igneous province. *Geochimica et Cosmochimica Acta*, 61(12), 2497–2504. [https://doi.org/10.1016/S0016-7037\(97\)00098-7](https://doi.org/10.1016/S0016-7037(97)00098-7)
- Montelli, R., Nolet, G., Dahlen, F. A., Masters, G., Engdahl, E. R., & Hung, S. H. (2004). Finite-frequency tomography reveals a variety of plumes in the mantle. *Science*, 303, 338–343. <https://doi.org/10.1126/science.1092485>
- Mosher, D. C., Shimeld, J., Hutchinson, D., Lebedeva-Ivanova, N., & Chapman, C. B. (2012). Submarine landslides in Arctic sedimentation: Canada Basin. *Adv. Nat. Technol. Hazards Res.*, 31, 147. [https://doi.org/10.1007/978-94-007-2162-3\\_13](https://doi.org/10.1007/978-94-007-2162-3_13)
- Mudie, P. J., Stoffyn-Egli, P., & Van Wagoner, N. A. (1986). Geological constraints for tectonic models of the Alpha Ridge. *Journal of Geodynamics*, 6(1–4), 215–236. [https://doi.org/10.1016/0264-3707\(86\)90040-2](https://doi.org/10.1016/0264-3707(86)90040-2)
- Muecke, G. K., Reynolds, P. H., & Avison, H. A. (1990). <sup>40</sup>Ar/<sup>39</sup>Ar geochronology of episodic magmatism during the late phase of Sverdrup Basin development, Canadian Arctic Islands (Vol. 15, p. 93). Ottawa: Geological Association of Canada/Mineralogical Association of Canada, Program with Abstracts.
- Mühe, R., Bohrmann, H., Garbe-Schönberg, D., & Kassens, H. (1997). E-MORB glasses from the Gakkel Ridge (Arctic Ocean) at 87°N: Evidence for the Earth's most northerly volcanic activity. *Earth and Planetary Science Letters*, 152(1–4), 1–9. [https://doi.org/10.1016/S0012-821x\(97\)00152-0](https://doi.org/10.1016/S0012-821x(97)00152-0)
- Mühe, R., Devey, C. W., & Bohrmann, H. (1993). Isotope and trace-element geochemistry of MORB from the Nansen-Gakkel Ridge at 86° North. *Earth and Planetary Science Letters*, 120(3–4), 103–109. [https://doi.org/10.1016/0012-821x\(93\)90233-Y](https://doi.org/10.1016/0012-821x(93)90233-Y)
- Mühe, R., & Jokat, W. (1999). Recovery of volcanic rocks from the Alpha Ridge, Arctic Ocean: Preliminary results. *Eos, Transactions of the American Geophysical Union*, 80(18), F1000.
- Mukasa, S. B., Shervais, J. W., Wilshire, H. G., & Nielson, J. E. (1991). Intrinsic Nd, Pb, and Sr isotopic heterogeneities exhibited by the Lherz alpine Peridotite massif, French Pyrenees. *Journal of Petrology*, Special Volume. [https://doi.org/10.1093/petrology/special\\_volume.2.117](https://doi.org/10.1093/petrology/special_volume.2.117)
- Münker, C., Weyer, S., Scherer, E., & Mezger, K. (2001). Separation of high field strength elements (Nb, Ta, Zr, Hf) and Lu from rock samples for MC-ICPMS measurements. *Geochemistry, Geophysics, Geosystems*, 2. <https://doi.org/10.1029/2001gc000183>
- Nejbert, K., Krajewski, K. P., Dubinska, E., & Pecskay, Z. (2011). Dolerites of Svalbard, north-west Barents Sea Shelf: age, tectonic setting and significance for geotectonic interpretation of the High-Arctic Large Igneous Province. *Polar Research*, 30. <https://doi.org/10.3402/polar.v30i0.7306>
- Nielsen, T. F. D., Turkov, V. A., Solovova, I. P., Kogarko, L. N., & Ryabchikov, I. D. (2006). A Hawaiian beginning for the Iceland plume: Modelling of reconnaissance data for olivine-hosted melt inclusions in Palaeogene picrite lavas from East Greenland. *Lithos*, 92, 83–104. <https://doi.org/10.1016/j.lithos.2006.03.038>
- Norman, M. D., & Garcia, M. O. (1999). Primitive magmas and source characteristics of the Hawaiian plume: Petrology and geochemistry of shield picrites. *Earth and Planetary Science Letters*, 168(1–2), 27–44. [https://doi.org/10.1016/S0012-821x\(99\)00043-6](https://doi.org/10.1016/S0012-821x(99)00043-6)
- Ntafos, T., & Richter, W. (2003). Geochemical constraints on the origin of the continental flood basalt magmatism in Franz Josef Land, Arctic Russia. *European Journal of Mineralogy*, 15(4), 649–663. <https://doi.org/10.1127/0935-1221/2003/0015-0649>
- Oakey, G. N., & Saltus, R. W. (2016). Geophysical analysis of the Alpha-Mendelev Ridge complex: Characterization of the high Arctic large Igneous Province. *Tectonophysics*, 691, 65–84. <https://doi.org/10.1016/j.tecto.2016.08.005>
- Olafsson, M., & Eggler, D. H. (1983). Phase-relations of amphibole, amphibole-carbonate, and phlogopite-carbonate peridotite—Petrologic constraints on the asthenosphere. *Earth and Planetary Science Letters*, 64(2), 305–315. [https://doi.org/10.1016/0012-821x\(83\)90212-1](https://doi.org/10.1016/0012-821x(83)90212-1)
- Olierook, H. K. H., Merle, R. E., & Jourdan, F. (2017). Toward a greater Kerguelen large igneous province: Evolving mantle source contributions in and around the Indian Ocean. *Lithos*, 282–283, 163–172. <https://doi.org/10.1016/j.lithos.2017.03.007>
- Paces, J. B., & Bell, K. (1989). Non-depleted sub-continental mantle beneath the superior province of the Canadian shield—Nd-Sr isotopic and trace-element evidence from midcontinent rift basalts. *Geochimica et Cosmochimica Acta*, 53(8), 2023–2035. [https://doi.org/10.1016/0016-7037\(89\)90322-0](https://doi.org/10.1016/0016-7037(89)90322-0)

- Patchett, P. J., White, W. M., Feldmann, H., Kielinczuk, S., & Hofmann, A. W. (1984). Hafnium rare-Earth element fractionation in the sedimentary system and crustal recycling into the Earth's mantle. *Earth and Planetary Science Letters*, *69*(2), 365–378. [https://doi.org/10.1016/0012-821x\(84\)90195-X](https://doi.org/10.1016/0012-821x(84)90195-X)
- Paul, M., Bridgestock, L., Rehkammer, M., van DeFliert, T., & Weiss, D. (2015). High-precision measurements of seawater Pb isotope compositions by double spike thermal ionization mass spectrometry. *Analytica Chimica Acta*, *863*, 59–69. <https://doi.org/10.1016/j.aca.2014.12.012>
- Pearce, J. A., & Stern, R. J. (2006). Origin of back-arc basin magmas: Trace element and isotope perspectives. *Geophysical Monograph Series*, *166*. <https://doi.org/10.1029/166gm06>
- Pease, V., & Coakley, B. (2018). Circum-Arctic lithosphere evolution. *Circum-Arctic Lithosphere Evolution*, *460*, 1–6. <https://doi.org/10.1144/Sp460.19>
- Pease, V., Drachev, S., Stephenson, R., & Zhang, X. (2014). Arctic lithosphere—A review. *Tectonophysics*, *628*, 1–25. <https://doi.org/10.1016/j.tecto.2014.05.033>
- Petrov, O., Morozov, A., Shokalsky, S., Kashubin, S., Artemieva, I. M., Sobolev, N., et al. (2016). Crustal structure and tectonic model of the Arctic region. *Earth Science Reviews*, *154*, 29–71. <https://doi.org/10.1016/j.earscirev.2015.11.013>
- Piepgras, D. J., & Wasserburg, G. J. (1980). Neodymium isotopic variations in seawater. *Earth and Planetary Science Letters*, *50*(1), 128–138. [https://doi.org/10.1016/0012-821x\(80\)90124-7](https://doi.org/10.1016/0012-821x(80)90124-7)
- Polteau, S., Hendriks, B. W. H., Planke, S., Ganerød, M., Corfu, F., Faleide, J. I., et al. (2016). The early cretaceous Barents Sea sill complex: Distribution, Ar-40/Ar-39 geochronology, and implications for carbon gas formation. *Palaeogeography, Palaeoclimatology, Palaeoecology*, *441*, 83–95. <https://doi.org/10.1016/j.palaeo.2015.07.007>
- Reiners, P. W. (2002). Temporal-compositional trends in intraplate basalt eruptions: Implications for mantle heterogeneity and melting processes. *Geochemistry, Geophysics, Geosystems*, *3*(2). <https://doi.org/10.1029/2001gc000250>
- Renne, P. R., Mundil, R., Balco, G., Min, K., & Ludwig, K. R. (2010). Joint determination of <sup>40</sup>K decay constants and <sup>40</sup>Ar\*/<sup>40</sup>K for the fish canyon sanidine standard, and improved accuracy for <sup>40</sup>Ar/<sup>39</sup>Ar geochronology. *Geochimica et Cosmochimica Acta*, *74*, 5349–5367. <https://doi.org/10.1016/j.gca.2010.06.017>
- Rooney, T. O., Mohr, P., Dosso, L., & Hall, C. (2013). Geochemical evidence of mantle reservoir evolution during progressive rifting along the western Afar margin. *Geochimica et Cosmochimica Acta*, *102*, 65–88. <https://doi.org/10.1016/j.gca.2012.08.019>
- Rowley, D. B., & Lottes, A. L. (1988). Plate-kinematic reconstructions of the North-Atlantic and Arctic-Late Jurassic to present. *Tectonophysics*, *155*(1–4), 73–120. [https://doi.org/10.1016/0040-1951\(88\)90261-2](https://doi.org/10.1016/0040-1951(88)90261-2)
- Rudnick, R. L., & Presper, T. (1990). Geochemistry of intermediate- to high-pressure granulites. *Granulites and Crustal Evolution*, *311*, 523–550. [https://doi.org/10.1007/978-94-009-2055-2\\_27](https://doi.org/10.1007/978-94-009-2055-2_27)
- Salters, V. J. M., & Hart, S. R. (1991). The mantle sources of ocean ridges, and island arcs—The Hf-isotope connection. *Earth and Planetary Science Letters*, *104*(2–4), 364–380. [https://doi.org/10.1016/0012-821x\(91\)90216-5](https://doi.org/10.1016/0012-821x(91)90216-5)
- Salters, V. J. M., & Stracke, A. (2004). Composition of the depleted mantle. *Geochemistry, Geophysics, Geosystems*, *5*, Q05004. <https://doi.org/10.1029/2003gc000597>
- Saltus, R. W., Miller, E. L., Gaina, C., & Brown, P. J. (2011). Regional magnetic domains of the Circum-Arctic: A framework for geodynamic interpretation. *Geological Society Memorier*, *35*, 49–60. <https://doi.org/10.1144/M35.4>
- Sato, H. (1977). Nickel content of basaltic magmas—Identification of primary magmas and a measure of degree of olivine fractionation. *Lithos*, *10*(2), 113–120. [https://doi.org/10.1016/0024-4937\(77\)90037-8](https://doi.org/10.1016/0024-4937(77)90037-8)
- Saunders, A. D., Jones, S. M., Morgan, L. A., Pierce, K. L., Widdowson, M., & Xu, Y. G. (2007). Regional uplift associated with continental large igneous provinces: The roles of mantle plumes and the lithosphere. *Chemical Geology*, *241*, 282–318. <https://doi.org/10.1016/j.chemgeo.2007.01.017>
- Saunders, A. D., Norry, M. J., & Tarney, J. (1988). Origin of MORB and chemically depleted mantle reservoirs: Trace element constrains. *Journal of Petrology, Special\_Volume*. [https://doi.org/10.1093/petrology/special\\_volume.1.415](https://doi.org/10.1093/petrology/special_volume.1.415)
- Saunders, A. D., Norry, M. J., & Tarney, J. (1991). Fluid influence on the trace-element compositions of subduction zone magmas. *Philosophical Transactions of the Royal Society A*, *335*(1638), 377–392. <https://doi.org/10.1098/rsta.1991.0053>
- Schmitz, M. D., Vervoort, J. D., Bowring, S. A., & Patchett, P. J. (2004). Decoupling of the Lu-Hf and Sm-Nd isotope systems during the evolution of granulitic lower crust beneath southern Africa. *Geology*, *32*, 405–408. <https://doi.org/10.1130/G20241.1>
- Schoene, B., Eddy, M. P., Samperton, K. M., Keller, C. B., Keller, G., Adatte, T., & Khadri, S. F. R. (2019). U-Pb constraints on pulsed eruption of the Deccan traps across the end-cretaceous mass extinction. *Science*, *363*, 862–866. <https://doi.org/10.1126/science.aau2422>
- Schoene, B., Samperton, K. M., Eddy, M. P., Keller, G., Adatte, T., Bowring, S. A., et al. (2015). U-Pb geochronology of the Deccan traps and relation to the end-cretaceous mass extinction. *Science*, *347*, 182–184. <https://doi.org/10.1126/science.aaa0118>
- Schouten, H. A., & Klitgord, K. D. (1986). Stable segmentation of central North-Atlantic Sea-floor. *Journal of the Geological Society of London*, *143*, 741–741.
- Sebai, A., Feraud, G., Bertrand, H., & Hanes, J. (1991). Ar-40/Ar-39 dating and geochemistry of tholeiitic magmatism related to the early opening of the central Atlantic Rift. *Earth and Planetary Science Letters*, *104*(2–4), 455–472. [https://doi.org/10.1016/0012-821x\(91\)90222-4](https://doi.org/10.1016/0012-821x(91)90222-4)
- Seyfried, W. F. Jr., & Mottl, M. J. (1982). Hydrothermal alteration of basalt by seawater under seawater-dominated conditions. *Geochimica et Cosmochimica Acta*, *46*(6), 985–1002. [https://doi.org/10.1016/0016-7037\(82\)90054-0](https://doi.org/10.1016/0016-7037(82)90054-0)
- Sheth, H. C. (1999). Flood basalts and large igneous provinces from deep mantle plumes: Fact, fiction, and fallacy. *Tectonophysics*, *311*(1–4), 1–29. [https://doi.org/10.1016/S0040-1951\(99\)00150-X](https://doi.org/10.1016/S0040-1951(99)00150-X)
- Sheth, H. C., Mahoney, J. J., & Chandrasekhar, D. (2004). Geochemical stratigraphy of Deccan flood basalts of the Bijasan Ghat section, Satpura Range, India. *Journal of Asian Earth Sciences*, *23*, 127–139. [https://doi.org/10.1016/S1367-9120\(03\)00116-0](https://doi.org/10.1016/S1367-9120(03)00116-0)
- Shorttle, O., MacLennan, J., & Piotrowski, A. M. (2013). Geochemical provincialism in the Iceland plume. *Geochimica et Cosmochimica Acta*, *122*, 363–397. <https://doi.org/10.1016/j.gca.2013.08.032>
- Sinton, J. M., Ford, L. L., Chappell, B., & McCulloch, M. T. (2003). Magma genesis and mantle heterogeneity in the Manus back-arc basin, Papua New Guinea. *Journal of Petrology*, *44*(1), 159–195. <https://doi.org/10.1093/petrology/44.1.159>
- Sobolev, A. V., Hofmann, A. W., Sobolev, S. V., & Nikogosian, I. K. (2005). An olivine-free mantle source of Hawaiian shield basalts. *Nature*, *434*, 590–597. <https://doi.org/10.1038/nature03411>
- Sofade, A. O. (2018). *Submarine alteration of seamount rocks in Canary Island: Insights from mineralogy, trace elements, and stable isotopes. Ph.D. Thesis*. Uppsala: Department of Earth Science, Uppsala University. 61 p. ISSN 1650–6553 Nr 442
- Sprain, C. J., Renne, P. R., Vanderkluisen, L., Pande, K., Self, S., & Mittal, T. (2019). The eruptive tempo of Deccan volcanism in relation to the cretaceous-Paleogene boundary. *Science*, *363*, 866–870. <https://doi.org/10.1126/science.aav1446>



- Staudigel, H., & Hart, S. R. (1983). Alteration of basaltic glass: Mechanisms and significance for the oceanic crust sea-water budget. *Geochimica et Cosmochimica Acta*, 47, 337–350. [https://doi.org/10.1016/00167037\(83\)902570](https://doi.org/10.1016/00167037(83)902570)
- Stevenson, R., Upton, B. G. J., & Steenfelt, A. (1997). Crust-mantle interaction in the evolution of the Ilimaussaq complex, south Greenland: Nd isotopic studies. *Lithos*, 40(2–4), 189–202. [https://doi.org/10.1016/S0024-4937\(97\)00025-X](https://doi.org/10.1016/S0024-4937(97)00025-X)
- Storey, B. C. (1995). The role of mantle plumes in continental breakup—Case-histories from Gondwanaland. *Nature*, 377, (6547), 301–308. <https://doi.org/10.1038/377301a0>
- Sugawara, T. (2000). Empirical relationships between temperature, pressure, and MgO content in olivine and pyroxene saturated liquid. *Journal of Geophysical Research*, 105(B4), 8457–8472. <https://doi.org/10.1029/2000jb900010>
- Sun, S. S., & McDonough, W. F. (1989). Chemical and isotopic systematics of oceanic basalts: Implications for mantle composition and process. In A. D. Saunders, & M. J. Norry (Eds.), *Magmatism in the ocean basins* (Vol. 42, pp. 313–345). London: Geological Society of London Special Publication.
- Sutter, J. F., & Smith, T. E. (1979). Ar-40-Ar-39 ages of diabase intrusions from Newark trend basins in Connecticut and Maryland—Initiation of central Atlantic rifting. *American Journal of Science*, 279(7), 808–831. <https://doi.org/10.2475/ajs.279.7.808>
- Sweeney, J. F. (1985). Comments about the Age of the Canada Basin. *Tectonophysics*, 114(1–4), 1–10. [https://doi.org/10.1016/0040-1951\(85\)90004-6](https://doi.org/10.1016/0040-1951(85)90004-6)
- Tailleur, L. L., & Brosge, W. P. (1970). Tectonic history of northern Alaska. In W. L. Adkison, & W. P. Brosge (Eds.), *Proceedings of the geological seminar on the North Slope of Alaska: American Association of Petroleum Geologists, Pacific Section* (pp. E1–E19). Oxnard, CA: Pacific Branch of AAPG.
- Tailleur, I. L., Mamet, B. L., & Dutro, J. T. (1973). Revised Age and Structural Interpretations of Nuka-Formation at Nuka-Ridge, Northwestern Alaska. *American Association of Petroleum Geologists Bulletin*, 57(7), 1348–1352.
- Takahashi, E. (1986). Melting of a dry peridotite K1b-1 up to 14 GPa—Implications on the origin of peridotitic upper mantle. *Journal of Geophysical Research*, 91(B9), 9367–9382. <https://doi.org/10.1029/JB091iB09p09367>
- Takahashi, E., Nakajima, K., & Wright, T. L. (1998). Origin of the Columbia River basalts: Melting model of a heterogeneous plume head. *Earth and Planetary Science Letters*, 162(1–4), 63–80. [https://doi.org/10.1016/S0012-821x\(98\)00157-5](https://doi.org/10.1016/S0012-821x(98)00157-5)
- Taylor, P. T., Kovacs, L. C., Vogt, P. R., & Johnson, G. L. (1981). Detailed aeromagnetic investigation of the Arctic basin.2. *Journal of Geophysical Research*, 86(Nb7), 6323–6333. <https://doi.org/10.1029/JB086iB07p06323>
- Thirlwall, M. F. (1995). Generation of the Pb isotopic characteristics of the Iceland plume. *Journal of the Geological Society of London*, 152(6), 991–996. <https://doi.org/10.1144/Gsl.Jgs.1995.152.01.19>
- Turner, G., Enright, M. C., & Cadogan, P. H. (1978). The early history of chondrite parent bodies inferred from <sup>40</sup>Ar-<sup>39</sup>Ar ages. In *Proceedings of the 9th lunar and planetary science conference* (pp. 989–1025). Houston, TX: NASA.
- Utzmann, A., Hansteen, T. H., & Schmincke, H.-U. (2002). Trace element mobility during subseafloor alteration of basaltic glass from ocean drilling program site 953 (off gran Canaria). *International Journal of Earth Sciences*, 91(4), 661–679. <https://doi.org/10.1007/s00531-001-0247-6>
- Van Wagoner, N. A., Williamson, M. C., Robinson, P. T., & Gibson, I. L. (1986). First samples of acoustic basement recovered from the Alpha-Ridge, Arctic-Ocean—New constraints for the origin of the ridge. *Journal of Geodynamics*, 6(1–4), 177–196. [https://doi.org/10.1016/0264-3707\(86\)90038-4](https://doi.org/10.1016/0264-3707(86)90038-4)
- Veizer, J. (1989). Strontium isotopes in seawater through time. *Annual Review of Earth and Planetary Sciences*, 17(1), 141–167. <https://doi.org/10.1146/annurev.earth.17.1.141>
- Vervoort, J. D., & Blichert-Toft, J. (1999). Evolution of the depleted mantle: Hf isotope evidence from juvenile rocks through time. *Geochimica et Cosmochimica Acta*, 63(3–4), 533–556. [https://doi.org/10.1016/S0016-7037\(98\)00274-9](https://doi.org/10.1016/S0016-7037(98)00274-9)
- Vervoort, J. D., Patchett, P. J., Albarede, F., Blichert-Toft, J., Rudnick, R., & Downes, H. (2000). Hf-Nd isotopic evolution of the lower crust. *Earth and Planetary Science Letters*, 181(1–2), 115–129. [https://doi.org/10.1016/S0012-821x\(00\)00170-9](https://doi.org/10.1016/S0012-821x(00)00170-9)
- Villeneuve, M., & Williamson, M. C. (2006). <sup>40</sup>Ar-<sup>39</sup>Ar dating of magmatism from the Sverdrup Basin magmatic province. In: *Proceedings of ICAM IV, mineral management SERV* (Vol. 206-215). Dartmouth: US Department of Interior.
- Vogt, P. R., Taylor, P. T., Kovacs, L. C., & Johnson, G. L. (1979). Detailed aeromagnetic investigation of the Arctic Basin. *Journal of Geophysical Research*, 84(Nb3), 1071–1089. <https://doi.org/10.1029/JB084iB03p01071>
- Vogt, P. R., Taylor, P. T., Kovacs, L. C., & Johnson, G. L. (1982). The Canada Basin—Aeromagnetic constraints on structure and evolution. *Tectonophysics*, 89(1–3), 295–336. [https://doi.org/10.1016/0040-1951\(82\)90042-7](https://doi.org/10.1016/0040-1951(82)90042-7)
- White, R., & Mckenzie, D. (1989). Magmatism at rift zones—The generation of volcanic continental margins and flood basalts. *Journal of Geophysical Research*, 94(B6), 7685–7729. <https://doi.org/10.1029/JB094iB06p07685>
- Willbold, M., & Stracke, A. (2006). Trace element composition of mantle end-members: Implications for recycling of oceanic and upper and lower continental crust. *Geochemistry, Geophysics, Geosystems*, 7, Q04004. <https://doi.org/10.1029/2005gc001005>
- Winchester, J. A., & Floyd, P. A. (1977). Geochemical discrimination of different magma series and their differentiation products using immobile elements. *Chemical Geology*, 20(4), 325–343. [https://doi.org/10.1016/0009-2541\(77\)90057-2](https://doi.org/10.1016/0009-2541(77)90057-2)
- Woodhead, J., Eggins, S., & Gamble, J. (1993). High-field strength and transition element systematics in island-arc and back-arc basin basalts—Evidence for multiphase melt extraction and a depleted mantle wedge. *Earth and Planetary Science Letters*, 114(4), 491–504. [https://doi.org/10.1016/0012-821x\(93\)90078-N](https://doi.org/10.1016/0012-821x(93)90078-N)
- Zindler, A., & Hart, S. (1986). Chemical geodynamics. *Annual Review of Earth and Planetary Sciences*, 14, 493–571. <https://doi.org/10.1146/annurev.earth.14.050186.002425>